NERC Scientific Facilities and Technology
Ion Microprobe Facility

University of Edinburgh
NERC Ion Microprobe Facility

2017 Annual Science Report

Ion Microprobe Facility
School of Geosciences
Kings Buildings
James Hutton Road
Edinburgh
EH9 3FE

http://www.ed.ac.uk/geosciences/facilities/ionprobe

Contents

Ion Microprobe Projects

Understanding the effects of ocean acidification and temperature on coral calcification: insights from the dissolved inorganic carbon chemistry of the coral calcification fluid

N. Allison[1], C. Cole[1], C. Hintz[2] & A.A. Finch[1]

[1]School of Earth and Environmental Sciences, University of St. Andrews, St. Andrews KY16 9AL, UK
[2] Faculty of Marine Sciences, Savannah State University, Savannah, Georgia, USA

Coral reefs are among the world's most biologically diverse ecosystems and are of substantial economic importance in terms of fisheries, tourism and coastal protection. Rising atmospheric CO_2 is causing ocean warming and has fundamentally affected seawater carbonate chemistry, lowering seawater pH. Understanding the effects of these changes is essential for predicting the future of coral reef ecosystems. However, attempts to assess increasing pCO_2 and temperature effects, either separately or in combination, have generated many contradictory observations with reports of both increased and decreased coral calcification [1]. Unraveling the source of the discrepancies between studies is key to accurately predicting the effects of increasing seawater pCO_2 and temperature in different coral species and reef environments. Coral calcification rates are positively correlated with the saturation states of the calcification fluid [2] suggesting that calcification fluid DIC chemistry is a prime driver of calcification. Understanding how coral calcification fluid DIC responds to changes in seawater pCO_2 and temperature is key to predicting the impact of future seawater temperature increases and ocean acidification on reef development.

The boron geochemistry of coral skeletons offers a method to reconstruct the dissolved inorganic carbon (DIC) chemistry of the coral calcification fluid [2]. In this study we cultured several genotypes of massive Porites spp. coral in a large-volume purpose built aquarium system at the University of St. Andrews, UK designed to maintain temperature, salinity and DIC system parameters within narrow limits [3]. *Porites* spp. are major components of coral reefs in the Indo-Pacific. Understanding the impact of rising seawater pCO_2 and temperature on the accretion ability of these reef building species is key to predicting the future of coral reefs. Imported corals were maintained at ambient seawater pCO_2 conditions for 2 months, adjusted to pCO_2 750 µatm over 1 month and then acclimated at this pCO_2 for 4 months at 28°C. The skeleton deposited over the subsequent 5 week period was identified by alizarin red stain for geochemical analysis. Seawater temperatures were then reduced to 25°C over a period of 4 weeks, corals were acclimated at this temperature for another month and then skeleton for analysis was again identified by alizarin red staining (Figure 1). At the end of this period corals were sacrificed and immersed in 3-4% sodium hypochlorite for ≥24 h with intermittent agitation to remove organic contamination, then rinsed and dried. Skeletal strips from the outermost surface of the colonies were sawn along the maximum growth axes and fixed in 25 mm epoxy resin blocks (Epofix, Struers Ltd.). Blocks were polished using silicon carbide papers (up to 4000 grade, lubricated with water) and polishing alumina (0.05 µm, suspended in water). We determined the skeletal $\delta^{11}B$ and B/Ca using the Cameca 1270 and spacing multiple SIMS analyses evenly spaced across sections bounded by the alizarin stain. The high spatial resolution of SIMS allows the analysis of primary coral

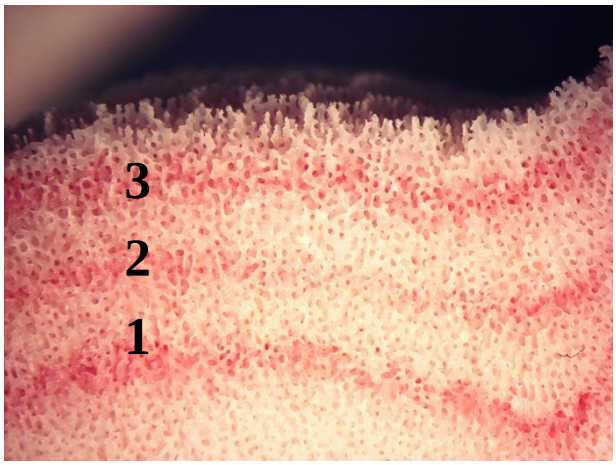

Figure 1. Cross-section though a cultured coral indicating the alizarin stain lines (numbered 1, 2 and 3. Aragonite between stain lines 1 and 2 was deposited at 28°C while aragonite deposited between stain line 3 and the outermost surface of the coral was deposited at 25°C. Aragonite deposited between stain lines 2 and 3 was deposited whilst the culture seawater temperature was changed. Image is 7 mm wide. The alizarin stain appears diffuse but actually occurs as a very fine line which is deposited across a 3 dimensional structure. Note this coral was cultured at low seawater pCO_2.

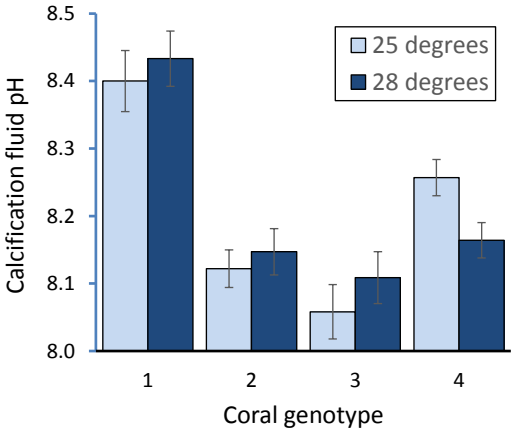

Figure 2. Calcification fluid pH reconstructed from skeletal $\delta^{11}B$ in 4 massive Porites spp. coral genotypes cultured at 750 µatm seawater pCO_2 and at 25 and 28°C. Error bars are 95% confidence limits of multiple SIMS analyses.

aragonite deposited during the 5 week stain periods even in corals cultured at high seawater pCO_2 which typically exhibit low linear skeletal extension rates (~400 µm in 5 weeks) deposited in irregularly shaped bands (Figure 1).

Results and Discussion

The pH of the calcification fluid used to precipitate the skeleton was estimated from skeletal $\delta^{11}B$ using the mean of 2 empirically-determined αB [4,5] and assuming that the $\delta^{11}B$ ECF is the same as culture seawater. Calcification fluid pH in these corals (Figure 2) is higher than that of the culture seawater (pH =7.81) but lower than that observed in field and cultured corals at ambient seawater pH (calcification site pH ≈ 8.5, [2]). Corals cultured at high seawater pCO_2 increase the pH of the calcification fluid above that of seawater by a greater magnitude than their counterparts cultured at low pCO_2 but are unable to ultimately attain the same high calcification fluid pH [6]. Calcification site pH was significantly higher in 3 of the 4 coral genotypes studied here at 28°C compared to 25°C (Figure 2, 2 tailed t test, $p \leq 0.05$). The calcification fluid pH is influenced by enzyme activities e.g. Ca-ATPase extrudes protons from the calcification fluid [7] while carbonic anhydrases catalyse the interconversion of CO_2 and HCO_3^- [8], thereby increasing fluid pH.

Enzyme activities may be both temperature and seawater pCO_2 dependent e.g. ocean acidification suppresses the gene expression and enzyme activities of carbonic anhydrases localised to the coral calcifying cells but increasing temperatures enhance these enzyme activities and may counteract the effect of seawater pCO_2 [8]. Our data indicate that temperature increases (below the coral bleaching threshold) can mitigate against the effect of ocean acidification on calcification site pH in massive *Porites* spp. corals. It is possible that future seawater temperature increases may offset the effects of ocean acidification in this coral genus at reef locations where corals live below their upper thermal stress thresholds. However, in practice, seawater temperature increases are unlikely to enhance calcification at most tropical reef locations where corals already exist close to their upper thermal tolerance limits. Future minor increases in seawater temperature at these sites are likely to induce widespread coral bleaching and thereby suppress coral calcification.

References

[1] J. Erez et al. (2011). Coral Reefs: An Ecosystem in Transition. Springer Science, New York. 151-176.
[2] N. Allison et al. (2014) Nature Communications **5**; 5741 doi: 10.1038/ncomms6741.
[3] C. Cole et al., (2018) Coral Reefs, doi.org/10.1007/s00338-018-1672-3.
[4] K. Klochko et al. (2006) Earth Planet. Sci. Lett. **248**, 276-285.
[5] O. Nir et al. (2015) Earth Planet. Sci. Lett. **414**, 1-5.
[6] A. Venn et al. (2012) Proceedings of the National Academy of Sciences of the USA **110**, doi: 10.1073/pnas.1216153110.
[7] F. Al Horani et al. (2003) Marine Biology **142,** 419-426.
[8] D. Zoccola et al (2016) Marine Drugs **14,** doi:10.3390/md14060109.

Cost-effective ^{17}O enrichment and NMR spectroscopy of mixed-metal terephthalate metal-organic frameworks

G. P. M. Bignami[1], Z. H. Davis[1], D. M. Dawson[1], S. A. Morris[1], S. E. Russell[1], D. McKay[1], R. E. Parke[1], D. Iuga[2], R. E. Morris[1] & S. E. Ashbrook[1]

[1]School of Chemistry, EaStCHEM and Centre of Magnetic Resonance, University of St Andrews, North Haugh, St Andrews, Fife, KY16 9ST, UK.
[2]UK 850 MHz Solid-State NMR Facility, Department of Physics, University of Warwick, Millburn House, Coventry, CV4 7AL, UK.

Scientific Report

Metal-organic frameworks (MOFs) are an important class of hybrid microporous materials, containing inorganic metal nodes and organic linkers. Among terephthalate-based MOFs, MIL-53 (MIL = Materiaux Institut Lavoisier) is characterised by a reversible breathing behaviour and the presence of difference possible metal centres (*e.g.*, Al, Ga or Sc) is known to affect the exact structural forms observed [1-3]. The cation disorder in MOFs containing different types of metal cations was investigated employing ^{17}O solid-state nuclear magnetic resonance (NMR) spectroscopy. NMR is an ideal tool for the characterisation of disordered materials owing to its exquisite sensitivity to the local, atomic-scale structure. However, the low natural abundance of ^{17}O (0.037%) requires expensive isotopic enrichment to acquire NMR spectra on a reasonable timescale. For this reason, cost-effective and atom-efficient synthetic pathways have been applied and developed to obtain ^{17}O-enriched Al, Ga, Sc and mixed-metal terephthalate MOFs. To evaluate the actual levels of ^{17}O enrichment, oxygen isotope data were acquired at the University of Edinburgh using a Cameca ims 1270 instrument. Samples were prepared by embedding the MOF powders in indium mounts, as shown in Figure 1, using a hydraulic press and then gold-coated. This packing stage, involving as-synthesised, calcined and hydrated MOF powders, proved to be very challenging in order to obtain a flat and polished surface stable for analysis.

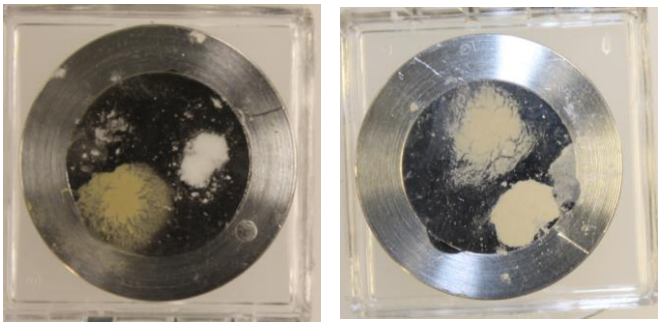

Figure 1. Photograph of the Al disks containing the samples embedded in indium.

The Al and mixed-metal Al and Ga MIL-53 materials isotopically enriched using the optimised synthetic pathways had enrichment levels ranging from 11-21% on the basis of the mass spectrometry measurements. These results not only allowed the evaluation of the actual level of isotopic enrichment, but also showed a significant variation of isotopic enrichment among different synthetic batches. This can be related to variations in the amount of isotopic reactant incorporated in the final MOF structures, shedding light on the reproducibility of the synthetic pathway optimised.

References

[1] T. Loiseau, C. Serre, C. Huguenard, G. Fink, F. Taulelle, M. Henry, T. Bataille and G. Férey, *Chem. Eur. J.*, 2004, **10**, 1373–1382.
[2] M. Vougo-Zanda, J. Huang, E. Anokhina, X. Wang and A. J. Jacobson, *Inorg. Chem.*, 2008, **47**, 11535–11542.
[3] J. P. S. Mowat, S. R. Miller, A. M. Z. Slawin, V. R. Seymour, S. E. Ashbrook and P. A. Wright, *Micropor. Mesopor. Mater.*, 2011, **142**, 322–333.

[PAGE INTENTIONALLY LEFT BLANK]

High spatial resolution analysis of zoned plagioclase from Mount St. Helens

J. Blundy[1], O. Melnik[2] & R. Dohmen[3]

[1]School of Earth Sciences, University of Bristol, Bristol BS8 1RJ, UK
[2]Institute of Mechanics, Moscow State University, 1 Michurinsky Prospekt, Moscow 119192, Russia
[3]Institut für Geologie, Mineralogie und Geophysik, Ruhr-Universität Bochum, D-44780 Bochum, Germany

Introduction

Complexly zoned plagioclase crystals are a ubiquitous feature of subduction zone volcanic rocks. Plagioclase zoning reflects a combination of pressure (P) and temperature (T) changes that have affected the magma system in which plagioclase was growing, together with any open system processes (crustal melting, magma mixing etc) that may have occurred at the same time. Unravelling these different controls on plagioclase chemistry is notoriously difficult because of the ambiguity of the various competing controls and the potential for diffusive re-equilibration during high-temperature storage of crystal prior to eruption. The aim of this project is to ally measurements of the major element composition of plagioclase (namely the $CaAl_2Si_2O_8$ anorthite component, An) with measurements of trace elements (Sr, Ba, Mg, Ti, K) at very high spatial resolution in zoned plagioclase from Mount St. Helens volcano (USA) in an attempt to establish the cause of the observed zoning patterns in terms of P-T changes and so unlock the testimony of individual crystals in terms of pre-eruptive magmatic processes and timescales. We term our approach "uncrystallisation modelling".

Modelling and Analytical Techniques

Uncrystallisation modelling involves sequential calculation of the change in P, T and melt fraction (F) required to step from one zone to the previous one in a zoned crystal, starting at the rim and adotping an estimated final temperature of crystallisation, e.g. from Fe-Ti oxide thermometry. The model requires that the system remains chemically closed on the scale of individual crystals and responds to changing P-T conditions in an equilibrium fashion. Parameterisation of plagioclase anorthite (An) content and F as functions of P and T can be made using equilibrium experimental data. Under these circumstances the partitioning of trace elements between crystal zones and the surrounding melt obey equilibrium partition relationships that are well known for plagioclase [1]. Thus trace element zoning data can be used to recover F, provided that diffusive relaxation is minimal.

High spatial resolution is a necessary condition for uncrystallisation modelling, not only to capture the very small spatial scale on which chemical heterogeneity occurs, but also to constrain timescales of diffusive equilibration, which can then be used to add a temporal dimension (t) to the method. In effect the aim is to recover P-T-t information from individual crystals. Conventional SIMS techniques, with 5 nA primary beam current, do not permit adequate spatial resolution (15 μm). To achieve the requisite 1-2 μm resolution we reduce the beam current to 0.02 nA. At these conditions the secondary ion signal is too weak to use kinetic energy filtering to remove isobaric interferences. For this reason careful calibration against matrix-matched standards is required. We used in-house Lake County labradorite and a newly developed labradorite standard, SPH1, which we have characterised by solution ICP-MS. Step profiles across crystals were designed to attain analytical precision of better than 3% relative for all elements at each point. Analysis times are of the order 1000 s per point.

Mount St. Helens

Mount St. Helens (MSH) volcano in the Cascades arc is one of the best-studied andesite/dacite, subduction-related volcanoes in the world. The iconic 1980-86 eruptions yielded silicic andesites or dacites with relatively monotonous major element compositions and scant evidence for magma mixing or other open system processes. These features make MSH an ideal volcano to apply uncrystallisation modelling. To this end we have parameterised the available H_2O-saturated experimental data for MSH [2-4] in terms of P, T, F, and the proportion and composition of plagioclase (An). We then measure high resolution chemical profiles from rim to core of selected zoned phenocrysts (e.g. Fig. 1). Four crystals were measured, two each from May and June 1980 eruptions.

Results

The measured profiles reveal significant small-scale variability in major and trace elements (Fig. 2). In general, crystal cores are richer in An and Sr and poorer in Ba than the rims, consistent with

progressive crystallisation. Uncrystallisation modelling indicates that the zoning can be ascribed to high-pressure (280-400 MPa) crystallisation of the cores and lower pressure crystallisation (100 MPa) of the rims. The crystallisation temperatures fluctuate around 880 °C, but are higher at rim (900 °C) than core (840 °C), likely due to latent heat release on crystallisation. The melt fraction decreases from core (0.85) to rim (0.70), as expected. The overall P-T-F evolution of individual crystals is consistent with that recovered from melt inclusions [5], but extends to higher pressures. These pressures correspond to depths beneath MSH where geophysical images indicate significant magma storage as partial melt. The abrupt transition from the deeper to the shallower parts of the crystal indicate rapid transfer of melt from the deep reservoir. Preliminary diffusion chronometry of the rims, based on Sr zoning [5], indicates that this magma ascent occurred on timescales of a few months prior to eruption. This has implications for monitoring MSH and other arc volcanoes.

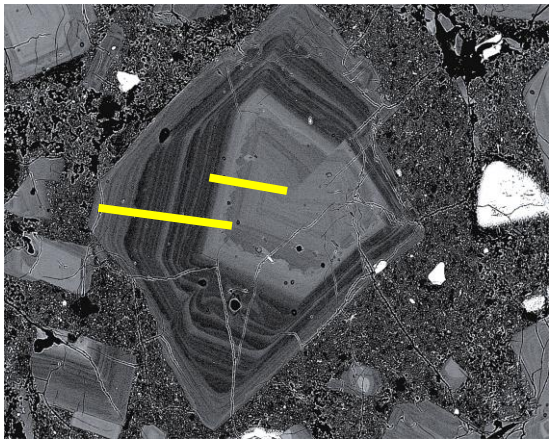

Figure 1. BSE image of plagioclase phenocryst SHKB24-11 from May 18th 1980 eruption. Crystal is approximately 1 mm across. The line of profile for Fig. 2 is shown in yellow. Note the abrupt transition from calcic core to oscillatory-zoned rim with calcic outermost zone.

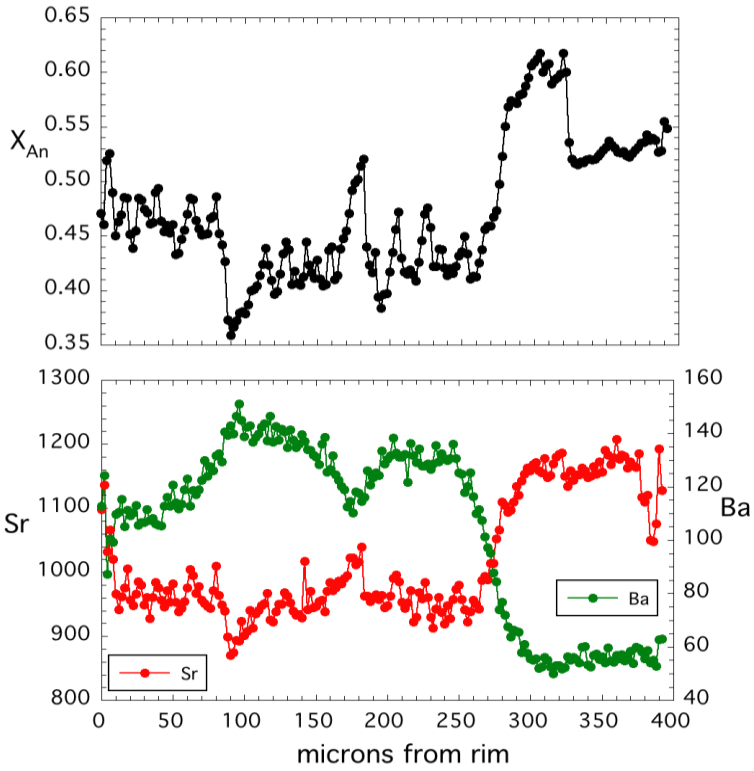

Figure 2. Chemical profiles from rim to core of SHKB24-11 determined by high-resolution SIMS: (top) molar fraction anorthite (X_{An}); (bottom) ppm Sr and Ba. According to our uncrystallisation modelling technique, the chemical characteristics of the core correspond to crystallisation at ~300 MPa; the rim grew at 100 MPa. The finescale Sr zoning preserved in the rim indicates pre-eruptive timescales of less than 0.4 years for rim growth.

References

[1] Dohmen & Blundy (2014) American Journal of Science **314**, 1319 –1372
[2] Rutherford *et al* (1985) Journal of Geophysical Research **85**, 90,2929-2947
[3] Rutherford & Devine (1988) Journal of Geophysical Research **93**, 11,949-11,959
[4] Gardner *et al* (1995) Bulletin of Volcanology **57**, 1-17
[5] Blundy *et al* (2008) USGS Professional Paper 1750, ch. 33
[5] Dohmen *et al* (2017) Reviews in Mineralogy and Geochemistry **83**, 535-575

Development of standards for volatile determination in apatite

R.A. Brooker[1], M.C.S. Humphreys[2] & J.C.M. de Hoog

[1]School of Earth Sciences, University of Bristol, Bristol. BS8 2HT, UK
[2]School of Earth Sciences, University of Durham, Durham. DH1 3LE, UK
[3] EIMF, School of GeoSciences, University of Edinburgh, Edinburgh EH9 3JW, UK

Rationale for Measurements

It is becoming increasingly apparent that the mineral apatite represents a remarkable opportunity to probe a range of processes in the magma plumbing systems beneath volcanoes, and even the processes that may play a role in the mechanism of porphyry copper mineralisation. The role of volatile species such as H_2O, CO_2, SO_2, Cl, & F, continues to emerge as one of the most important areas of research in magma evolution, of particular importance due to the devastation of explosive volcanic eruptions. As magmas rise and decompress, the different volatiles exsolve at different rates related to variable solubilities. However, many of these volatiles have vanished from the system by the time we get to study the rocks.....they are after all, volatile and the cork has been popped. As a result, the complex volatile history is notoriously difficult to track, the 'how and when' of volatile escape remaining poorly understood. Where melt inclusions are trapped by crystals they can record a snap shot, but recent studies have shown how post-entrapment alteration can make interpretation difficult. As a result, the search continues for an alternative, ubiquitous and robust means to monitor volatile activity in magmatic processes. Increasingly, the answer appears to be the mineral apatite which is often present to record both volcanic and intrusive events.

Apatite is particularly common in the more explosive volatile rich magmas that typify arc magmatism and the plutonic equivalents that occasionally produce ore bodies. It has the general formula $Ca_5(PO_4)_3X$ where X is crystal site that accommodates F^-, Cl^-, & OH^-, but has also been shown to host CO_3^{2-} [1] and possibly S^{2-} (reduced sulphur). CO_3^{2-} and SO_4^{2-} (oxidized sulphur) can also replace PO_4^{3-} in the main structure [1]. This covers all the major volatile species released by magmas, with S and Cl being particularly important to ore forming processes. The problem has been to measure a full, complete set of volatiles in natural apatites. Traditionally, F and Cl were measured using an electron probe (EMPA) and the rest of the X site was assumed to contain OH. However, we have shown CO_3^{2-} can also enter the site [1] with some speculation that S^{2-} and even O^{2-} might also occupy the channel.

To add complication, we have shown how difficult F can be to analyse accurately using EMPA [2] and that vacancies are also clearly present in the channel [1], so just measuring F and Cl and calling the rest OH is clearly not accurate. Both experiments and modelling work by ourselves [1,3] and others has shown how apatite records the melt volatile content in a systematic way that can be applied to model pre-eruptive degassing histories, but this is only possible with the development of a set of standards to measure all volatile species in the mineral apatite and the ion probe appears to be the perfect technique. We have filtered a large collection of gem quality apatites to come up with a set of 12 standards with volatiles determined by the best possible techniques; accurate EMPA for F and Cl, LECO bulk analysis for CO_2 and SO_2 and TEAC for H_2O. However, the bulk analysis requires some assessment of the homogeneity in the samples, some of which are cm sized and clearly have some degree of zonation in some major or trace elements. This study was designed to develop best practice on the Cameca 1270 and perform transects from core to rim to identify the extent of any volatile zonation.

Standards Data

The dataset for ~500 analyses made using the Cameca 1270 are shown in Fig. 1. The number of spots for each apatite depends on the sample size (min 10, max 50) and represent one or more transects from core to rim. The results illustrate which samples are the most reliable and which might be suited to calibrate for any given volatiles over a given concentration range. Clearly some samples are zoned for certain volatiles, but not others. Knowing the spatial distribution and relative size of any heterogeneity allows a maximum uncertainty error to be applied to bulk data. The extensive pre-screening of apatite samples (involving visual examination, CL, IR, EMPA) has ensured that the majority of these standard samples have no zones or single distinct thin zones confined to the outer rim. The exception being Linopolis (LIN a or c in Fig.1) which has distinct zonation for most components except water. This

study will allow final standard block to be made with sections of core used to ensure a restricted range of values. This will be made available to other workers.

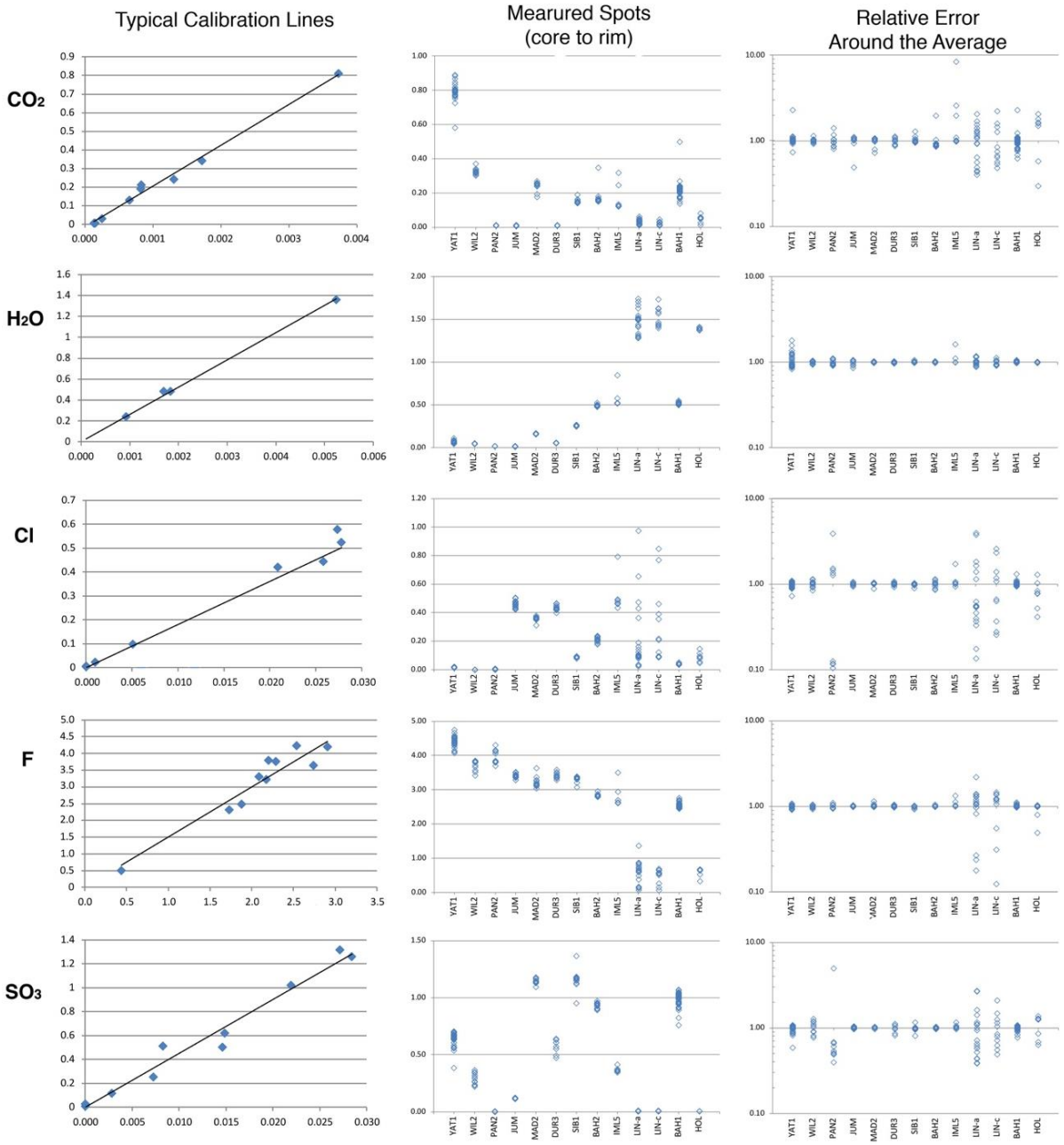

Figure 1. The first column shown a typical 1270 calibration for each volatile species. The standards values for each apatite (y-axis) were obtained via TEAC for H_2O, LECO for CO_2 and SO_2 (converted to SO_3) and EMPA for F and Cl. This is expressed as the elemental value or converted to a more useful oxide value as shown. These are plotted against the counts at relevant mass values for each volatile ratioed to the counts for oxygen on the x-axis (C/O, OH/O, Cl/O, F/O, S/O). The slope can then be used to determine concentrations in unknowns. The middle columns show the range of concentrations measured across a given apatite standard and the right column shows the same data expressed as a relative error.

References/Publications

[1] Riker J., Humphreys, M.C.S., Brooker, R.A., De Hoog, J.C.M. & EIMF. (2018) American Mineralogist 103: 260-270; [2] Stock, M. J., Humphreys, M., Smith, V. C., Johnson, R. D. & Pyle, D. M. (2015). American Mineralogist 100, 281-293; [3] Stock, M.J., Humphreys ,M.C.S., Smith,V.C., Isaia, R., Brooker, R.A., Pyle, D.M. (2018) J. Petrol. In Press

Trace element partitioning between sulphate phases and silicate melts in arc magmas: preliminary technique development

R.A. Brooker, J.D. Blundy & M. Hutchinson

School of Earth Sciences, University of Bristol, Bristol BS8 21RJ, UK

Rationale

There is an emerging view that arc magmas may commonly be saturated in sulphate, producing anhydrite or even immiscible calcium-sulphate melts. However, these phases are rarely preserved in natural samples due to their high water solubility in the surface environment. We currently have no data on the distribution of trace elements between these sulphate phases and silicate glass that might indicate the involvement of this phase in igneous (and ore-forming) processes. The main project aims to address this omission using experimentally generated samples that simulate natural magmas and developing an analytical protocol for SIMS including a set of relevant standards. However, the sulphate melts produced in the experiments do not quench to a glass, instead forming a lamella texture as shown in Fig. 1, with a phase close to $CaSO_4$ surrounded by phases lower in Ca. This raises some analytical questions.

In order to determine if analysis of this quench texture was possible by SIMS and constrain the best conditions, a one-day trail was performed on two experimental run products which were also analysed by laser ablation ICP-MS (see Fig. 1) and EMPA. The experiments were doped with a selected suit of trace elements mostly at the 50-100 ppm level (see Fig. 2 and 3). Due to the texture, it is clear a large spot size is required to get a representative analysis of the quenched sulphate melt.

Figure 2 illustrates the generally excellent agreement between the laser and SIMS data and the values for trace element are also within a reasonable range for the doping levels in the silicate melt (the dominant phase by mass). The sulphate melt shows a bigger range of concentrations allowing some interesting partition values to be calculated in Fig. 3. There are some discrepancies between the laser and ion probe data, but these can be partly explained for the major elements as large scale uneven distribution in the quench texture (as determined by EMPA element mapping). Other discrepancies in certain traces will be investigated further using a newly developed anhydrite standard set. But overall, we have shown that the quench texture should not be an obstacle to the objectives of the main application.

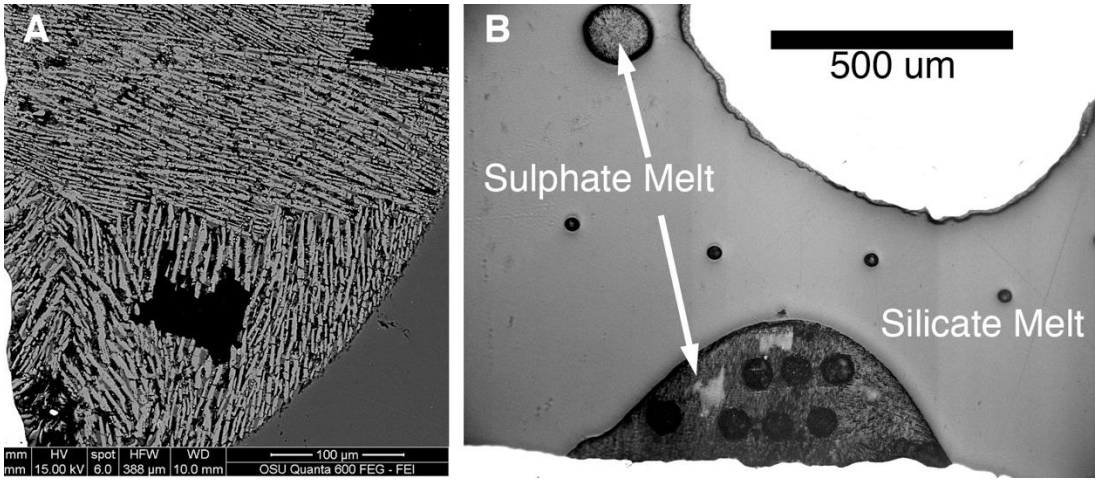

Figure 1. Sulphate melt textures. In a) the BSE image shows the quench texture, typical of sulphate melts and with the lighter phase being the $CaSO_4$ rich component. This also illustrates the 'plucking' of samples that occurs during polishing (black). In b), the laser ablation pits are visible in the silicate and sulphate melts. These were polished away for SIMS analysis.

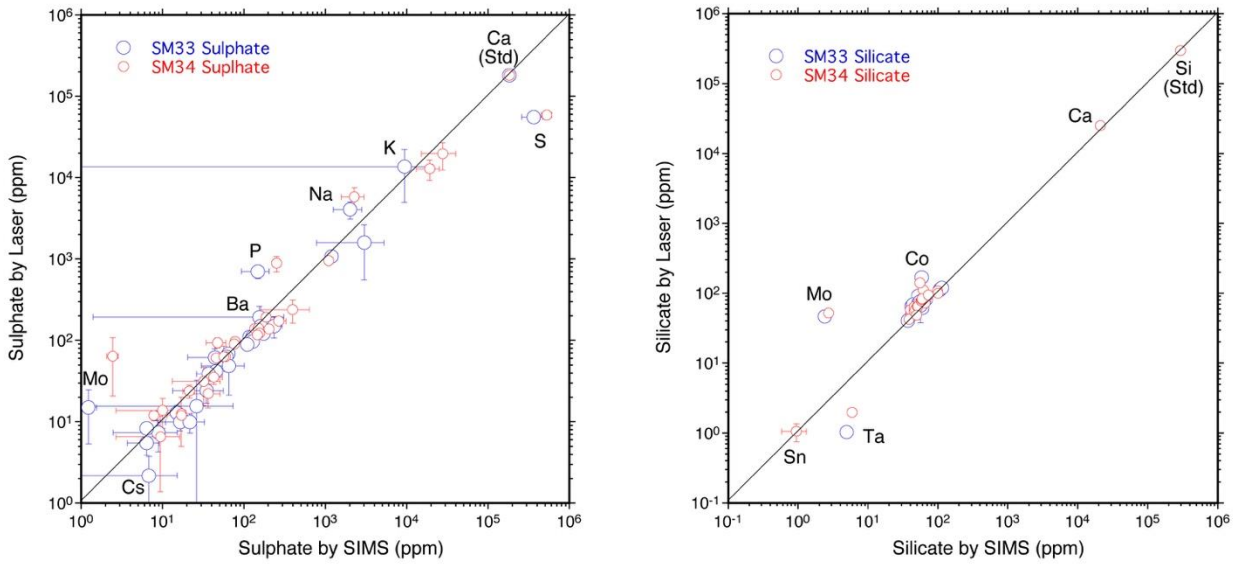

Figure 2. Comparison of data for laser vs SIMS for two experiments SM 33 and SM 34. For the sulphate melt the data are standardized to Ca and for the silicate melt to Si (both measured by EMPA). The outlier elements are labelled. The silicate melt data shows most of the trace elements close to their doping levels of 50-100 ppm

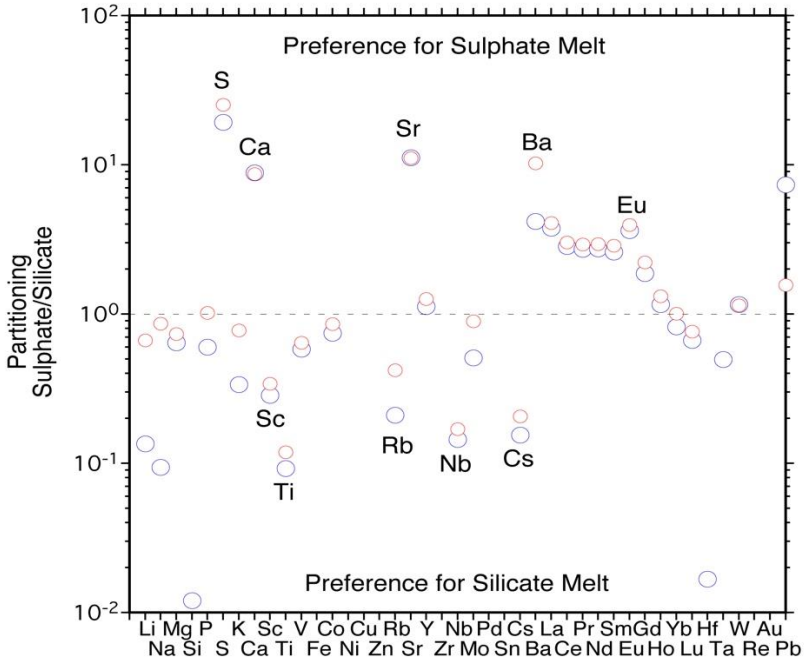

Figure 3. Partitioning between sulphate and silicate melt for the two experiments SM33 (blue) and SM34 (red). Clearly Ca and S favour the sulphate melt to form the major $CaSO_4$ component, as do Sr and Ba due to similar charge and size. There is some fractionation of the REE with lights favouring the sulphate over heavies (note Eu anomaly).

Investigating magma storage depths beneath Kick-'em-Jenny and Bequia volcanoes using melt inclusions

M. Camejo[1,2], J. Blundy[1] & E. Melekhova[1]

[1]School of Earth Sciences, University of Bristol, Bristol BS8 1RJ, UK
[2]Seismic Research Centre, University of the West Indies, St Augustine, Trinidad and Tobago

Scientific motivation for investigation

Seismic studies on the Lesser Antilles arc have highlighted significant variations in crustal thickness along-strike which may be linked to the petrogenesis of magmas and subsequent erupted compositions. Such variations are especially evident in the southern third of the arc from St. Vincent to Grenada. Although substantial work has been done on determining the depth of melt generation for bordering volcanic islands St. Vincent and Grenada, little is known about similar conditions for the central Grenadines. We therefore attempt to fill this petrological gap, starting with the two volcanoes making up the terminal ends of the Grenadines archipelago: Kick-'em-Jenny and Bequia. Melt inclusion studies will determine pre-eruptive volatile budgets and constrain magma storage depths. For the active submarine Kick-'em-Jenny volcano, such information will be useful for future hazard assessment.

Methods

We analysed trace element and volatile (H_2O and CO_2) concentrations in melt inclusions from Kick-'em-Jenny lavas and Bequia cumulates at the Edinburgh Ion Microprobe Facility. Saturation pressures were then calculated using the MagmaSat algorithm [1], which were converted to the depths melts existed before erupting.

Results and discussion

Kick-'em-Jenny

Melt inclusion data provide evidence for a highly pressurized system at depth (Fig. 1a). This has implications for the type of eruptive activity expected especially if gases are not periodically exsolved from the magmatic system. When melt inclusion entrapment depths are matched with pre-eruptive earthquake depths from the volcano's two most recent eruptions, two preferred magma storage regions are inferred: ~ <6km and ~ >9km. Melt inclusion data also show that more recent activity (2013/14 deposits) is concentrated in the uppermost magma storage region, while 1972 activity tapped in to both upper and lower magma chambers (Fig. 1b).

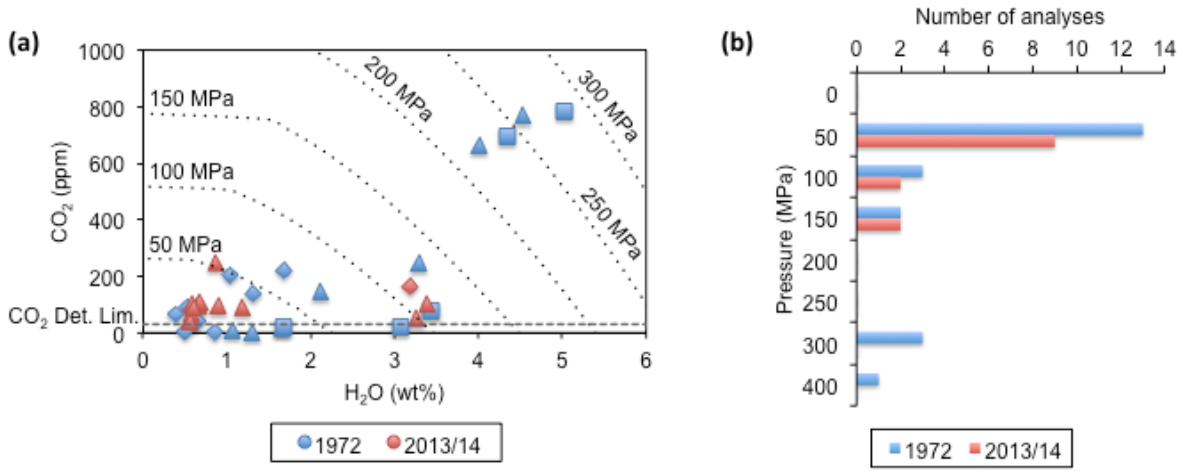

Figure 1. (a) Volatile concentrations of CO_2 and H_2O in Kick-'em-Jenny melt inclusions from 1972 and 2013/14 deposits. Isobars calculated using the Magmasat solubility model [1]. Melt inclusion hosts denoted as follows: diamond, olivine; square, clinopyroxene; triangle, amphibole. (b) Melt inclusion entrapment pressures for a given analysis.

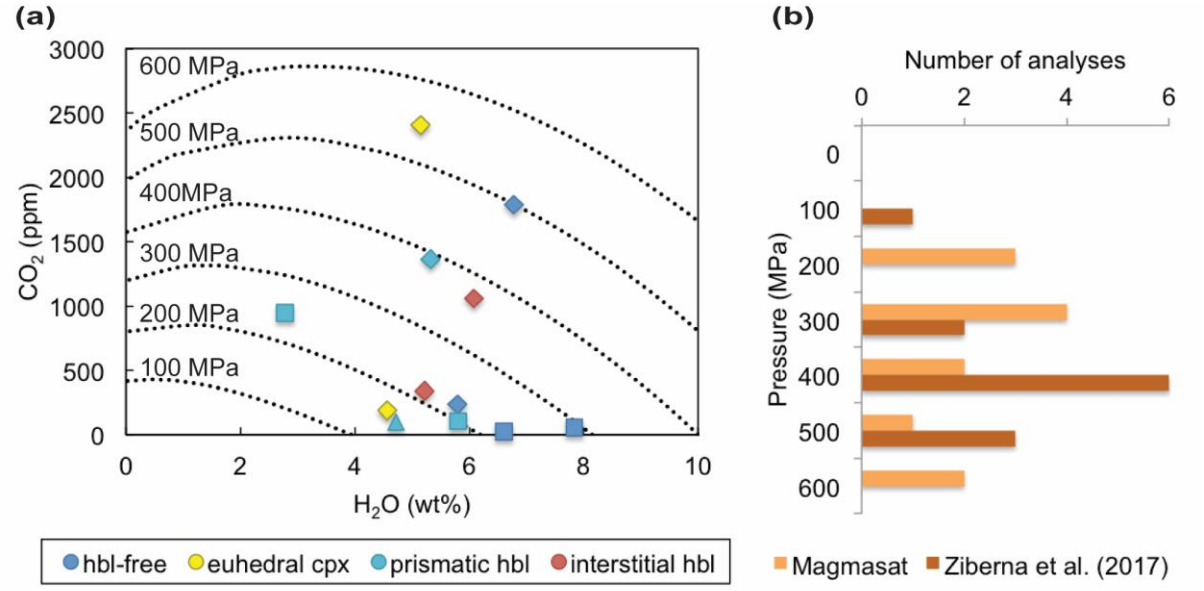

Figure 2. (a) Volatile concentrations of CO_2 and H_2O in Bequia melt inclusions. Isobars calculated using the Magmasat solubility model [1]. Melt inclusion hosts denoted as follows: diamond, olivine; square, clinopyroxene; triangle, amphibole. Colours denote cumulate textural groups. (b) Melt inclusion entrapment pressures for a given analysis matched by pressures calculated using the multiple reaction approach of [2].

If this is an accurate representation of the configuration of more recent eruptions, it means that such shallow magma intrusion can potentially be a contributor to flank collapse. This increases the tsunami threat posed by this submarine volcano.

Bequia

Melt inclusion data show that cumulates are sourced from crustal mush regions spanning a broad depth range of 6 to 21 km, with corresponding pressures of 162 to 571 MPa and crystallising under water contents of up to 7.8 wt. % (Figure 2). Such a spread would facilitate the reactive infiltration of hydrous melts with diverse compositions during magma differentiation.

References

[1] M. S. Ghiorso and G. A. R. Gualda, "An H_2O-CO_2 mixed fluid saturation model compatible with rhyolite-MELTS," *Contributions to Mineralogy and Petrology*, vol. 169, pp. 1-30, 2015; [2] L. Ziberna, E. C. R. Green, and J. D. Blundy, "Multiple-reaction goebarometry for olivine-bearing igneous rocks," *American Mineralogist*, 2017.

Tracking magma temperature changes using gas chemistry

M. Cassidy

Department of Earth Sciences, University of Oxford, Oxford, OX1 3AN UK

Scientific Report

This documents reports on the results gained from a 1 day pilot study at EIMF in November 2017.

Motivation

I am attempting to understand how some gases (S, Cl, F) behave during temperature fluctuations within the shallow magma body, by measuring these species in experimental glasses. The hypothesis being that these species partition between the melt and fluid phase as a function of temperature, and thus may provide a means of detecting magma temperature fluctuations by measuring volcanic gas at the surface.

Volcanic gas monitoring of active volcanoes mostly measures SO_2 and CO_2, because previous experimental work has shown that the content of H_2O, CO_2 and SO_2 in the melt is predominantly controlled by pressure, therefore SO_2 and CO_2 are often used as proxies for deep magma ascent due to their different solubility depths [1,2]. However many volcanic eruptions are sourced from magmas that reside from shallow reservoirs and not supplied by deeper mafic inputs to the system (e.g. Kelud volcano [3]). These eruptions are can triggered instead by overpressures in the magma chamber due to enhanced crystallisation. In these instances, gas monitoring of traditional volatile species will be unable to detect changes relating to magmatic ascent before eruptions.

Recent studies suggest that the temperature of a residing magma reservoir may dictate the explosivity of an impending eruption [3, 4, 5]. This is because temperature has a fundamental role in controlling the magma's rheology, which determines the magma's ability to retain magmatic volatiles. However, there is a very poor understanding of how these and other gases, such as halogens, partition from the melt and fluid phases at varying temperatures. Studies on Cl, suggest that it has its partitioning does not vary with pressure [6], offering promise for Cl and the other halogens, that temperature may be the principle factor controlling it fluid/melt partitioning.

In my current work I have conducted petrological experiments at various pressures, temperatures and XH_2O (degree of water saturation in the fluid phase) on Kelud volcanics (Indonesia). I have constrained the magmatic storage conditions before both explosive and effusive eruptions. This work has unveiled shallow a magma storage body at ~50 MPa, but with variable temperatures and XH_2O ratios between explosive & effusive eruptions., I used my pilot day on the SIMS (9th November 2017) to measure the S, Cl and F contents of my five of my experimental glass products from Kelud. The samples chosen were isobaric (50 MPa) and ranged in temperature from 1000, 1050, to 1100°C and XH_2O (0.55 – 1). An average of 7 analyses per sample were conducted, averages were calculated along with standard deviation. The precision was good for water-saturated experiments, but there was more heterogeneity in the water under saturated experiments. Along with my unknown samples, secondary standards (MPI Ding reference materials), were also measured to check for reproducibility and accuracy.

Outcomes

The data show some very promising results (Fig 1). There is a 200 ppm difference in F glass content over 100° C temperature change, and 750 ppm difference in glass content for Cl over the same temperature range. This shows that the halogens may partition from melt/fluid phase during temperature changes within the magmatic body at shallow depths. Furthermore, Cl concentration also changes as a function of the degree of water saturation, this may very useful for understanding if magmas are water saturated before eruptions, a condition recognised to trigger eruptions. S contents were already degassed at these low pressure, and thus the effect of temperature would be limited.

These data may help us determine changes that occur within the magma chamber, for example a reduction of Cl and F relative to other gases may suggest that the magma is cooling and crystallising at shallow pressures. If successful, this would significantly help scientists monitor activity and improve our ability to forecast eruptions.

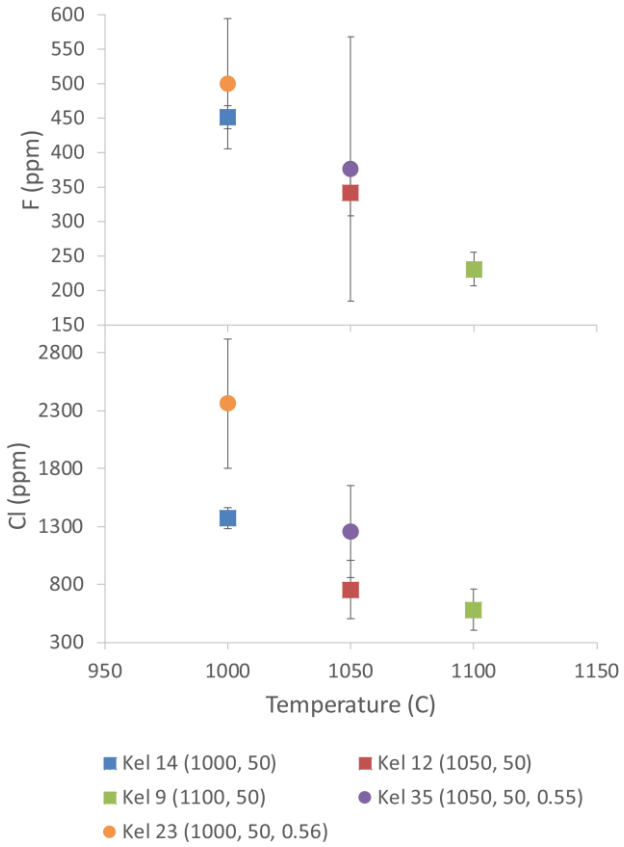

Figure 1. Plot of Cl & F content in experimental glass as a function of temperature and XH_2O. Points plotted represent an average of at ~7 analyses with their standard deviations plotted as bars.

Future work

These results are very interesting, but they require extra work to understand if that same changes occur with different magma types, different conditions at different volcanic systems. To this end I am conducting further isobaric experiments on more silicic compositions in order to constrain the F, Cl changes across different temperatures. Furthermore, I would like to extend the measurements beyond just Cl, and F and measure the other halogens, such as Br and I on the SMIS, which may tell us more about the state of magma at depth. I will be applying to the EIMF in April 2018 to gather more SIMS data to build on these initial exciting results.

References

[1] Surono et al. (2012) J. Volcanol. Geotherm. Res. 241–242, 121–135.
[2] Moor, J. M. et al. (2016) J. Geophys. Res. Solid Earth 1–15.
[3] Cassidy, M. et al. (2016) Geology 44.
[4] Ruprecht, P. & Bachmann, O. (2010). Geology 38, 919–922.
[5] Koleszar, A. M. et al.,(2012). J. Volcanol. Geotherm. Res. 219–220, 1–14.
[6] Lesne et al., (2011). J. Pet, 52, 9, 1737-1762

SIMS U-Pb dating of detrital zircons from Cretaceous volcanogenic sediments in Cyprus used to determine the age of arc magmatism and, combined with geochemical data, develop a new model of Tethyan subduction in the E. Mediterranean region

G. Chen & A. Robertson

School of GeoSciences, University of Edinburgh, Edinburgh EH9 3JW, UK

Introduction

The main aim of the ion-probe dating of separated zircon crystals was to determine if the age of arc-derived volcaniclastic sediments in W Cyprus (Kannaviou Formation) [1-2] is similar to that of felsic tuffaceous rocks in the Kyrenia Range, N Cyprus (Fourkovouno Formation) [3], and to develop a new tectonic model depending on the results obtained. A parallel one-day pilot ion probe study of volcanic glass from W Cyprus discovered that the composition is similar to some products of continental margin arc volcanism. Taking both data sets together, a new plate tectonic model of the Eastern Mediterranean is proposed, as promised in the dating proposal.

Results and Interpretation

The dating proved to be difficult (as expected) because not all of the grains separated for analysis proved to be zircon, because the crystals were small and many contained cracks or impurities making them unsuitable for analysis. The U-Pb crystallisation ages obtained range from 578.9±6.3 Ma to 78.8±0.9 Ma (n=18). Two xenocrystic zircons were possibly derived from the adjacent terrigenous sequence of the Mesozoic Mamonia Complex. Several crystals yielded unreliable results because of high common lead (n=2) or inherited zircon cores (n=1). Five zircons gave reversely discordant ages due to excess radiogenic Pb. The remaining eight grains yielded a reliable Concordia age of 80.44±1.0 Ma (Campanian) (Fig. 1a). Petrographic and sedimentological evidence suggest that the zircons were mainly supplied together with fall-out tephra in a deep-marine setting. Therefore, the determined age is interpreted as the time of crystallisation of the source arc-related volcanics.

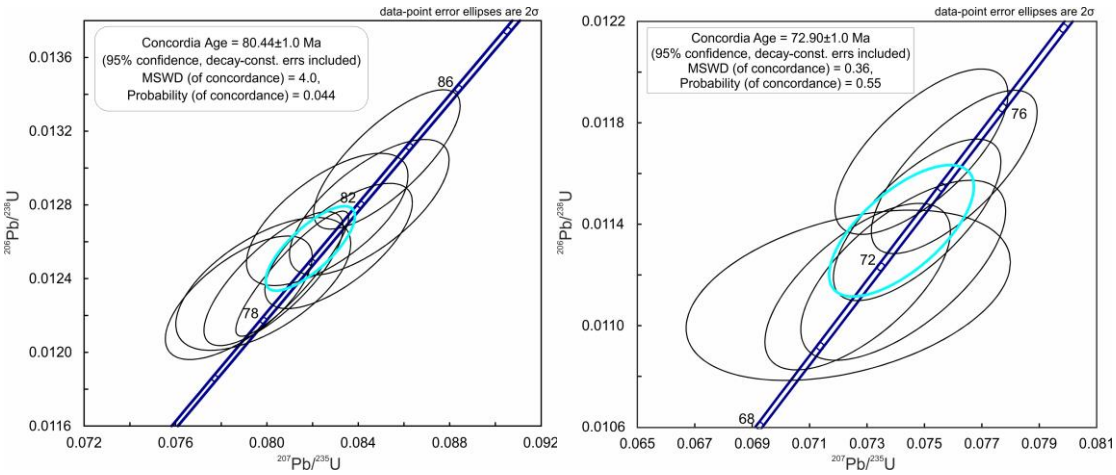

Figure 1. (a) Eight concordant analyses of zircons from the Kannaviou Formation, yielding a Concordia age of 80.44±1.0 Ma; (b) Six concordant analyses for the Fourkovouno Formation, yielding a Concordia age of 72.9±1.0 Ma.

The U-Pb dating of zircons (n=12) from north Cyprus (Fourkovouno Formation) was again difficult owing to paucity of suitable zircons, most of which yielded discordant ages, ranging from 71.3±0.9 Ma to 589.9±6.3 Ma. The results from several other grains also had to be discarded; i.e. one xenocryst, poorly luminescent grains (n=3), a high common lead grain (n=1) and reverse-discordant zircons (n=2). A reliable Concodia age of 72.9±1.0 Ma was calculated for the remaining six grains, which is interpreted as the primary crystallization age of these pyroclastic felsic tuffaceous rocks (Fig. 1b).

For comparison, as in the proposal, a sample from the base of the structurally overlying continental margin sequence (Kiparisso Vouno Formation) yielded concordant analyses (64 out of 99

grains analysed) that dominantly group in the Ediacaran-Cryogenian age range, together with small populations of Late Cretaceous (Cenomanian-Coniacian; 95-87 Ma), Carboniferous (350-310 Ma), Tonian (1000-850 Ma) and Archean ages. The dominant Ediacaran-Cryogenian zircon populations are likely to have been recycled from Palaeozoic sandstones within the Tauride-Anatolide continent to the north. However, prior to Triassic rifting of the Southern Neotethys, initial derivation was from the NE Africa/Arabian-Nubian Shield of north-Gondwana [4]. The Palaeozoic zircons reflect Variscan magmatism within the Tauride-Anatolide continent [4], whereas the Late Cretaceous zircons are likely to record continental margin arc magmatism in SE Turkey [3].

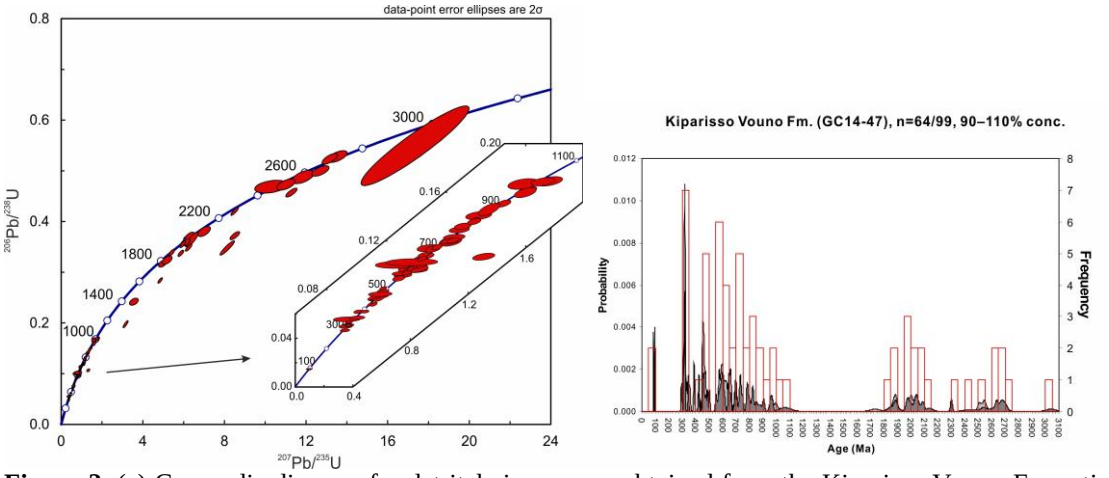

Figure 2. (a) Concordia diagram for detrital zircon ages obtained from the Kiparisso Vouno Formation (GC14-47); (b) Probability-density distribution of the zircon ages obtained from the Kiparisso Vouno Formation (GC14-47).

Taking account of all of the available age, geochemical and other relevant evidence, the Campanian (80.44±1.0 Ma) volcaniclastic Kannaviou Formation was sourced from an incipient continental margin arc, whereas the Late Campanian (72.9±1.0 Ma) Fourkovouno Formation erupted in a later-stage Andean-type active continental margin setting. The arc magmatism took place along the northerly, active continental margin of the Southern Neotethys [1, 2, 4, 7]. The older, Kannaviou Formation and the younger, Fourkovouno Formation arc volcanism is interpreted as the products of early and more advanced northward subduction beneath the Tauride microcontinent. It is suspected that similar arc products in some other areas were removed by subduction-erosion, or concealed by continental collision. Subduction continued to affect the northern continental margin of the Southern Neotethys (Kyrenia Range) during the Maastrichtian (Late Cretaceous). This lead to the accumulation of the over-riding Kiparisso Vouno Formation and related subduction-influenced extensional volcanism possibly in a back-arc setting [3]. Continental collision was delayed until the Miocene [3].

The aims of the research proposal where, therefore, achieved successfully, including development of a new tectonic model, although ideally we would have liked to have more viable U-Pb ages from the two volcaniclastic units.

References

[1] A. H. F. Robertson (1977) Journal of the Geological Society, **134**, 269-292.

[2] M. F. Gilbert and A. H. F. Robertson (2013) Geological Society, London, Special Publications, **372**, 273-298.

[3] A. H. F. Robertson et al. (2012) Geological Magazine, **149**, 264-290.

[4] T. Ustaömer et al. (2012) Geological Society, London, Special Publications, **372**, 49-74.

Boron and B isotope behaviour during serpentinite dehydration

E. Clarke[1], J.C.M. De Hoog[1], J. Harvey[2], B. Debret[3], L. Kirstein[1] G. Bromiley[1]

[1]School of GeoSciences, University of Edinburgh, Edinburgh EH9 3JW, UK
[2]School of Earth and Environment, University of Leeds, Leeds LS2 9JT, UK
[3]Department of Earth Sciences, University of Cambridge, Madingley Road, Cambridge CB3 0EZ, UK

Introduction

The incorporation of volatiles, particularly water, into the mantle by subduction has played a crucial role in the evolution of our planet: water incorporation triggers partial melting, which feeds the re-supply of volatiles to Earth's atmosphere via arc volcanism and the creation of continental crust. Without these processes, it is unlikely that Earth could sustain life (certainly complex terrestrial life), making deep water recycling a key contributor to Earth habitability.

A strong candidate for transporting water and other volatiles into the mantle is serpentinite due to its high water content and widespread presence in subducting lithosphere. Along with water, serpentinites contain high concentrations of B and other fluid mobile elements. These elements are released at depth during dehydration, and the boron isotope ratio ($\delta^{11}B$) can be used to track these fluids. It is a powerful tracer of water in the mantle due to the large differences between mantle rock (~ -10‰) and seawater (~ +40‰). However, secondary olivine, formed by the dehydration of serpentine during subduction, has been found to contain significant concentrations of B[1,2,(this study)].

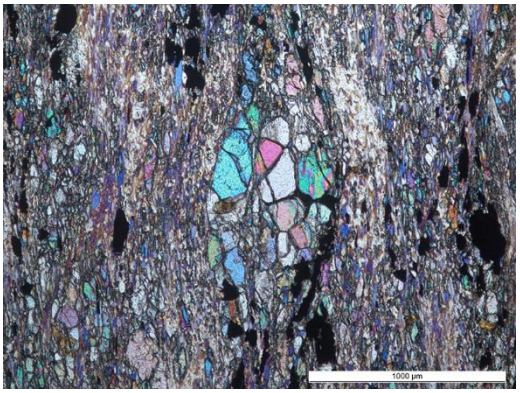

Fig. 1 Secondary olivine in serpentine matrix (Zermatt-Saas). Cross-polarised light micro-photograph.

This retention of B during dehydration could fractionate boron isotopes and undermine current assumptions of the $\delta^{11}B$ of serpentinite fluids. In addition, evidence for open system serpentinite dehydration is also presented. Therefore, to use $\delta^{11}B$ as a geochemical tracer of water, the behaviour of B and its isotopes during serpentinite dehydration must be fully understood. Here we present in–situ B and B isotopic analysis of serpentine and secondary olivine (Fig. 1) to investigate B behaviour during serpentinite dehydration.

Results and discussion

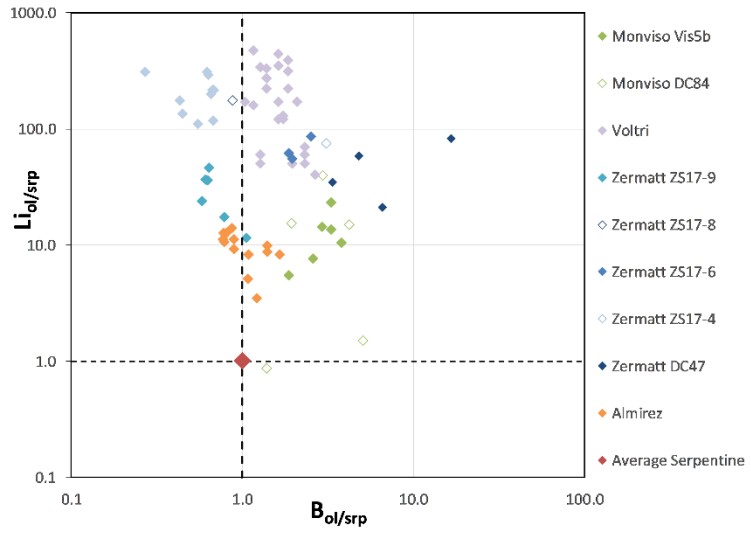

Figure 2 Boron and Li concentrations in olivine compared to that of antigorite in the same sample

Secondary olivines often show higher concentrations of B than serpentine in the same sample (6.4-17.1ppm) and always show higher Li concentrations (0.2-11.5 ppm) Fig. 2). This evidences complex open system behaviour during dehydration with secondary olivines inundated with excess B and Li potentially sourced from dehydrating meta-sediments, altered oceanic crust or other serpentinite bodies (or a mixture of these). Those

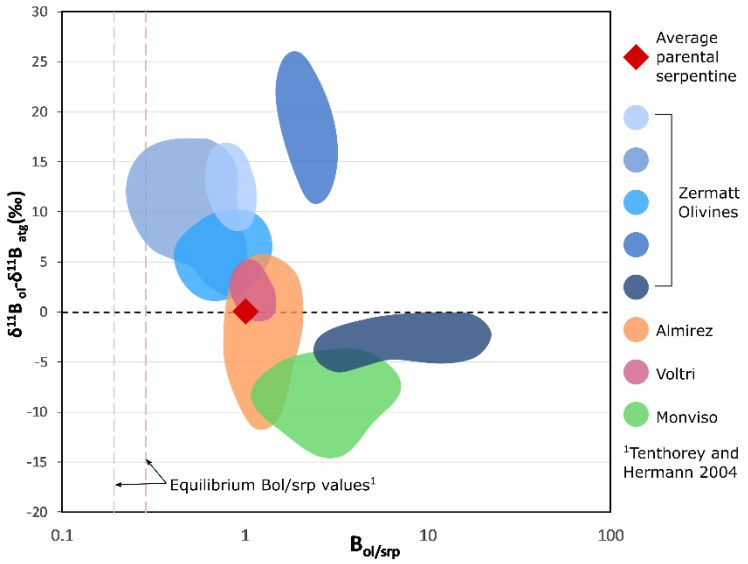

Figure 3 Boron and δ^{11}B values of olivine compared to that of antigorite in the same sample. Equilibrium Bol/srp calculated experimentally in Tenthorey and Hermann 2004[6]

samples which show relatively small influence of external fluids, i.e., more closed system behaviour (i.e. $B_{ol} < B_{srp}$) also show elevated δ^{11}B values in the olivine compared to serpentine from the same sample (Fig. 3). This suggests that B isotopic fractionation occurs during serpentine dehydration, probably due to a difference in B coordination in olivine and serpentine[3], where olivine preferentially incorporates ^{11}B. Since low pH fluids share the same preference, this ~12‰ fractionation has been used to calculate average predicted fluid composition. The 3-way mixing plot (Fig. 4) demonstrates that slab fluids of around 60% serpentinite origin are required to create the high δ^{11}B values of arc lavas. Further implications include a high δ^{11}B value for slab residue, which introduces the potential traceability of subducted slabs throughout the mantle.

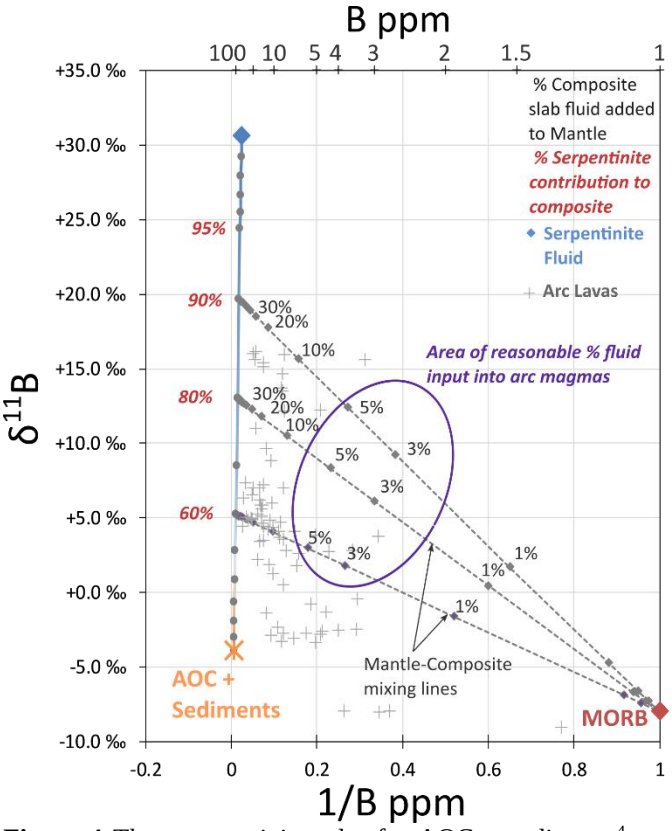

Figure 4 Three-way mixing plot for AOC + sediments[4] + serpentinite fluid + MORB plotted against range of arc lavas.

Analytical details

Instrumental boron isotope fractionation during analysis of different minerals (olivine, serpentine) was evaluated using ultramafic glass reference materials (GOR128-G and GOR132-G) and serpentine minerals analysed independently by TIMS[5].

Significant instrumental mass fractionation of ~ 8‰ in the serpentine standards was recorded and applied to the presented data.

References

[1] Scambelluri et al. (2004) EPSL **222**, 217-234
[2] De Hoog et al. (2014) CMP **167** (3):1–15
[3] Ingrin et al. (2014) Am Mineral 99, 2138-2141
[4] Tonarini et al. (2011) EPSL **301**, 275-284
[5] De Hoog et al. (2017) Goldschmidt Abstracts #872
[6] Tenthorey and Hermann. (2004) Geology 32, 865-868

Tracing serpentinite dehydration along the Lesser Antilles arc: volatile & trace element signatures of melt inclusions

G. F. Cooper[1], J. D. Blundy[2] & C. G. Macpherson[1]

[1]Department of Earth Sciences, Durham University, Durham, DH1 3LE, UK
[2] School of Earth Sciences, Wills Memorial Building, University of Bristol, Bristol, BS8 1TH

Introduction

Within subduction zones, the down going slab contributes a distinct geochemical flavour to arc magmas. Subducted serpentines, associated with ultramafic slab lithologies, play a crucial role in supplying H_2O and selected trace elements, including boron and halogens to arc magmas. This study investigates the role of serpentine dehydration along the Lesser Antilles arc using melt inclusions from volcanic samples and plutonic xenoliths from the whole length of the Lesser Antilles arc (Fig. 1). Serpentinite is a common component in fracture zones which intersect the Lesser Antilles Arc. By analysing melt inclusions from the whole length of the arc, we can investigate if there are any systematic increases in fluid addition and a corresponding change in fluid chemistry at locations where oceanic fracture zones intersect.

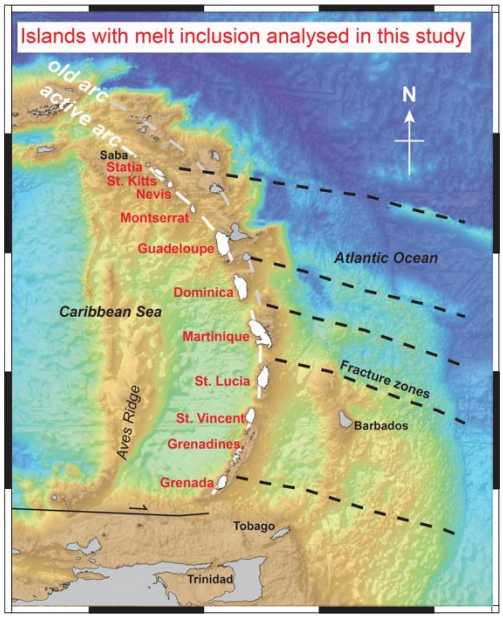

Fig. 1. Map of the Lesser Antilles arc. Island from which MI's were analysed are in red. Approximate locations of fracture zones are shown (dashed lines).

Results

More than 200 melt inclusions have been analysed for volatiles (H_2O, CO_2), light elements (Li, B, F, Cl) and a selected range of trace elements (Rb, Sr, Y, Zr, Nb, Cs, Ba, La, Ce, Sm) over two analytical sessions (Oct 2017 & Jan 2018) using the Cameca IMS-4f. The majority of melt inclusions were hosted in clinopyroxene, although a number hosted in plagioclase, orthopyroxene, olivine and amphibole were measured for comparison. After Ion Microprobe analysis, melt inclusions were analysed for major elements by EPMA at the University of Bristol. Melt inclusions range from basalts to high SiO_2 rhyolites (50-78 wt. % SiO_2). The lesser evolved melts can be classified as Low-MgO high alumina basalts (MgO=1.8-3.5 wt. %, Al_2O_3=15.3-19.1 wt %).

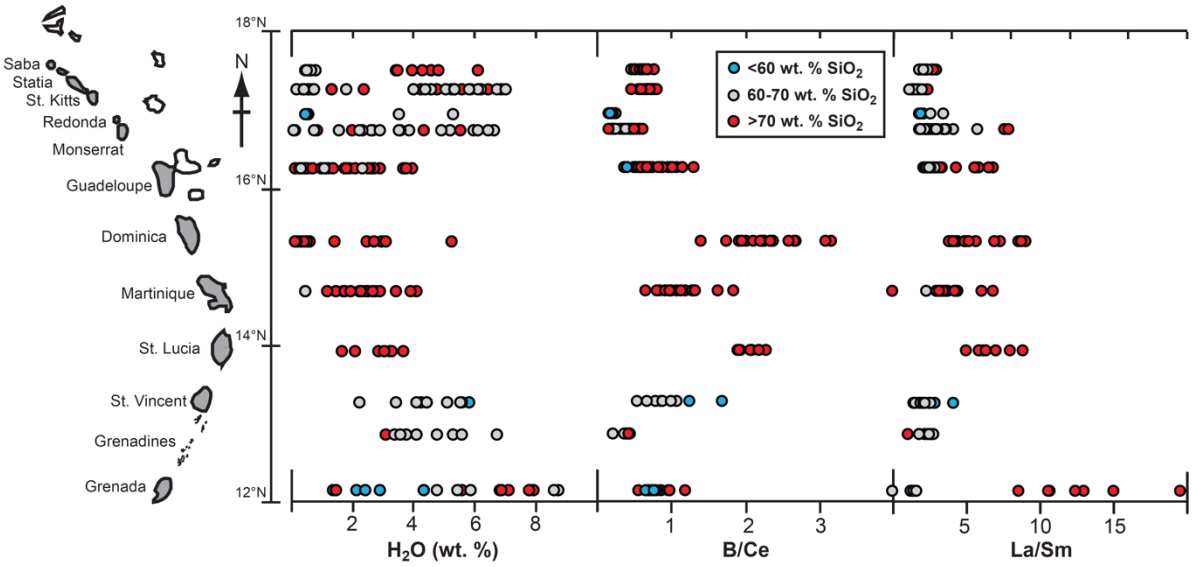

Fig. 2. Along-arc variation in water and selected trace element ratios in all measured melt inclusions. Data is coloured based on the SiO_2 content of the melts.

Melts from along the length of the Lesser Antilles are characterised by high water contents. Melt inclusions cover a large range in H_2O (0.1-9.1 wt. %), MI's also display a large range in CO_2 contents from 0-760 ppm. Each individual island also shows a large range in water contents (Fig. 2). It is likely that many of the the MI's have lost their primary water contents and therefore water concentrations alone may no be the best way to trace the supply of volatiles from the slab. The ratios of fluid mobile elements, such as B/Ce (Fig. 2) may suggest variations in the supply of fluids from the slab. High B/Ce in the central arc (Fig. 2) indicate an excess in B, and potentially the involvement of serpentinite source. Other trace-element ratios, such as B/Nb, B/Zr and La/Sm (Fig. 2) follow a similar pattern, with elevated ratios in the central arc. Whereas other ratios such as Ba/La don't show a systematic variation. The highest La/Sm values are found in melt inclusions from Grenada, which may be due to partial melting, the influence of sediments and/or high temperature and pressure fluids. Grenada also shows the highest Cl values (up to 1 wt. %).

Many of the melt inclusions are highly evolved (>70 wt. % SiO_2) and therefore many trace element signatures are likely to be controlled by differentiation within crustal storage regions. These processes will mask those obtained from the source. This is evident in the increase in B concentrations in melts >70 wt. % SiO_2 from <10 ppm to >20 ppm. These effects will therefore need to be considered when interpreting this dataset.

Key Findings

This study has produced a unique melt inclusion dataset from the Lesser Antilles which has revealed:

- large along-arc variations in trace element signatures which suggest there is a variation in the supply of fluids to the arc.
- Dominica shows the largest range in trace element ratios and the highest water contents. This is consistent with geophysical signals, such as elevated B values [1] as well as the highest eruption volumes [2].
- Basaltic melt inclusions are rare in the Lesser Antilles and melts are commonly more evolved than the composition of their host rock. This suggests that much of crystal cargo is stored in evolved crystal mushes, which are later remobilised by lesser-evolved ascending melts.
- Many of the islands have distinctive geochemical signatures, which is likely the result of both source variation, differentiation and crustal assimilation. Melt inclusions from Grenada in the south of the Lesser Antilles, have unique trace element signatures indicative of partial melting and sediment in the source.

Further Work

To further this study, we aim to measure the boron isotopic composition in a sub-set of the same melt inclusions, coupled with amphibole crystals within the same samples. By analysing B isotopes, we aim to to test whether sources of fluids are distinct between different islands in the arc. By using the variations in trace elements shown in this study, we can be selective in targeting melt inclusions for future isotopic analysis. The B enrichment in the central Lesser Antilles (Fig. 2) suggests a greater involvement of fluids and therefore, we can expect these melts to carry more positive $\delta^{11}B$ values (e.g. [3]).

References

[1] Sclaphorst et al. (2016) Geophysical Journal International **204**, 1405
[2] Wadge (1984) Geology **12**, 555-558
[3] De Hoog & Savov (2018) In Boron Isotopes, Advances in Isotope Geochemistry, 217-247

A new record of Eoarchaean to Hadean (?) crustal evolution in the Superior Province

J. Darling[1], C. Storey[1] & D. Moser[2]

[1]School of Earth and Environmental Sciences, University of Portsmouth, PO1 3QL, UK
[2]Department of Earth Sciences, University of Western Ontario, London ON, N6A 5B7, Canada

Scientific Background

The composition and evolution of Earth's earliest crust remains a major unknown in the geological evolution of our planet, largely due to the severely restricted rock record of the first 1 billion years of Earth's evolution. Whether this time period was dominated by mafic crust [1–3] or included large amounts of continental crust [4–7] remains hotly debated, but has major implications for the evolution of the crust-mantle system and early atmosphere, as well as boundary conditions for the origin of life.

Opportunities to test models of early lithospheric processes rely on extremely rare exposures of ancient (>3.5 Ga) crust. The known rocks of this age are highly deformed and metamorphosed, making petrological data and bulk rock geochemical records difficult to interpret. The accessory mineral zircon is commonly found in crustal rocks and is resilient to metamorphic disturbance, providing the best possible material for direct interrogation of early crustal evolution. A particularly powerful approach involves the in situ measurement of U-Pb, Hf and O isotopes, which are used to characterize the nature and origin of the magma source from which the zircon crystallized, and the time since this source separated from the upper mantle. Together, these systems provide patterns of crustal growth that reflect regional geodynamics, and powerful tools for resolving the timing and proportion of juvenile crust formation versus crustal reworking [2,3,7,8].

The recent discovery of Eoarchaean (3.6 to 4.0 Ga), to possibly Hadean (>4.0 Ga), meta-igneous and meta-sedimentary rocks in the Nuvvuagittuq Supracrustal Belt (NSB) offers a new opportunity to investigate the processes of early crustal growth using these techniques. Amphibolites in the belt record very early differentiation of the lithosphere during the active lifespan of the 146Sm-142Nd system (T1/2 ≅0.07 Ga [9]), and have reported ages as old as 4.406 ± 0.015 Ga [10,11]. Further evidence for a Hadean origin comes from a 4.1 ± 0.1 Ga 147Sm-143Nd isochron age for intrusive gabbroic sills [11]. However, interpretation of both of these whole-rock Nd ages has been fiercely debated, due to the highly metamorphosed nature of the belt [12], and the geological significance of 142Nd anomalies [13,14]. A range of Eoarchaean granitoids intrude the belt, providing a minimum age of 3.8 Ga [15] and insights into early crustal differentiation.

We have identified new zircon records in the NSB [15], including targets that will provide new U-Pb age constraints on the intrusion of (Hadean?) gabbros and detrital grains that uniquely offer broad sampling of this ancient part of the Superior Province, including units that may not be exposed. These zircon suites have tremendous potential to resolve whether these are Earth's oldest rocks, and provide new insights into the mechanisms of growth, maturation and recycling of Earth's early crust.

Samples and methods:

Ion-microprobe (IMS 1270) oxygen isotope ratio measurements of zircon domains were undertaken on targeted via detailed scanning electron microscope (SEM) imaging at the University of Portsmouth (secondary electron, backscattered electron, cathodoluminescence, CL). Following ion-microprobe analyses of U-Pb isotopes in the same grains (scheduled for May 2018), Hf isotope measurements will be undertaken on selected sub-grain domains at the University of Portsmouth with the SIMS U-Pb and O isotope data. Two sets of newly discovered zircon targets are being analysed:

1. Detrital zircons from semi-pelitic schist N09-23A in the NSB [15]. Preliminary U-Pb data from from a small population (50 grains) indicate a deposition age of ca. 3.4 Ga, with zircon ages up to 3.8 Ga, demonstrating that these grains offer a broad sampling of local Eoarchaean (and older?) crust.

2. Irregular cores in zircons from two metagabbros with a controversial whole-rock Sm-Nd age of 4.1 ± 0.1 Ga. These zircon cores are interpreted to be preserved magmatic zircon domains that are variably replaced by 2.7 Ga metamorphic zircon growth (Fig. 2).

Results:

New scanning electron microscope imaging has revealed that detrital zircons in semi-pelitic schist N09-23A have a diverse range of internal growth and alteration structures, including many grains with rounded cores that are overgrown by later zircon growth with oscillatory-zonation that is typical of magmatic zircon (Fig. 1). This demonstrates that the population records a broad sampling of >3.4 Ga magmatism. The metagabbro zircon grains are predominantly sector zoned, suggestive of a metamorphic origin, but around one-quarter of grains contain cores that are dark in CL that may reflect original magmatic zircon.

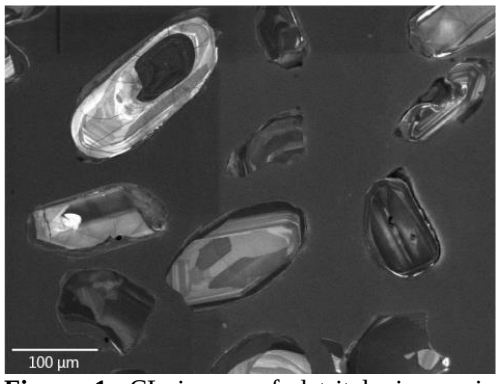

Figure 1: CL image of detrital zircons in sample N09-23A, showing varied growth textures and core-overgrowth structures.

In November 2017, oxygen isotope ratios were measured in these zircons using the CAMECA IMS 1270 at EIMF. Two hundred and thirty measurements were made on the samples, targeting different growth domains in both the detrital and metagabbro zircons. Analyses were normalised to the zircon reference material 91500, which was also used to correct for instrumental drift throughout each session (linear correction). The overall precision of $\delta^{18}O$ measurements in 91500 for the session was ± 0.04 ‰ (2σ; n = 117). The Plesovice and Kim5 zircon reference materials were run as secondary standards, yielding mean $\delta^{18}O$ values of 8.14 ± 0.06 ‰ (n = 42) and 5.24 ± 0.18 ‰ (n = 39) respectively, both within uncertainty of reference values [16,17].

In the detrital zircon population of N09-23A, measured $\delta^{18}O$ values range from 3.1 to 7.8 ‰. This range spans from values that are lower than those found in zircon that is in high-temperature equilibrium with the mantle (5.3 ± 0.6 ‰; [17]), to some of the highest values measured in Eoarchaean zircon. The latter are indicative of magma sources that include a significant amount of recycled supracrustal material. The significance of these values, in terms of secular evolution of magmatic processes, will be revealed via U-Th-Pb isotope analyses that are scheduled to be undertaken at EIMF in May 2018. Ten out of twelve analyses from metagabbro zircons, including both cores and sector-zoned overgrowths, fall within the range of mantle zircon. Two further analyses of sector-zoned overgrowths have slightly enriched $\delta^{18}O$ of up to 6.6 ‰.

Further research:

Geochronology of the zircon targets will be undertaken by measuring U-Th-Pb isotopes in the same textural domains as the oxygen isotope analyses. This work is planned for May 2018, using the EIMF CAMECA IMS 1270. Subsequently, hafnium isotopes and trace elements will be measured by laser ablation (multi-collector)-inductively-coupled-plasma mass-spectrometry at the University of Portsmouth.

References

[1] Reimink J.R. et al., 2016, Nat. Geosci. Advance. Online Pub.; [2] Kemp A.I.S. et al., 2010, EPSL 296, 45-56; [3] Kemp A.I.S et al., 2015, Precam. Res. 261, 112-26; [4] Harrison T.M., 2009, Annu. Rev. Earth Planet. Sci. 37, 479-505; [5] Wilde S.A. et al. 2001, Nature 409, 175-8; [6] Harrison T.M. et al., 2005, Science 310, 1947-50; [7] Dhuime B. et al., 2012, Science 335, 1334-7; [8] Næraa T. et al, 2012, Nature 485, 627-630; [9] Kinoshita N. et al., 2011, Science 335, 1614–7; [10] O'Neil J. et al., 2008, Science 321, 1828–32; [11] O'Neil J. et al., 2012, Precam. Res. 221, 23–44; [12] Cates N.L. & Mojzsis S.J., 2007, EPSL 255, 9–21; [13] Guitreau M. et al., 2013, EPSL 362, 171–81; [14] Roth A.S.G. et al., 2013; EPSL 361, 50–7; [15] Darling J.R. et al., 2014, Am. J. Sci. 313, 844–76; [16] Gao, Y.-Y. et al, 2015, Scientific Reports 5:16878; [17] Valley, 2005, CMP 150, 561-580.

Zircon in ultramafic rocks: potential fingerprints of crust-mantle interaction

T. Dempster[1], J. Faithfull[2] & J. MacDonald[1]

[1]School of Geographical and Earth Sciences, University of Glasgow, Glasgow G12 8QQ, UK
[2]The Hunterian, University of Glasgow, Glasgow G12 8QQ, UK

The project aimed to assess the origin of zircon megacrysts in ultramafic rocks from the Lewisian gneiss complex in NW Scotland and the robustness of their oxygen and U-Pb isotopic systems during subsequent tectonothermal events. Although the zircons from this locality have been the subject of previous isotopic investigations [1,2,3], these studies failed to assess their origin or recognise the complex growth history, including multiple generations of zircon.

Zircon typically occurs as an accessory mineral in silicic and intermediate igneous rocks [4], however zircon megacrysts (Fig. 1) are locally abundant, forming >10 vol% within pervasive orthopyroxenite veins in peridotite host rocks in the Archaean Lewisian gneiss complex. Two generations of zircons are present with up to 1 cm megacrystic zircon (Fig. 2) and a later smaller equant population located around the megacryst margins (Fig. 3). Patterns of zoning, together with REE and oxygen isotopic geochemistry indicate that the megacrysts crystallized from melts with a crustal affinity, whereas the equant zircons formed by in-situ recrystallisation within the ultramafic host. The two generations yield $^{207}Pb/^{206}Pb$ ages of 2,464±12 Ma and 2,465±11 Ma for the megacrysts and equant zircons respectively, contemporaneous with granulite facies events in the adjacent gneisses [5]. Thus the vast majority of zircon crystallization occurs within a relatively short timescale, associated with elevated temperatures.

Figure 1. Hand specimen of orthopyroxenite vein with abundant large pink zircon megacrysts.

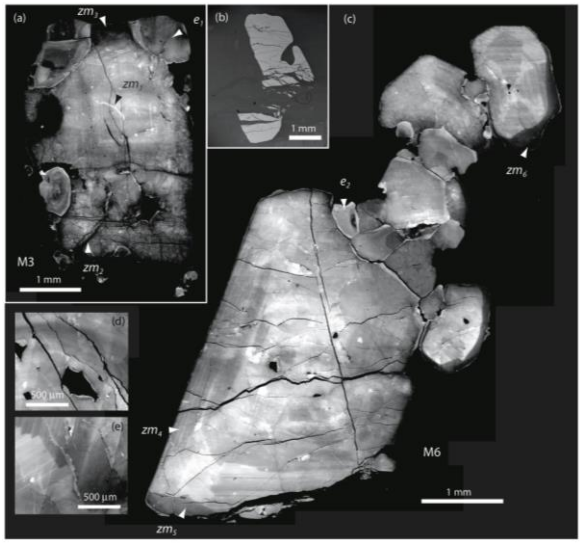

Figure 2. Cathodoluminescence (CL) images of zircon megacrysts with oscillatory zoning, some marginal and fracture related zoning.

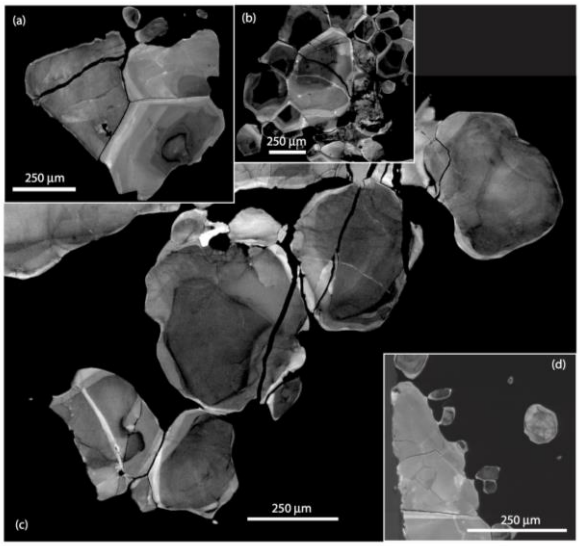

Figure 3. Cathodoluminescence images of late equant/granoblastic generation of zircon that forms around the margins of zircon megacrysts.

In general, the zircon compositions match well with those reported from xenocrysts within some kimberlites [6,7] although oxygen isotope compositions typically have a more crustal affinity (Fig. 4). The zircon REE (Fig. 5) and isotopic geochemistry confirms that the cm-thick veins probably formed by metasomatic interaction between the ultramafic host rocks and Si-rich melts [10,11] derived from

partial melting of the adjacent granulite facies orthogneisses. This interaction produced abundant orthopyroxene and, within the thicker veins, phlogopite, pargasite, scapolite and feldspars [11].
The zircons display a range of late deformation features, however identical U-Pb ages to the host zircons are recorded by most of the dark CL zircon in different fracture systems. Although the luminescence does correlate with actinide content it shows no relationship with other trace element concentrations. It is concluded that radiation damage to the zircon lattice may be a dominant control on the luminescence. Late cross-cutting bright CL-filled fractures do record younger U-Pb ages of ca 2417 Ma, compatible with localized fluid infiltration and deformation associated with the emplacement of the Scourie dyke swarm [12].

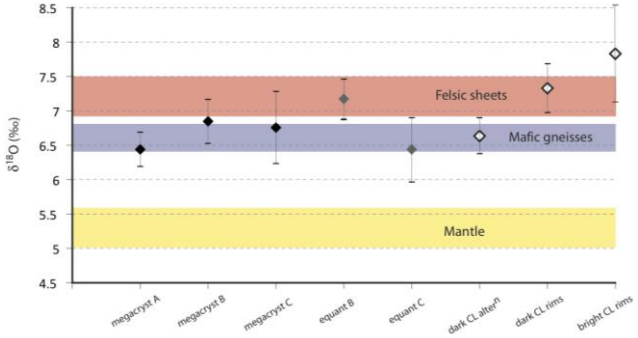

Figure 4. Oxygen isotope compositions of zircons in comparison to those determined for nearby Lewisian gneisses [8] and typical mantle values [9].

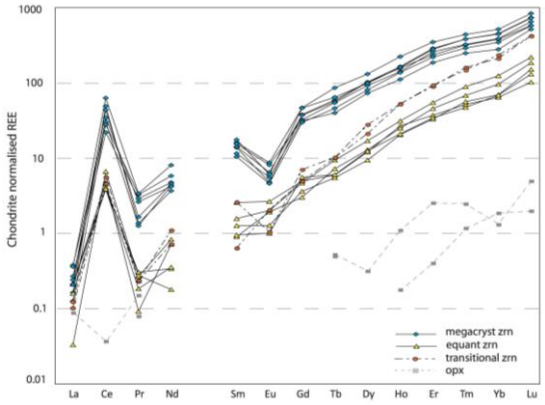

Figure. 5 Chondrite normalised REE plot showing distinctive REE signatures of different zircon generations (data from earlier EIMF pilot study)

Zircon megacrysts locally form a major component of the mineral assemblage of the veins and appear to be physically concentrated during movement of the siliceous melts. Their unusual size is linked to the suppression of zircon nucleation and increased solubility in the Si-undersaturated melts [13]. Although reports of zircon in mantle lithologies other than from kimberlites are unusual [14,15], the metasomatism between crustal melts and peridotite may represent an important analog for processes in the mantle wedge above subducting slabs. The crystallization of abundant zircon in this metasomatic environment has implications for geochemical budgets of melts generated in the mantle and may in part account for the widely reported depletion of HFSE in arc magmas [16,17,18].

References

[1] S.M. Reddy et al. (2006) Geology **34**, 257-260
[2] N.E. Timms et al. (2006) Geochemical Transactions **7**, 10
[3] N.E. Timms and S.M. Reddy (2009) Chemical Geology **261**, 11-23
[4] P.W.O. Hoskin and U. Schaltegger (2003). Reviews in Mineralogy **53**, 27-62
[5] J.M. MacDonald et al. (2015). Precambrian Research **260**, 55-75
[6] E.A. Belousova et al. (1998) Mineralogical Magazine **62**, 355-366
[7] J. Konzett et al. (2000). Contributions to Mineralogy and Petrology **139**, 704-719
[8] I. Cartwright and J.W. Valley (1992). Journal of the Geological Society of London **149**, 115-125
[9] J.W. Valley (2003) Reviews in Mineralogy **53**, 343-385.
[10] M. Marocchi et al. (2009) Mineralogy and Petrology **95**, 251-272
[11] T. Sekine and P.J. Wyllie (1982) Contributions to Mineralogy and Petrology **81**, 190-202
[12] J.H.F.L Davies and L.M. Heaman (2014) Precambrian Research **249**, 180-198
[13] U. Schaltegger et al. (2015) American Mineralogist **100**, 83-94
[14] H-Y. Li et al. (2016) Journal of Geophysical Research (Solid Earth) **121**, 687-712
[15] Y. Liu et al. (2009) Journal of Petrology **51**, 537-571
[16] P.B. Kelemen et al. (1990) Nature **345**, 521-524
[17] C. Münker et al. (2004) Earth and Planetary Science Letters **224**, 275-293
[18] M.F. Thirlwall et al. (1994) Journal of Petrology **35**, 819-838

Ion microprobe analysis of $^{18}O/^{16}O$ and $^{28}Si/^{30}Si$ in Cretaceous cherts

J. A. D. Dickson

Department of Earth Sciences, University of Cambridge, Cambridge CB2 3EQ, UK

Introduction

The proposed origins for chert are diverse and in many instances controversial. Attention has recently been focused on Cretaceous cherts from the large offshore hydrocarbon reservoirs of the South Atlantic where chert forms an important component of the reservoir rocks. The oxygen and silica isotopic composition of silica phases in these cherts provides an important monitor of the temperature, composition and origins of the fluids from which they precipitated.

The silica phases present in these cherts include intimately mixed chalcedony, quartzine, microquartz, and megaquartz. It is possible to isolate some but not all of these phases for separate analyses. Bulk analyses, however, inevitably homogenises the variations present in these silica varieties while ion microprobe analyses not only allows these phases to be separated but allows variation within them to be discerned [1].

Analyses and results

The spatial resolution afforded by the Ion probe is demonstrated by Figure 1 that show variation in the silica phases that could not be obtained by conventional bulk analyses.

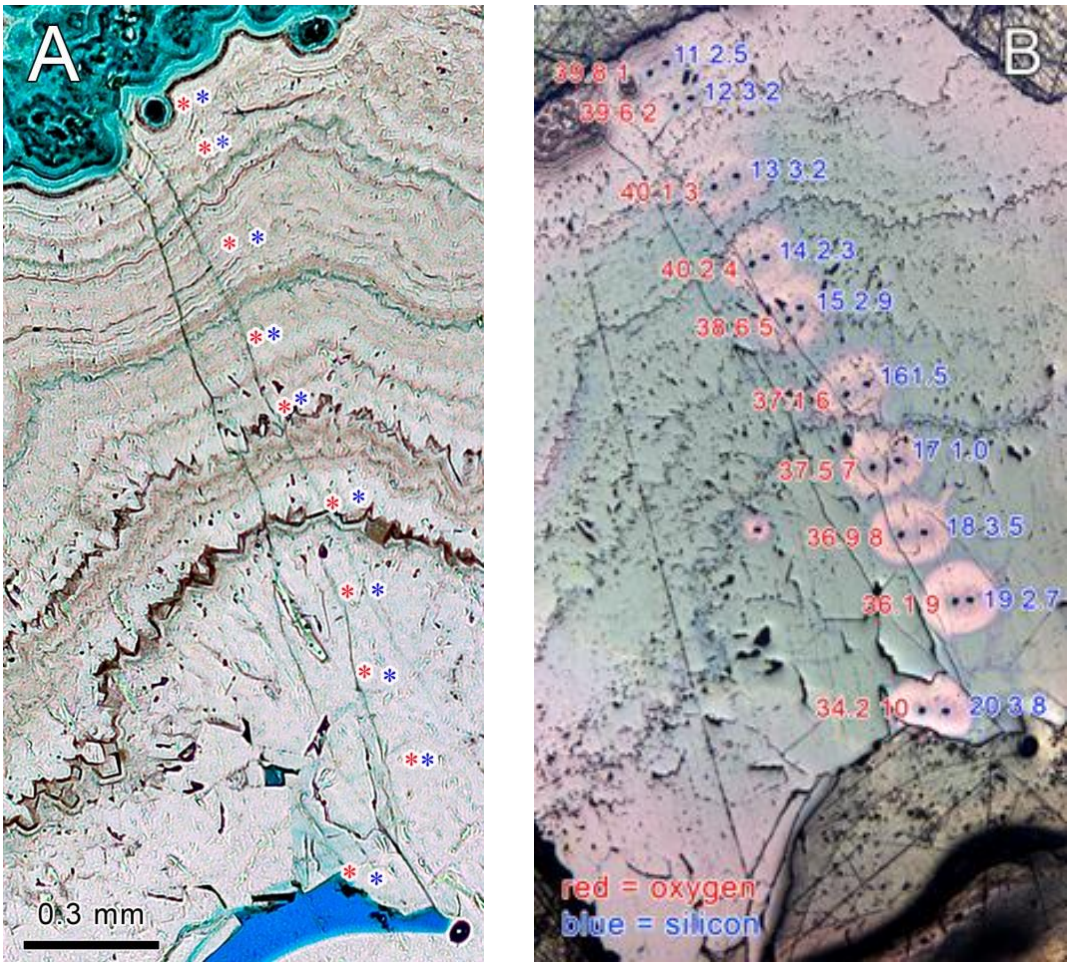

Figure 1. Colloform chalcedony at top, banded chalcedony center, mega quartz towards base and blue coloured pore at bottom. A. Transmitted light image, location of analysis spots B. Reflected light image taken after analyses, corners are composed of indium and analysis spots shown with data.

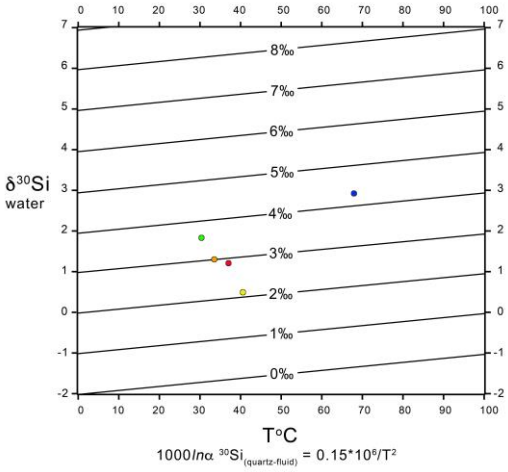

Figure 2. Graphical representation of equilibrium relationship between $\delta_{18}O$ value of water, temperature, and the $\delta_{18}O$ value of quartz using Ligang et al., equation [3]: the $\delta_{18}O$ means of the five silica type are plotted as colour coded dots, microquartz green, chalcedony brown, early quartz red, intermediate quartz yellow and mega quartz blue

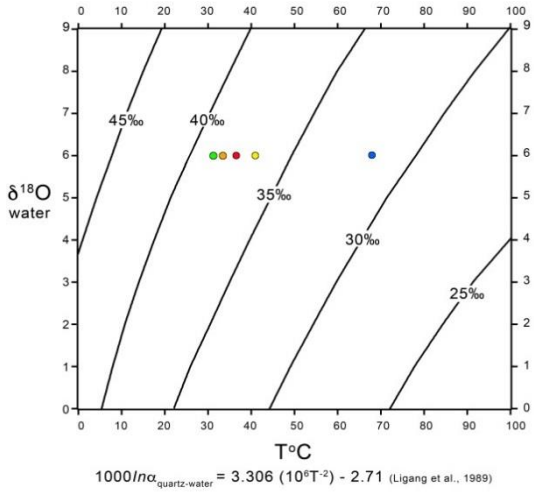

Figure 3. Graphical representation of equilibrium relationship between $\delta_{30}Si$ value of dissolved silica in water, temperature, and the $\delta_{30}Si$ value of quartz using Pollington et al. (2016) equation; the $\delta_{30}Si$ means of the five silica type are plotted as colour coded dots, microquartz green, chalcedony brown, early quartz red, intermediate quartz yellow and mega quartz blue

Conclusions

The exceptionally high $\delta^{18}O$ VPDB values from microcrystalline quartz forming the original framework of the cherts and early chalcedony cements are matched in published data only by analyses of Lake Magadi cherts [2]. The high $\delta^{18}O_{VPDB}$ values of microcrystalline quartz and chalcedony, if they were equilibrium precipitates and formed in highly evaporated waters such as found in African Rift Valley lakes (~ +7‰ $_{SMOW}$), indicates they were precipitated at temperatures ~ 30°C (Figure 2). The later mega quartz with lower $\delta^{18}O$ values if also precipitated from water of similar $\delta^{18}O_{SMOW}$ composition precipitated at temperatures ~ 65°C.

The ~2‰ difference in $\delta^{30}Si$ values between chalcedony and early microcrystalline quartz, and late megaquartz cement indicates a different source of silica (Figure 3).

The isotope data from the chert analysed in this study indicate they precipitated around 30°C from highly evaporated lake waters; they are not hydrothermal hot spring deposits. A paragenetic sequence thought the early silica cements show an ~ 3‰ decrease in $\delta^{18}O$ values; the late megaquartz has distinctly lower $\delta^{18}O$ ~32‰. The $\delta^{30}Si$ values of the early silica falls from an early value ~3.5‰ to 2.0‰; the late megaquartz reverses this trend, its $\delta^{30}Si$ value is ~ 4.2‰. The mega quartz cement precipitated last in the sequence of silica precipitates during burial and at a temperature that was perhaps applied by others to the early silica leading to their interpretation that they were high temperature hydrothermal deposit [5].

References

[1] A.Saller et al. (2016) AAPG Bulletin **100**, 1135-1164
[2] J.R.O'Neil and R.L.Hay.E. (1973) Earth Planetary Science Letters **19**, 257-266
[3] Ligand et al. (1989) Economic Geology, 84, 1643-1650.
[4] Pollington et al. (2016) Chemical Geology 421, 127-142.
[5] Poros et al., (2017) AAPG Search and discovery Article #51413.

U-Pb ages of Lewisian zircons – validation of previously contaminated analyses

S. Fischer[1], P. Cawood[1,2], C. Hawkesworth[1,3]

[1]School of Earth & Environmental Sciences, University of St Andrews, St Andrews KY16 9AL, UK
[2]School of Earth, Atmosphere & Environment, Monash University, Clayton Campus, Victoria 3800, Australia
[3]School of Earth Sciences, University of Bristol, Wills Memorial Building, Clifton BS8 1RJ, UK

Background of samples

Here we report results of U-Pb analyses on zircons obtained from high-grade mafic migmatitic orthogneisses, their leucosomes as well as meso-scale crustal melt bodies from the mainland Lewisian complex. The Lewisian complex in the NW of Scotland comprises Archaean and Palaeoproterozoic gneisses of predominantly tonalitic, trondhjemitic and granodioritic composition with minor mafic and metasedimentary units and has been subdivided into the granulite facies central region and the amphibolite facies northern and southern regions [1]. Finer subdivision into discrete blocks (interpreted as distinct tectonic terranes) has been based largely on U-Pb dating on zircons; the number and exact boundaries of these blocks is still subject to debate [e.g. 2, 3; and references therein].

To test the terrane model focussing on mafic lithologies and to understand the effect of partial melting of lower mafic Archaean crust on the geochemistry of zircon, we analysed zircons from melanosome and leucosome portions of mafic migmatites as well as cross-cutting felsic sheets from three separate localities: Cnoc Gorm within the Laxford shear zone, Scouriemore within the Assynt block, and Loch an Èisg Brachaidh within the Gruinard block.

Contamination of previous analyses

The zircons for which results are reported here had been previously analysed for oxygen isotopes, U-Pb isotope dating (both on the Cameca 1270) and trace element analyses (on the Cameca 4f). Results of these analyses were outlined in our 2016 EIMF report and are therefore not repeated here. One issue with these previous analyses, however, was a significant amount of common Pb, which is measured and detected as ^{204}Pb. Ideally, zircon should contain no detectable or only very low amounts (a few ppb) of ^{204}Pb. During the first round of analyses, all spots had ^{204}Pb concentrations of at least 10–15 ppb, with a median of values at ca. 15 ppb. Although significantly higher values probably indicate disturbance of the U-Pb system, these consistent contents of ca 15 ppb ^{204}Pb, including analyses on standard zircon 91500, were attributed to surface contamination introduced during polishing. Galena is present in one of the samples, and, although not actively picked, a grain may have been accidentally introduced to a mount or galena was present as secondary material in cracks of mounted mineral grains. During polishing on the same lap, this would then have been smeared onto all mounts. Although no untoward behaviour in the data was observed, a session to repeat the U-Pb analyses was scheduled at EIMF, the results of which are presented here.

Results

After trace element analysis (part of the initial analytical strategy), all mounts were cleaned by hand using ethanol and cotton wipe and then rinsed with distilled water and re-coated. Since the existing O/U-Pb/trace element pits were now too deep, and also likely filled with (potentially contaminated) material during cleaning, new spots were re-analysed close-by or within the same zonation (as identified in BSE/CL images).

This second session gave much better results. Common lead was absent or low in most spots that were previously around 10 – 15 ppb, with a median of all new analyses at 0.9 ppb. Previously high ^{204}Pb areas (i.e. > or >> 15 ppb) were largely still high (albeit lower than during the first session) and are therefore interpreted as genuinely disturbed portion of zircon, often close to cracks or in high-U, probably metamict, parts. Analysed ratios and calculated ages are generally within a few percent of previous analyses and ^{207}Pb/^{206}Pb-ratios of old versus new analyses correlate well (Fig. 1).

Considering the hypothesis of contamination with galena derived common Pb from within one of the samples, it is reasonable to use an old Pb isotopic composition for common Pb correction, as the galena would be fairly old, probably related to the ca 2.48 Ga Inverian event. Using old (2.5 Ga) instead of modern day Pb values in the corrections for common Pb yields better ^{208}Pb/^{206}Pb$_{predicted}$

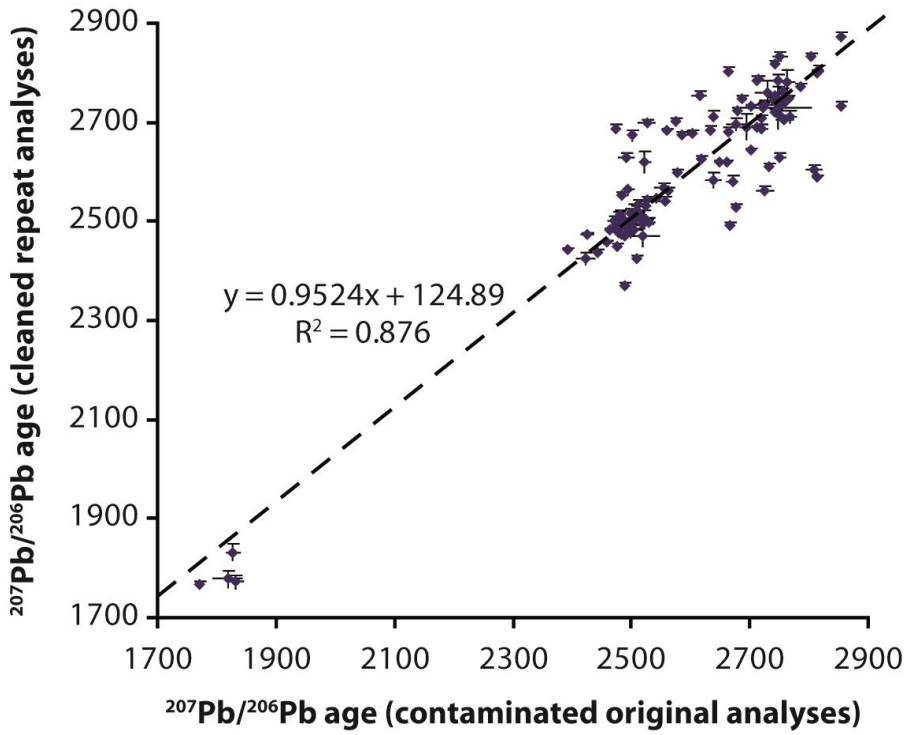

Figure 1. Comparison of original and repeat age analyses. Pairs that had one or both ages rejected on the basis of higher than threshold values for ^{204}Pb (see text for details) or discordance were removed. Also, three analyses with an obvious mismatch between the two ages were removed. 26 of the 125 pairs that have two usable ages have ages that are identical within 1σ.

versus $^{208}Pb/^{206}Pb_{measured}$ ratios (i.e. closer to 1), supporting this approach and suggesting that the Pb contaminant has indeed an old Pb isotope composition.

In cases where (a) original and repeat give the same age (either exactly or within error), (b) both analyses don't show any evidence of disturbance, and (c) the repeat is free of ^{204}Pb, the original analyses show contamination typically within the range of a few ppb (lowest value 2.6 ppb) up to about 20 ppb ^{204}Pb, but most commonly 10 – 15 ppb. In uncontaminated samples, ^{204}Pb contents of up to 10 ppb are typically acceptable as good data, provided no other proxy (e.g. discordance, more than 3 % common Pb correction, more than 10 % divergence of measured $^{208}Pb/^{206}Pb$ form the predicted ratio) indicates disturbance. Consequently, the contaminated data set can be considered to be of reliable quality where ^{204}Pb values are below ca 30 ppb, i.e. the sum of a generally acceptable ^{204}Pb content of ca 10 ppb plus the added surface contamination of up to 20 ppb (the latter value identified by comparison of the corresponding original, contaminated and repeat, uncontaminated analyses).

Conclusions

The results of the cleaned, previously common lead-contaminated, zircons presented here confirmed the data obtained from the same domains of the contaminated grains. This shows that, where a minor to moderate surface contamination is indicated by detection of ^{204}Pb on standard zircons known to be free of common lead (such as zircon 91500), the applied corrections account well for this contamination and data can be relatively confidently used despite the contamination. The repeat analyses were placed adjacent to, or within the same growth domain of, the previous analyses, which in turn were performed on the craters left by previous oxygen isotope analyses. The reproduction of ages within error shows that U-Pb isotope data from analyses on pre-existing SIMS pits, in this case from O isotope analyses, are not significantly affected by those analyses.

References

[1] Peach *et al.* (1907) Memoirs of the Geological Society; [2] P. Kinny & C. Friend (2005) Journal of the Geological Society, **162**, 175–186

Volatile contents of basaltic glass from the Galápagos Spreading Centre

M. Gleeson, S. Gibson & M. Stock

Department of Earth Sciences, University of Cambridge, Downing Street, Cambridge, CB2 3EQ, UK

Introduction

The Galapágos Archipelago is an archetypal example of the interaction of a deep-seated mantle plume with a nearby mid-ocean ridge [1,2,3]. Previous geochemical studies have shown that the isotopic variability exhibited by enriched, transitional and normal MORB from the Galapágos Spreading Centre (GSC; Figure 1)[4,5] is a consequence of melt contributions from three distinct components within the Galapagos mantle plume. By using analysis of volatile elements (H, F) in submarine basalts from the GSC we aim to: (i) quantify the volatile contents of these different mantle sources and (ii) gain a greater understanding of their origin and how plume-ridge interaction contributes to the global cycling of volatiles.

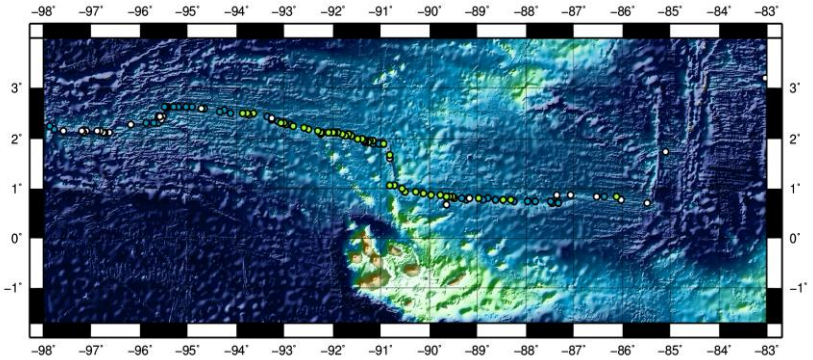

Figure 1. Location of enriched (green), transitional (blue) and normal MORB (white) samples along the GSC analysed for volatiles in this study and that of Cushman et al.[4]

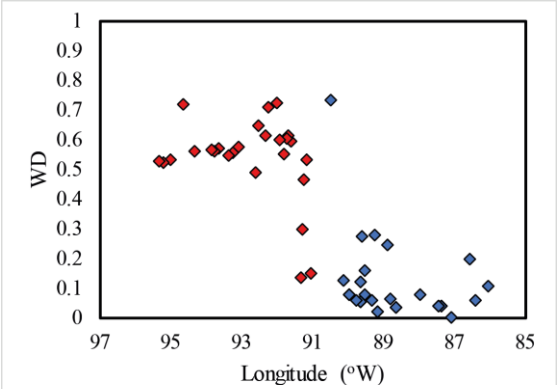

Figure 2 Relative contribution from the Wolf-Darwin mantle plume component to basalts erupted along the GSC

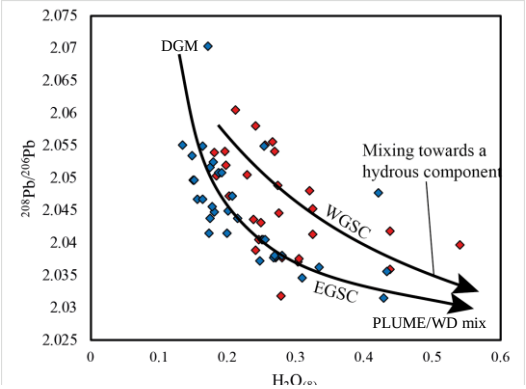

Figure 3 Mixing trajectories between hydrous and anhydrous mantle components along the Galapágos Spreading Centre.

Results

The results of our SIMS pilot project for basaltic glasses from both the western and eastern Galápagos Spreading Centre, together with previously published data from the western GSC of Cushman et al.[6], shows that H_2O and F concentrations are highest near the 91°W transform fault (Figure 2). This represents the closest point on the GSC to the mantle plume. H_2O correlates strongly with Ce (as suggested for other studies[5]) whereas F is strongly correlated with Nd. The concentrations of Cl are clearly influenced by varying degrees of assimilation of NaCl-rich brines.

Broad correlations between isotopic parameters and volatile concentrations in GSC basalts indicate that there is a volatile-rich component common to both the eastern and western GSC (Figure 3). However, our pilot project has revealed that key differences (e.g. variations in H_2O/Ce ratios) exist between the western and eastern segments that are not influenced by this common volatile-rich component. Mantle melting models involving both physical (e.g. rates of plume upwelling) and chemical parameters (mantle source compositions) will provide further insights into the volatile contents of the different mantle sources present along the ridge.

References

[1] Schilling J.G. et al. (1982) J Geoph Res **87** (B7); [2] Christie, DM et al. (2005) G^3 6(1); [3] Gibson SA et al. (2015) G^3 16 (5); [4] Schilling JG et al. (2003) G^3 4 (10); [5] Ingle S et al. (2010) G^3 11 (4); [6] Cushman B et al. (2004) G^3 5 (8)

[PAGE INTENTIONALLY LEFT BLANK]

Spatial variations in magmatic plumbing systems and the controls on magmatic volatile contents across the Galapagos archipelago

M. Gleeson[1], S. Gibson[1] & M. Stock[1]

[1]Department of Earth Sciences, University of Cambridge, Cambridge, CB2 3EQ, UK

CONTENT KEPT CONFIDENTIAL UPON AUTHORS' REQUEST

[PAGE INTENTIONALLY LEFT BLANK]

Tracking subduction dehydration and fluid-rock interaction in high-pressure metamorphic phengite using boron isotopes

R. Halama[1], M. Konrad-Schmolke[2] & J.C.M. De Hoog[3]

[1]School of Geography, Geology and the Environment, Keele University, Keele ST5 5BG, UK
[2]Department of Earth Sciences, University of Gothenburg, 40530 Gothenburg, Sweden
[3]School of GeoSciences, University of Edinburgh, Edinburgh EH9 3JW, UK

Introduction

Boron (B) isotopes have great potential to track water cycling and fluid-rock interaction in metamorphic rocks from subduction zone settings. The B stable isotope system is particularly useful for the investigation of sources and mechanisms of fluid-induced mass transfer in subduction zones because information from B as fluid-mobile trace element can be combined with B isotopic information [1]. In this study, we are investigating the boron concentrations and B isotope compositions of white mica, the major mineral host for boron and a phase that is stable over a wide range of temperatures and pressures in subduction-related metamorphic rocks [2]. We address the hypothesis that deeply subducted metamorphic rocks reflect dehydration in the down-going plate and evaluate the effects of subsequent fluid-rock interaction during exhumation in chemically overprinted samples that exhibit step-like compositional zoning in white mica.

Results

We analysed white mica from six high-pressure (HP) terranes that comprise various subduction-related metamorphic rocks (Fig. 1), including the Raspas Complex (Ecuador), the Franciscan Complex (California), the Münchberg Massif (Germany) and the Western Alps (Sesia Zone, Dora Maira UHP Unit, Lago di Cignana Unit). The samples represent a wide range of P/T conditions experienced by subducting plates.

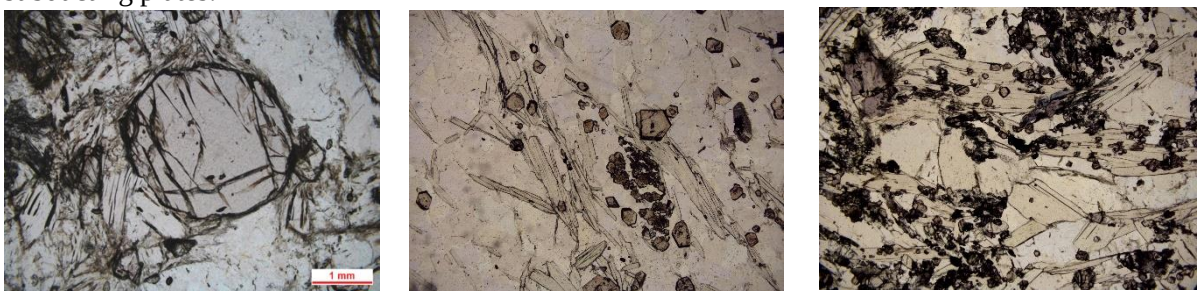

Fig. 1: Representative photomicrographs of white mica analysed in this study. Left: Pyrope quartzite from Dora Maira. Middle: Phengite-garnet quartzite from Lago di Cignana (image width is ~2 mm). Right: Eclogitic micaschist from the Sesia Zone (image width is ~4 mm).

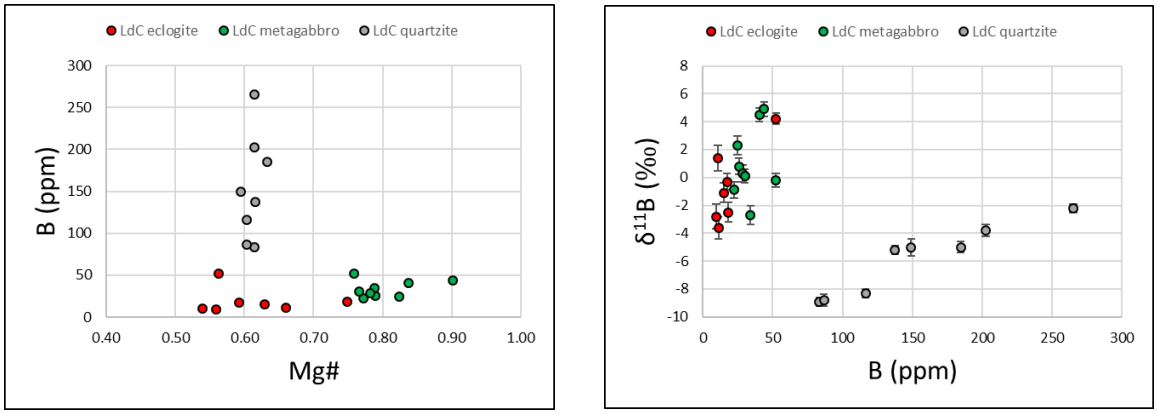

Fig. 2: Boron concentrations and B isotope composition of phengites from three different rock types of the Lago di Cignana area (Italy, Western Alps).

We first evaluate the effects of protolith composition by investigating 3 different rock types from the same locality (Lago di Cignana), which have experienced the same P/T evolution and the same peak P-

T conditions of 620 ºC and 2.8 GPa (Fig. 2). In the metabasic rocks, B contents in white mica are moderately low (10-50 ppm) and $\delta^{11}B$ value scatter between -4 and +4. In contrast, white mica from the quartzite has high B contents (up to 260 ppm) and shows a positive correlation between B and $\delta^{11}B$. These results highlight the influence of the protolith on the B elemental and isotopic signatures.

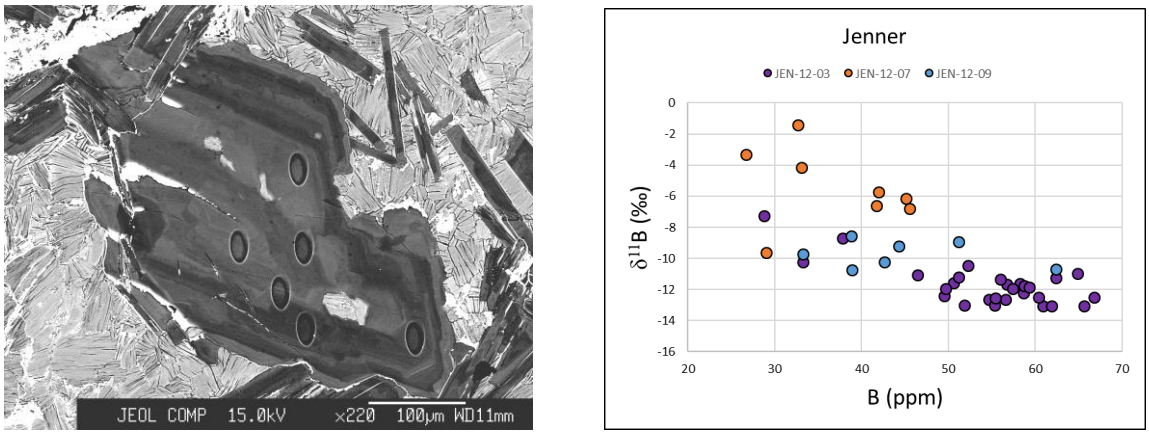

Fig. 3: Complex zoning in phengite from overprinted eclogite (back-scattered electron image) and boron data from Jenner (Franciscan Complex, California).

Metasomatic overprinting is particularly prominent in blueschists and eclogites from the Franciscan Complex (Fig. 3). White mica typically exhibits several chemically distinct zones, but there is no correlation of major element chemistry with $\delta^{11}B$. Overall, the samples show a negative correlation of $\delta^{11}B$ with B contents, suggesting that B with highly negative $\delta^{11}B$ was added via fluid-rock interaction during the retrograde overprint.

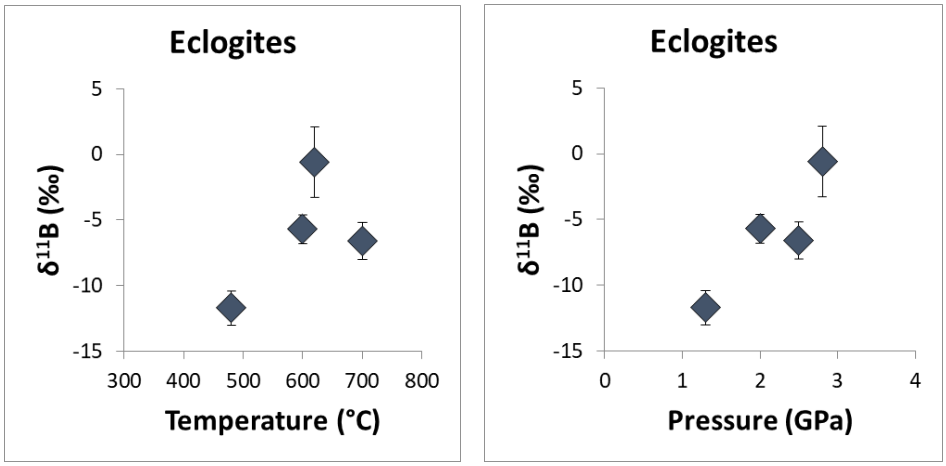

Fig. 4: Average B isotopic composition in phengites from eclogites that equilibrated at distinct pressure-temperature conditions.

Focusing on eclogites from 4 different localities, we can evaluate the relationship of B contents and $\delta^{11}B$ values with increasing depth in the subduction zone. The expectation was that B concentrations and $\delta^{11}B$ values in the residual rocks decrease with increasing degree of metamorphism. Our data show that all eclogites have negative $\delta^{11}B$ values, but only some fall outside the range of typical mantle values. There is no clear correlation of $\delta^{11}B$ with temperature and a positive correlation with pressure. Further work will evaluate whether these systematics are due to limited effects of dehydration on $\delta^{11}B$ due to high contents of stable phengite remaining in the rock and/or B isotopic re-equilibration on the retrograde P/T path.

References

[1] M. Konrad-Schmolke and R. Halama (2016) Lithos **208-209**, 393-414
[2] R.Halama et al. (2014) Geochimica et Cosmochimica Acta **126**, 475-494

Numerical constraints on Cambrian ocean temperatures

T. H. P. Harvey[1], T. W. Hearing[1,2], M Williams[1], S. E. Gabbott[1], P. R. Wilby[2] & M. J. Leng[3]

[1]School of Geography, Geology and the Environment, University of Leicester, Leicester, LE1 7RH, UK
[2]British Geological Survey, Keyworth, NG12 5GG, UK
[3]NERC Isotope Geoscience Facility, British Geological Survey, Keyworth, NG12 5GG, UK

CONTENT KEPT CONFIDENTIAL UPON AUTHORS' REQUEST

[PAGE INTENTIONALLY LEFT BLANK]

Calculating the initial H_2O and CO_2 contents of basaltic arc magmas using stable isotope fraction

E. C. Hughes[1], G. Kilgour[2], H. M. Mader[1] & J.D. Blundy[1]

[1]School of Earth Sciences, University of Bristol, Bristol BS8 1RF, UK
[2]Wairakei Research Centre, GNS Science, Taupo, New Zealand

Introduction

Melt inclusions (MIs) are tiny pockets of melt, trapped inside crystals as they grow from the magma, providing a unique insight into the pre-eruptive melt. The H_2O and CO_2 content of MIs are commonly analysed by SIMS to infer the initial volatile content of magmas and estimate the depth at which these MIs were trapped to help understand volcanic plumbing systems. Ideally, MIs quench to a glass upon eruption, providing a pristine record of the pre-eruptive melt, but there are various post-entrapment processes which can affect the volatile content of MIs. This is especially true in the case of H_2O, as H can diffuse quickly to re-equilibrate with changing conditions.

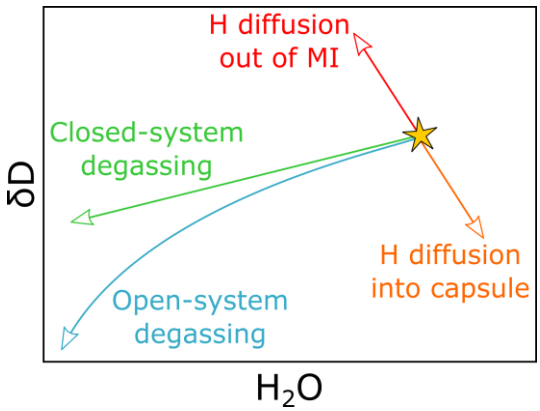

Figure 1. Schematic relationships between δD and H_2O for various processes that effect melt inclusions and experiments.

Hydrogen isotopes provide a method to try and unravel these processes and infer whether the H_2O content has been modified by post-entrapment processes (Figure ***1***). If they have retained their initial H_2O signature, H isotopes may also provide information about the degassing process (open vs. closed) and initial H_2O contents (Figure ***1***). Previous studies [1] have found that the H_2O fractionation factor between vapour and melt ($\Delta^{H2OT}_{v\text{-}m}$) is a function of H_2O content as the proportion of H_2O_{mol} and OH^- in the melt varies with H_2O_T. These fractionation factors have different signs ($\Delta^{H2Omol}_{v\text{-}m} < 0$, $\Delta^{OH}_{v\text{-}m} > 0$), although overall $\Delta^{H2OT}_{v\text{-}m} > 0$ resulting in an isotopically lighter melt [2].

Experimental glasses

To investigate the controls on H isotopes during degassing, experimental glasses were made in an internally-heated pressure vessel (IHPV – Leibniz Universität Hannover, Germany) at 1250 °C and 1, 3, 5 and 7 kbar using a basaltic glass composition with 0 – 5 wt% initial H_2O in Au-Pd capsules. The samples were analysed using a thermal conversion elemental analyser (TCEA – University of Oregon, USA) to obtain the bulk glass H_2O and δD to compare to SIMS analysis. H_2O was estimated using the H^+/H_2^+ ratio as the background was low enough for this relationship to be used as glass chips were mounted in indium. SIMS and TCEA measurements agree well for H_2O and δD, although variations in glass composition did slightly affect the SIMS measurements of δD (Figure *2*).

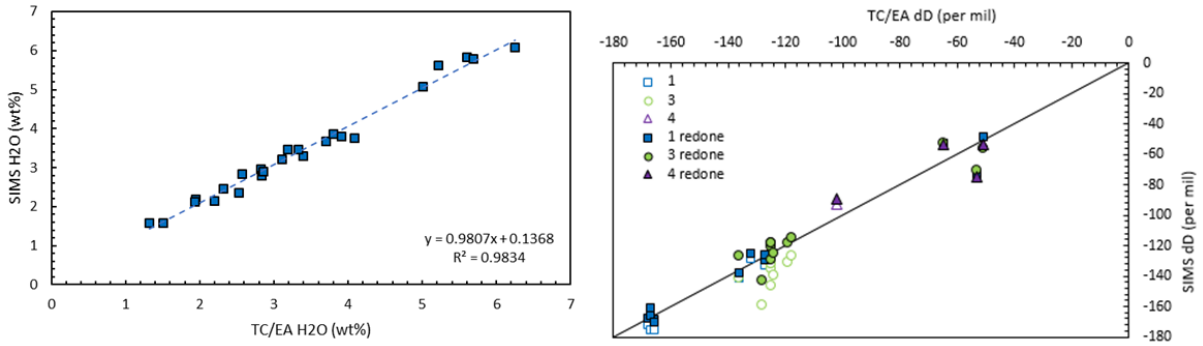

Figure 2. SIMS against TCEA H_2O (left) and δD (right). For δD open symbols are where three independent glasses were used for calibration and closed symbols where the experimental glasses were used for calibration.

Unfortunately, H diffused into the capsule during experiments meaning that the experiments were not a closed system to H_2O and δD is affected by both diffusion and degassing. δD is influenced by capsule size as surface area to volume ratio is important, therefore δD becomes lighter with decreasing capsule size (Figure 3). Excluding the 5 kbar data (green) (and for a single capsule size): at a specific pressure, δD becomes heavier with increasing H_2O; for an initial H_2O content, δD becomes lighter with decreasing pressure; and δD becomes heavier with increasing CO_2 (Figure 3). This is contrary to previous experimental data on closed-system degassing which found that the melt gets lighter with progressive degassing (Figure 1). Either these relationships are simply due to H diffusion into the capsule during the experiment or CO_2 may have an important effect on the fractionation factor.

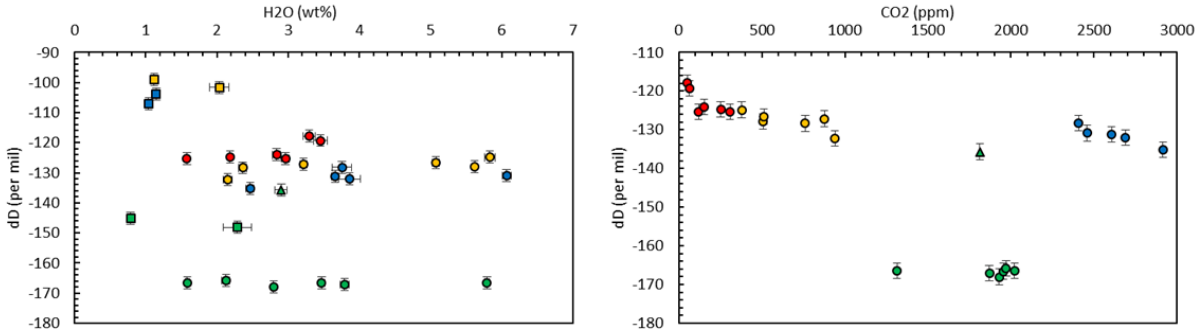

Figure 3. δD against H_2O (left) and CO_2 (right) where symbol colour indicates pressure (red = 1, yellow = 3, green = 5, blue = 7 kbar) and shape indicates capsule size (triangle = large, square = medium, circle = small).

Melt inclusions

Olivine- and pyroxene-hosted melt (and some matrix glass) from Etna (Italy), Rangitoto (New Zealand), Stromboli (Italy) and Yasur (Vanuatu) were also analysed. Stromboli and Yasur may have suffered H diffusion out of the melt inclusion, although the values at Yasur are within the range found at Aoba, Vanuatu [3]. Etna and Rangitoto may be showing a combination of degassing and H diffusion but there is significant scatter in the data. Further data will be collected on these melt inclusions (e.g., size, CO_2, $\delta^{13}C$, major/minor element composition, Fe^{2+}/Fe_T, etc.) to understand the results fully.

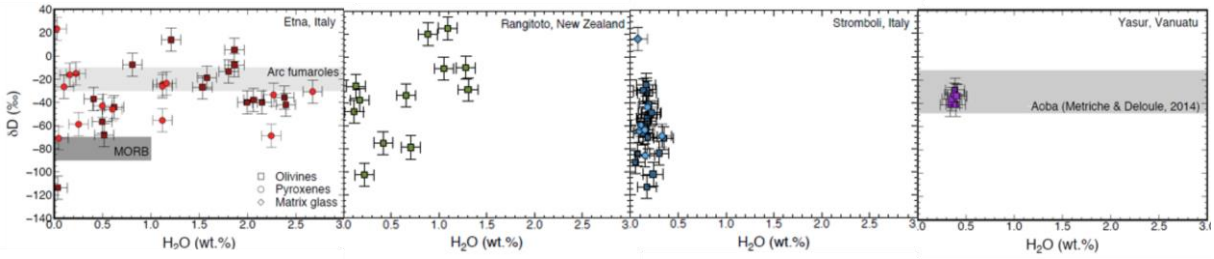

Figure 4. δD against H_2O for olivine- and pyroxene-hosted melt inclusions (and matrix glass) from (left to right) Etna, Italy; Rangitoto, New Zealand; Stromboli, Italy; and Yasur, Vanuatu.

References

[1] F. Pineau et al. (1998) Chemical Geology **147**, 173-184
[2] J.C.M. De Hoog et al. (2009) Chemical Geology **266**, 256-266
[3] N. Métrich & E. Deloule (2014) Lithos **206-207**, 400-408

Halogen behaviour within peralkaline magmas and the implications for REE transport and concentration

F. Iddon & M. Edmonds

Earth Sciences, University of Cambridge, CB2 3EQ, UK

Introduction:

Economic deposits of Rare Earth Elements (REE) are not common, however industrial demand has been rapidly increasing. Carbonatite and peralkaline igneous complexes are the primary sources of REE, as well as other key trace metals. Defined as having an excess of alkalis with respect to aluminium, peralkaline systems commonly occur in areas undergoing continental rifting, such as the active Main Ethiopian Rift (MER) (Fig. 1). Alkali-related volatile retention during fractionation, leads to enrichment and late exsolution of F and Cl in peralkaline residual fluids. It has been shown that REE partition strongly into these halogen-rich fluids under magmatic conditions, particularly due to alkalis and F delaying crystallisation of phases such as zircon, that preferentially allow REE into their structures. However, beyond a very limited number or experimental studies published in the 1990s, there has been little attempt to observe F, Cl and REE behaviour in natural peralkaline systems and information about magmatic volatiles in continental rift settings is limited.

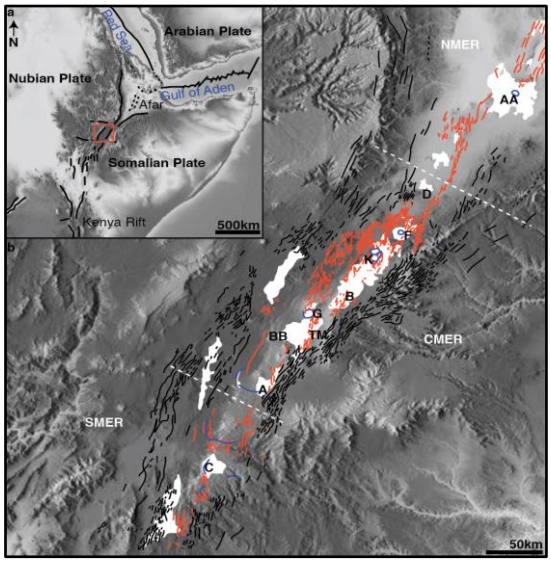

Above, figure 1: Map showing the MER, a northerly segment of the EARS (Inset). Peralkaline calderas are outlined in dark blue, with their deposits highlighted in white. The red lines represent the Wonji Fault Belt, the black lines represent the older border faults. K= Kone and A= Aluto.

Strategy:

Phenocrysts of quartz and olivine were picked from crushed fractions of samples from Aluto and Kone volcanoes in the MER (Fig. 1). The samples were all scoria or pumice, chosen to minimise the effect of volatile loss from the crystal-hosted melt inclusions. Crystals with melt inclusions were polished then mounted in epoxy for volatile and trace element analysis using Secondary Ion Mass Spectrometry (SIMS) at the University of Edinburgh. Matrix glass fragments were also analysed for comparison. Melt inclusions and matrix glass were then analysed for major elements using electron microprobe at Cambridge.

Results and Discussion:

The quartz-hosted melt inclusions show extreme halogen enrichment with up to 9500 ppm F and 3600 ppm Cl, this is correlated with melt evolution, displayed by a positive relationship with SiO_2 and highly incompatible Zr (Fig. 2). These high values likely reflect protracted fractional crystallisation, initial starting halogen content also appear to be high (Fig. 2). The matrix glasses typically show slightly lower halogen contents, indicating removal during late stage exsolution. The disparity between melt inclusion and matrix glass concentrations is more extreme in the F data, with a sizable population of very F-rich melt inclusions causing this skew (Fig. 2). The behaviour of the REE mirrors these trends, with a

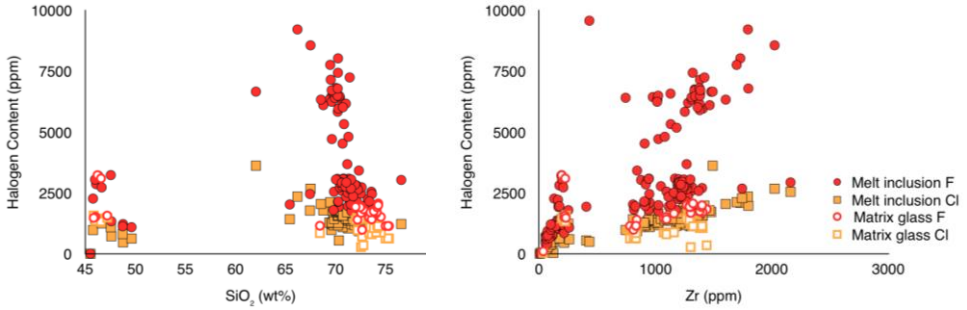

Figure 2: Halogen content in melt inclusions and matrix glass against SiO_2 (top) and Zr (bottom).

positive correlation between both LREE and HREE with SiO_2 and Zr (Fig. 3). HREE show lower enrichment and concentrations do not increase at the same rate as the LREE (Fig. 3). Again, matrix glasses typically show slightly lower values, this might suggest a degree of partitioning into halogen-rich fluids. There is a strong correlation between halogen and REE contents. The correlation appears stronger with Cl as the very F-rich melt inclusions do not display similarly higher REE contents (Fig. 4). Cl/F and LREE/HREE ratios show a weak positive correlation (Fig. 5) that may indicate preferential coupling of Cl and LREE behaviour, and F and HREE behaviour as predicted by experimental work [1-2].

Water contents were also analysed, showing that these peralkaline melts are very hydrated. Quartz and alkali feldspar-hosted melt inclusions recorded up to 8 wt% H_2O (Fig. 6). Olivine-hosted melt inclusions recorded up to 2 wt% H_2O in the mafic melts analysed (Fig. 6). There is no clear correlation between H_2O and the halogens, or the REE. Halogens and REE remain at high concentrations as H_2O is steadily lost, showing how late stage any exsolution must occur. The relationship between H_2O and CO_2 saturation has been used to make estimates of magma storage depths. The evolved peralkaline magmas at Aluto were likely stored at depths of up to 10 km (Fig. 7), slightly deeper than suggested by RhyoliteMELTS modelling [3] and at the deeper end of geophysical estimates [4].

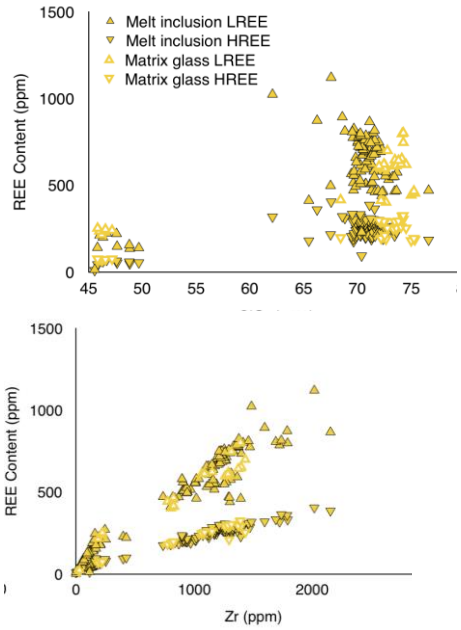

Figure 3: ΣREE content in melt inclusions and matrix glass against SiO_2 (left) and Zr (right).

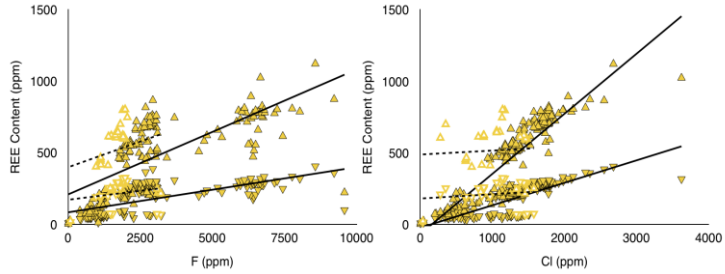

Figure 4: REE content in melt inclusions and matrix glass against F (left) and Cl (right). Solid lines show best fit linear regressions for melt inclusion data, dashed lines show best fit linear regressions for matrix glass data.

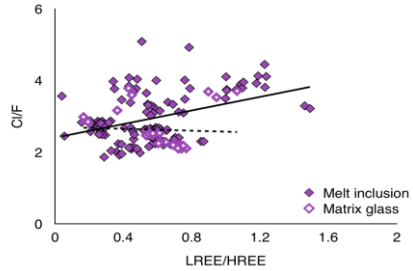

Figure 5: Cl/F against LREE/HREE. Solid lines show best fit linear regressions for melt inclusion data, dashed lines show best fit linear regressions for matrix glass data.

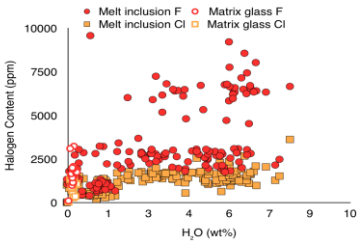

Figure 6: H_2O content in melt inclusions and matrix glass against halogen contents.

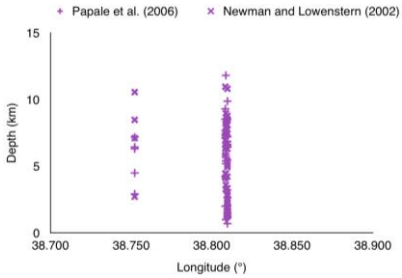

Figure 7: Plot showing estimates of magma storage depth at Aluto volcano based on H_2O and CO_2 saturation using both the methods described in Papale et al. (2006) and Newman and Lowenstern. (2002).

References

[1] Flynn and Burnham (1978) Geochim Cosmochim Acta 42, 679-684; [2] Kerrich and Fryer (1979) Can J Earth Sci 16, 440-458; [3] Gleeson et al. (2017) J Volc Geotherm Res 337, 44–61; [4] Wilks et al. (2017) J Volc Geotherm Res 340, 52–67.

Pilot K-Ca dating study of K-feldspar

S.P Kelley & R.W. Hinton

School of GeoSciences, University of Edinburgh, Edinburgh EH9 3JW, UK

Overview

This report is the result of a one day pilot study to test the application of K-Ca dating to K-feldspar using a gem quality sample of known age. ^{40}K undergoes a branched decay to ^{40}Ar (10%) and ^{40}Ca (90%) giving rise to K-Ar and K-Ca decay schemes. Measurement of $^{40}K/^{40}Ca$ for geochronology is difficult as the parent and daughter share the same mass and so cannot be measured without chemical separation and separate measurement. This has previously been very challenging, so the K-Ca system has rarely been applied as a geochronometer, despite interest in the system going back many decades.

Recent innovative work using the Cameca 1270 Ion Probe in Edinburgh by Richard Hinton has developed a technique to determine K-Ca dates from individual ion beam spots. Richard and myself used a one day pilot study to assess the capability to measure K-Ca ages on a homogeneous gem quality sample. Our motivation was to demonstrate the capability and compare the results of K-Ca spot age determinations with millimetre scale age/diffusion profiles for K-Ar ages measured in the same grain using a UV laser ablation noble gas mass spectrometry technique that I have already published [1]. We hoped to demonstrate both reproducibility but also capability to measure small K-Ca age variations and use the comparison to estimate relative closure temperatures for the two systems. The potential for K-Ca dating may have applications in several areas including subduction zones, authigenic overgrowths and extra-terrestrial samples.

Analyses

The pilot study was undertaken in October 2017 and all analyses were undertaken by Richard Hinton assisted where possible by Simon Kelley. The beams measured were $^{40}K^{2+}$, $^{40}Ca^{2+}$, $^{42}Ca^{2+}$ $^{44}Ca^{2+}$, ^{28}Si and $^{41}K^{+}$. Klokken (1.2Ga) K-feldspar was used as comparison although the Itrongay K-feldspar proved to be as stable as the standard with very low 'common calcium' Ca contents, yielding $^{40}Ca/^{44}Ca$ as high as 350 which is remarkably radiogenic for the technique. All signals increased with time but were mitigated by measuring ratios of K, Ca and Si to monitor fractionation. Given that there is a large (5mm sq) polished surface on the gem quality Itrongay K-feldspar it may a good standard for the future.

Over 20 spots were analysed varying the conditions and acquisition to optimise the data. Following optimisation we acquired a profile of ages from the grain edge to the core over a distance of around 2mm. The data indicated an age of 480±10Ma (Figure 1), within errors of earlier TIMS measurements of Itrongay feldspar K-Ca age. The $^{40}Ca/^{44}Ca$ intercept was close to 47.1 as expected, confirming the approach and low 'common calcium' values.

Outcomes

The results of the pilot study indicate that K-feldspar K-Ca ages can be very stable and reproducible and that the closure temperature is significantly higher than the K-Ar system, in contrast to work on biotite which indicates a K-Ca closure similar or lower than K-Ar. The pilot data were incorporated into a NERC proposal submitted in January 2018 (outcome awaited). The proposal was led by Craig Storey in Portsmouth (who had earlier used the Edinburgh Ion Probe to analyse biotite) and included Edinburgh and the Open University. The work has also led to a second day of pilot data funded by Edinburgh University to analyse muscovite, again comparing diffusion/age profiles to estimate closure temperatures.

We will report the outputs from both K-feldspar and Muscovite studies at the Goldschmidt conference in Boston in August 2018 [2]. We hope to acquire sufficient K-feldspar and muscovite data for an initial paper which will be the first inter-comparison and will lead to future proposals for funding to pursue applications such as dating authigenic K-feldspar overgrowths.

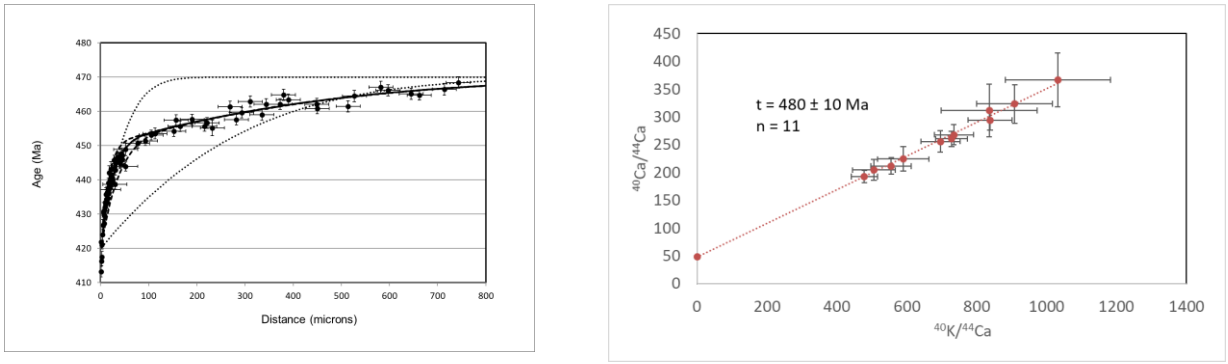

Figure 1. On the left: Ar-Ar Age profile illustrating 50Ma age variations from the grain edge to the core over 800 microns. On the right: An Isochron diagram illustrating pilot data acquired on the Cameca 1270 instrument in October 2017. Note that there is little age variation in K-Ca as indicated by the Isochron and that the age is at the top end of that indicated by Ar-Ar profile.

References

[1] S. Flude et al. (2014). Geological Society Special Publication. Advances in $^{40}Ar/^{39}Ar$ Dating: from Archaeology to Planetary Sciences 378, 265-275.

[2] S.P. Kelley et.al. (2018) Infering Diffusion rates and closure K-Ca dating of micas and K-feldspar. Abstract Goldschmidt, 2018, Boston.

A role for biogenic sulfur in fixing precious metals in layered intrusions?

A.P. Kelly & B. O'Driscoll

School of Earth and Environmental Sciences, University of Manchester, Oxford Road, Manchester M13 9PL

Introduction and background

Base-metal sulfides play a key role in controlling platinum-group element (PGE) enrichments in basaltic magma chambers. However, there are open questions surrounding the source of the S that 'fixes' the precious metals in these important ore deposits. Some classic models invoke a high-temperature (magmatic) origin, with segregation of the sulfide from the magma as immiscible droplets following magma fractionation, or mixing with magma of a different composition. However, another proposed mechanism involves the assimilation of S-rich country (sedimentary) rocks into the magma chamber, forcing sulfide liquid saturation and unmixing. The S isotope system is a potentially powerful tool for assessing magma-crust interactions. In particular, the involvement of significant amounts of crustally-derived S, as sulfide or sulfate, should be manifest in the $\delta^{34}S$ (general form: $([^{34/32}S_{Sample}/^{34/32}S_{Standard} - 1])*1000$) isotopic composition in terms of its deviation from 0 ±2‰ (the range representative of mantle-derived S). The ~60 Ma Rum layered intrusion (NW Scotland) is a useful locality to examine the role of crustal contamination in providing the S for PGE-enrichment in magmatic environments. It contains chromitite seams that are enriched to ppm levels in Pt and Pd[1]. At the level of emplacement of the Rum intrusion, a sequence of Mesozoic rocks crop out including Jurassic mudstones characterised by relatively light $\delta^{34}S$ (i.e., -33.8 to -14.7‰), as well as Proterozoic sandstones that have a $\delta^{34}S$ range of +1.4 to +4.7‰[2]. A number of studies have reported isotopically light bulk rock $\delta^{34}S$ compositions for various igneous rocks associated with the Rum intrusion[1]. For example, a sulfide-bearing troctolite in the lower portion of the layered intrusion has been reported to have $\delta^{34}S$ as low as -14.8‰[2]. A satellite peridotite plug to the north of the layered intrusion has also been documented with relatively light $\delta^{34}S$ (-18.3‰)[2]. In both of these cases, assimilation of Jurassic mudstones has been implicated as the driver for sulfide saturation and ^{32}S enrichment. However, S isotope compositions have not previously been reported for the Rum PGE-rich chromitite horizons.

Objectives and sample details

The primary aim of this study is to elucidate the role of sedimentary-derived S in driving sulfide saturation in the Rum magmas, as well as investigate the length-scales over which S isotope heterogeneity, if present, occurs in Rum sulfide-bearing cumulates. A corollary aim is to assess whether or not formation of specific base-metal sulfide phases has exerted a control on S isotope fractionation[3]. In order to achieve these goals, we employed secondary ionisation mass spectrometry (SIMS) to measure the S isotope compositions of individual sulfides in the rocks described above. One of the samples studied is the ~2 mm thick Unit 7-8 chromitite, reportedly the most PGE-enriched material on Rum[1]. Although sulfide grains in the peridotite and troctolite samples studied are on the order of 300-500 µm in diameter (**Figs. 1a,b**), the Unit 7-8 chromitite sulfides are <30 µm in size. All of our sulfide analyses are considered to be 'primary', i.e., away from areas of alteration or grain edges. The sulfides are predominantly pyrrhotite, pentlandite or chalcopyrite. In all samples, sulfides occur both as single-phase anhedral grains or composite blebs (**Fig. 1**).

Results and preliminary interpretations

Our data reveal significant isotopic disequilibrium in all of the samples studied, preserved at length-scales of several centimetres to tens of microns (**Fig. 1**). In the satellite plug, a range of $\delta^{34}S$ of -15.2 – -5.3‰ is measured in a sample area of ~5 cm^2. In the sulfide-bearing troctolite in the layered intrusion, a range of -12.7 – -3.5‰ is revealed over an area of ~3 cm^2. In the Unit 7-8 chromitite, where Pt+Pd abundances total ~3.5 ppm, we find a range of >10‰ $\delta^{34}S$ (-4.3 – +5.9‰) in an area of <1 cm^2. The isotopic heterogeneity present in the satellite plug and the troctolite points to the involvement of a country rock assimilant in driving sulfide saturation. However, the sub-mm length-scales over which $\delta^{34}S$ variations occur suggest that a secondary alteration mechanism (S loss, degassing) cannot be completely ruled out. It is difficult to explain the chromitite seam $\delta^{34}S$ values by country rock assimilation – no country rocks with $\delta^{34}S > +4.7$‰ have been reported from Rum. Loss of S (as SO_2 or H_2S) cannot easily explain fractionations of up to +6‰ $\delta^{34}S$ in the residual sulfide by Rayleigh

fractionation either. In order to explain the range of chromitite $\delta^{34}S$ values, we are investigating the possibility that the Rum parental magmas may have been derived from sub-continental lithospheric mantle with relatively heavy $\delta^{34}S$ compositions. Loss of SO_2 from the resultant sulfide liquid fraction would then drive $\delta^{34}S$ to relatively light values[4]. At the liquidus temperatures of the parental melts (~1300°C), much or all of the S present would need to be lost to account for the fractionation observed (down to -4.3‰). Given that appreciable (albeit accessory) quantities of sulfide remain in the chromitites, it might be more likely that S loss occurred at <800°C, perhaps in conjunction with crystallisation of the base-metal sulfides, when only 40-50% of the S budget would need to be lost as SO_2. In addition to providing new constraints on the grain-scale distances over which S isotope heterogeneity occurs in the Rum PGE-rich chromitites, our $\delta^{34}S$ data hint at a potentially important postcumulus phase of degassing that may have been responsible for producing the rich and diverse platinum-group mineral assemblage in these rocks.

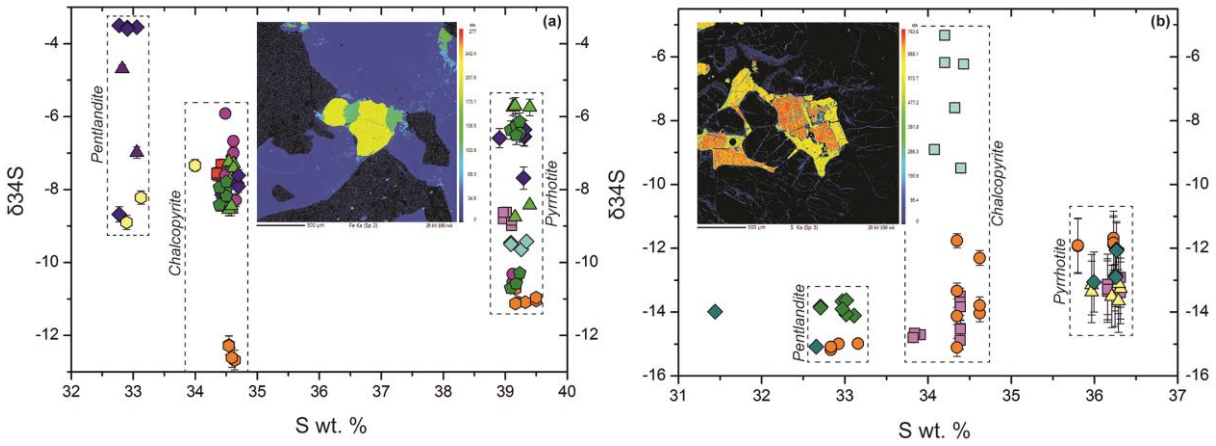

Figure 1. $\delta^{34}S$ versus S concentration (wt.%) for sulfides from the troctolite (a) and the peridotite plug (b). Pentlandite, chalcopyrite and pyrrhotite data are shown for each sample (labelled). In each plot, symbols of the same colour/shape represent measurements from the same sulfide grain. Many grains are composite, containing two or even three phases. In (a), 11 separate sulfide grains are represented and in (b), 6 sulfide grains are represented. Inset in each plot illustrates an element map of an example composite grain from each sample, in (a) Fe map with pyrrhotite (yellow) and pentlandite (green) and (b) S map with a pyrrhotite core (red) and a chalcopyrite/pentlandite rim (yellow). In some cases $\delta^{34}S$ uncertainties are smaller than the symbol height so are not visible.

References

[1] B. O'Driscoll et al. (2009) Earth and Planetary Science Letters **286**, 41-51
[2] M.R. Power et al. (2003) Geological Magazine **140**, 499-512
[3] C. Laflamme et al. (2016) Chemical Geology **444**, 1-15
[4] E.M. Ripley et al. (2003) Geochimica et Cosmochimica Acta **67(15)**, 2805-2817.

Appendix: analytical procedure, data processing and standards

Sulfur isotope measurements were carried out using the Cameca 1270, on polished mounts that each included standard grains of pyrite (Sierra), pyrrhotite (Alexo), chalcopyrite (Nifty) and pentlandite (VMSO)[3]. Negative secondary ions were produced by a 2.6 nA, 10 kV, Cs^+ primary beam of ~1 µm diameter. A pre-analysis sputter time of 60 s in spot mode was used to remove surface contamination. The average drift-corrected external precision ($\delta^{34}S$, based on the standard error of the mean) on standards Sierra, Alexo, VMSO and Nifty, over a 5 day analytical campaign, was ±0.06‰, ±0.11‰, ±0.03‰ and ±0.04‰, respectively. The 2σ analytical uncertainty (*AU*) was calculated by combining the drift-corrected standard measurement for a given day with the uncertainty on the individual measurement in question, using the following equation:

$$AU = \sqrt{\left(\frac{SEM(std\ measurement)}{\delta 34S(std\ measurement)}\right)^2 + \left(\frac{SEM(sample\ measurement)}{\delta 34S(sample\ measurement)}\right)^2}$$

Are Stromboli melts supersaturated with respect to carbon dioxide?

E. Liu[1], M. Edmonds[1] & B. Houghton[2]

[1]Department of Earth Sciences, University of Cambridge, Cambridge CB2 3EQ, UK
[2]University of Hawaii, Honolulu, Hawaii, 96822

Motivation and hypothesis

Melt inclusion arrays are mixtures of diverse melts, with variable amounts of fractionation and degassing occurring during magma ascent and storage (e.g., [1]). Melt inclusions from Skuggafjoll, Iceland [2] suggest that geochemically "depleted" melts (arising from larger degrees of mantle melting) rising rapidly through the crust may become supersaturated with respect to CO_2, corroborating experimental results that suggest CO_2 supersaturation can occur at even modest decompression rates [3]. Furthermore, trace element variability in Skuggafjoll melt inclusions can be explained by mixing between depleted supersaturated melts and degassed enriched melts. Thus, correlations between CO_2 and measures of trace element enrichment (e.g. Ce/Y, Nb) indicate that magma mixing can be an important control on melt inclusion volatile compositions [2]. This interpretation challenges the long-held view that melt inclusion H_2O-CO_2 concentrations reflect the equilibrium conditions of entrapment and has implications for the use of CO_2-H_2O systematics of melt inclusions to estimate entrapment pressures (e.g. [4]).

We hypothesise that paroxysmal eruptions at Stromboli, Italy, are fed by rapidly ascending melts that become supersaturated with respect to CO_2, delaying degassing to low pressures. However, the co-eruption of both crystal-rich scoria and vesicular pumice attests to magma mixing [5,6]. To test our hypothesis, and deconvolve the effects of magma mixing and degassing in controlling measured CO_2, olivine crystals in bomb samples from the paroxysmal activity at Stromboli during April 2003 were selected to investigate the volatile-trace element systematics.

Methods

Olivine macrocrysts in the size range 0.5–2 mm were hand-picked from a crushed scoria bomb, mounted in epoxy resin, and polished to expose glassy melt inclusions. Only bubble-free inclusions were selected for further analysis. Volatile (CO_2, H_2O) and rare earth elements (REEs) were analysed by secondary ion mass spectrometry (SIMS) using the Cameca ims-4f at the University of Edinburgh. Following SIMS, major and volatile (S and Cl) elements in the same inclusions were measured by electron microprobe (EPMA) using the Cameca at the University of Cambridge. The composition of the host olivine was measured immediately adjacent to the analysed inclusions. In total, 58 melt inclusion glasses and 7 matrix glasses were analysed by both SIMS and EPMA.

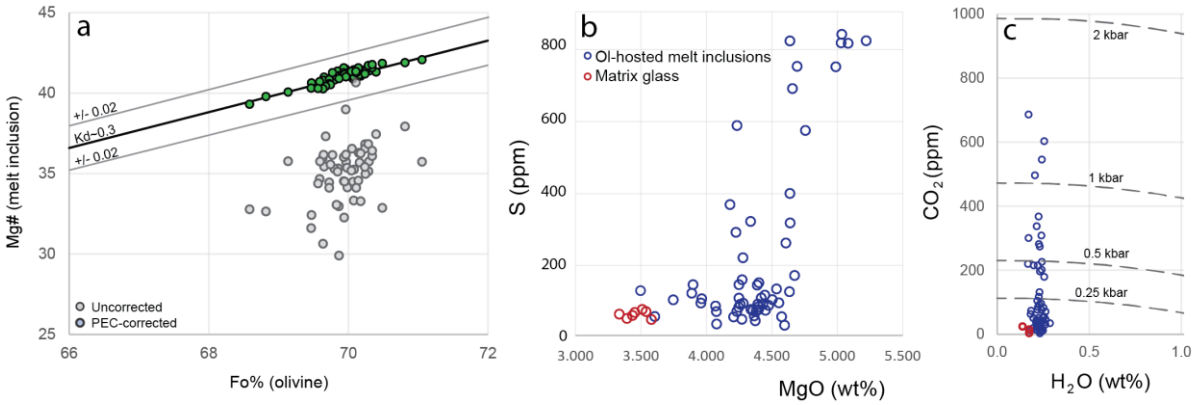

Figure 1: (a) Host olivine forsterite content versus melt inclusion Mg# before (open circles) and after (green filled circles) post-entrapment crystallisation (PEC) correction. PEC corrections were performed by incremental addition of the host olivine composition to the inclusion composition until reaching an equilibrium $Kd^{ol\text{-}liq}_{Fe\text{-}Mg}$ value of 0.30 [6]; (b) S contents of olivine-hosted melt inclusions (blue symbols) and matrix glasses (red symbols) as a function of MgO wt%; (c) H_2O and CO_2 contents of melt inclusions and matrix glasses overlain by isobars calculated using SolEx [4].

Results

Melt inclusions (MIs) are hosted in relatively Fe-rich olivines (Fo = 70.0 ± 0.4 mol%). Minor post-entrapment crystallisation corrections of 0.5 to 6.0% were required to bring the MIs into equilibrium with their host crystal. MI glasses are shoshonitic (highly potassic basaltic melt) in composition, and are almost indistinguishable in both major and trace elements from the matrix glass. PEC-corrected CO_2 contents in the MIs range from < 25 ppm (detection limit of SIMS analyses) to 506 ppm. H_2O contents are homogeneous with an average of 0.25 ± 0.13 wt% (Fig. 1c).

Elements that are incompatible during mantle melting (e.g., Ba, Nb, Nd, Zr) and REEs are strongly correlated with each other (Fig. 2a), and with minor incompatible elements measured by EPMA (e.g., P_2O_5). CO_2 is moderately positively correlated with Sr (r=0.6), and weakly with Sc and Y (r=0.35). CO_2 and Nb are weakly negatively correlated (r= -0.35).

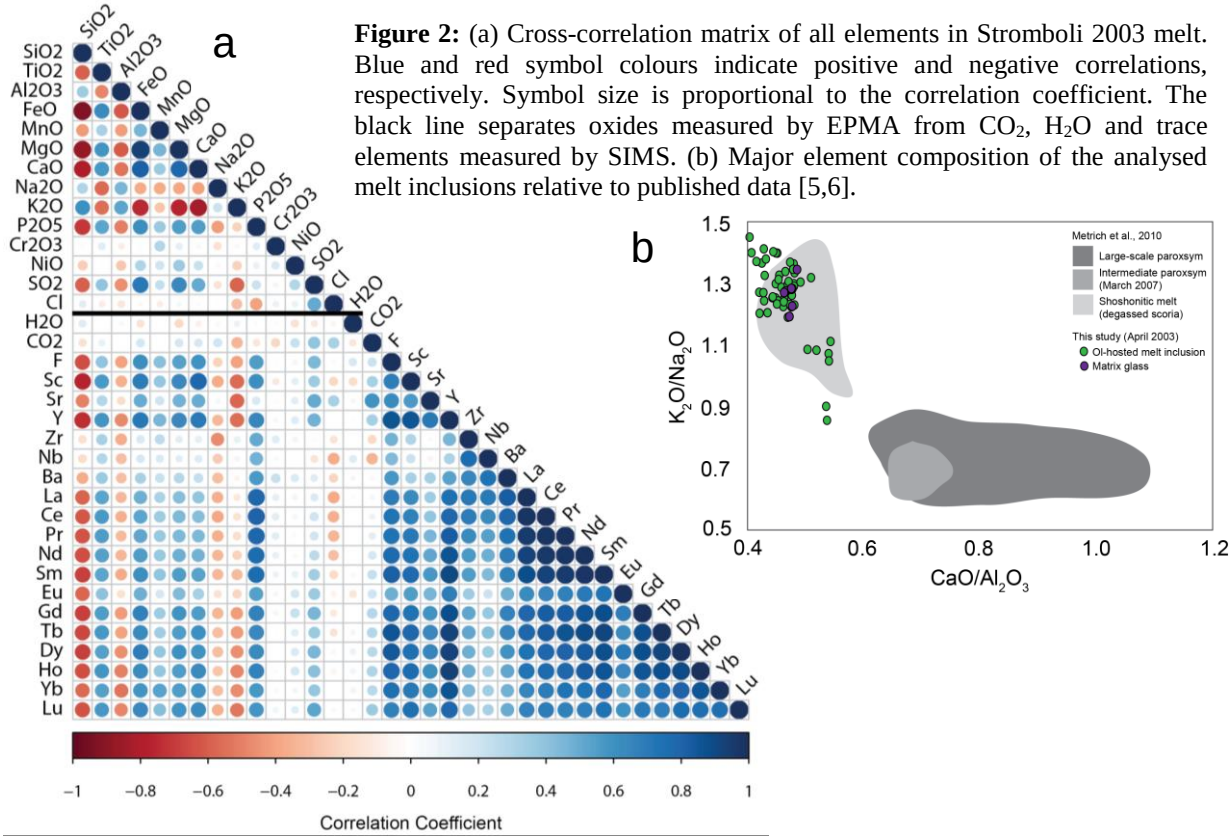

Figure 2: (a) Cross-correlation matrix of all elements in Stromboli 2003 melt. Blue and red symbol colours indicate positive and negative correlations, respectively. Symbol size is proportional to the correlation coefficient. The black line separates oxides measured by EPMA from CO_2, H_2O and trace elements measured by SIMS. (b) Major element composition of the analysed melt inclusions relative to published data [5,6].

Discussion

CO_2–H_2O contents measured in the Stromboli 2003 MIs correspond to volatile saturation pressures mostly <0.25 kbar, although several less degassed inclusions extend to higher pressures of ~1–1.5 kbar (calculated using SolEx; [4]) The shoshonitic melt compositions are at the evolved end of published MI data for Stromboli, (Fig. 2a; [5,6]) and, together with the low total volatile concentrations, indicate that considerable differentiation (decompression crystallisation) and degassing occurred prior to low pressure entrapment. Our sampled melt inclusions appear to sample the recycled, degassed crystal-rich melt that is characteristic of background Strombolian activity and which is erupted alongside primitive volatile-rich melt during paroxysmal eruptions [6]. The slight negative correlation between CO_2 and Nb indicates that CO_2 is not behaving truly incompatibly during ascent and fractional crystallisation, and instead hints at mixing between variably enriched melts. However, the restricted range of CO_2 contents in our MIs limits our ability to robustly test the initial hypothesis, and further work is required to explore the volatile-trace element systematics in more primitive MIs sampling a wider compositional range.

References [1] Sides et al., 2014, Nature Geoscience, 7(6); [2] Neave et al., 2013, Earth and Planetary Science Letters 400; [3] Pichavent et al., 2013, Contributions to Mineralogy and Petrology, 166(2); [4] Witham et al., 2012, Computers & Geosciences, 45; [5] Metrich et al., 2001, Journal of Petrology, 42(8); [6] Metrich et al., 2010, Journal of Petrology, 51(3).

Does small scale volatile heterogeneity exist in the Iceland plume?

S. Matthews[1], O. Shorttle[1,2], J. Maclennan[1]

[1]Department of Earth Sciences, University of Cambridge, Downing Street, Cambridge, CB2 3EQ, UK
[2]Institute of Astronomy, University of Cambridge, Madingley Road, Cambridge, CB3 0HA, UK

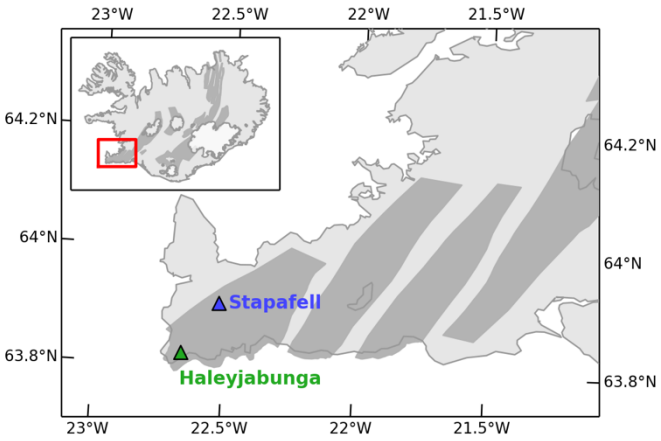

Figure 1. Locations of Stapafell and Haleyjabunga on the same rift segment on the Reykjanes peninsula. Dark grey corresponds to the active rift zones.

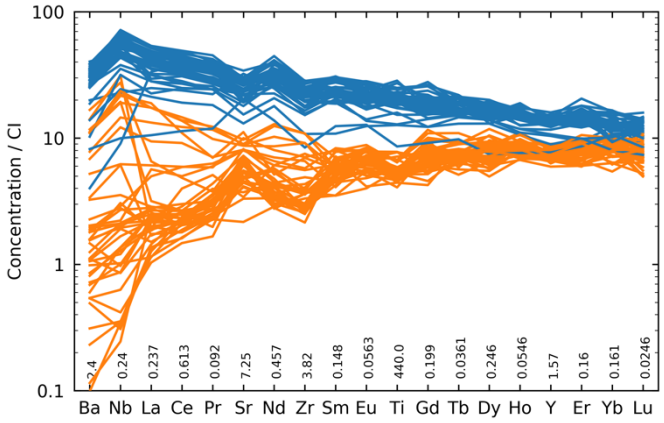

Figure 2. Trace element concentrations normalised to CI chondrite for melt inclusions from Stapafell (blue) and Haleyjabunga (orange).

Motivations

Earth's rocky mantle is a significant chemical reservoir hosting not only a majority of the planet's lithophile elements, but also possibly much of its volatile inventory[1]. However, despite their significance, our understanding of the spatial distribution of volatile elements in the mantle remains poorly understood. Progress has been hampered in part by the very property that makes the volatile elements so interesting: their tendency to undergo a decoupled transport history, via degassing (H, C), diffusion (H, F), immiscibility (C, S) and interaction with the hydrosphere (H, C, Cl, B).

In Iceland, lithophile trace elements and radiogenic isotopes have revealed the presence of depleted, recycled and primordial material heterogeneously distributed on a scale as small as individual volcanic systems[2]. Since mantle transport and storage processes, such as diffusion, operate on characteristic length scales for each element, understanding the length scale over which the mantle remains heterogeneous is a vital step in characterising mantle volatile transport.

Samples

We analysed volcanic rocks from two eruptions separated by only ~10 km (Figure 1), which sample different mantle domains and are internally highly chemically heterogeneous[2]. Since the erupted magma has experienced a long history of mixing and loss of volatile elements by degassing, we analysed melt inclusions hosted in the olivine macrocrysts. Melt inclusions form as crystals incorporate tiny droplets of magma during growth at high pressure, and so provide an undegassed and unmixed record of the magma volatile inventory.

Results

Figure 2 illustrates the geochemical diversity recorded by the melt inclusions from the two eruptions: Stapafell displays enriched geochemical signatures, consistent with a mantle source of recycled origin, implied by radiogenic isotope observations[3]. In contrast, Haleyjabunga mostly preserves more depleted melts, consistent with a considerable depleted mantle component in its mantle source.

Our volatile element results are summarised in Figure 3, alongside selected literature data from Iceland and the mid-ocean ridge system. The volatile elements have been normalised to lithophile trace elements which are thought to behave in a similar way during mantle melting (i.e. they have similar partition coefficients). Applying this normalisation largely removes the effects of melting, and magma residence in the crust, allowing mantle trends to be resolved.

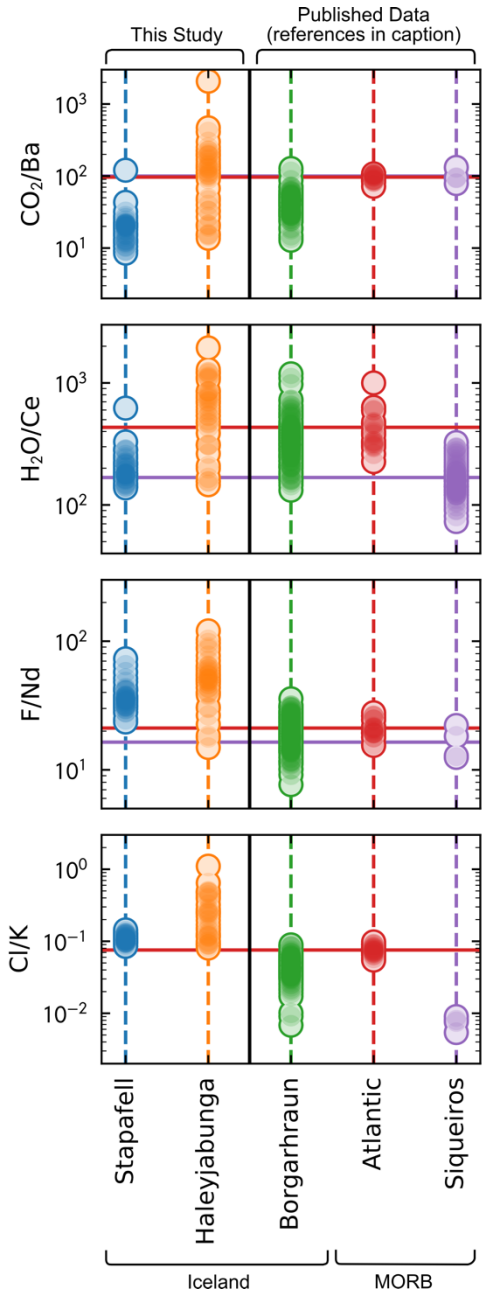

Figure 3. Volatile- trace element ratios in melt inclusions from the eruptions studied here, and other selected eruptions from Iceland (Hauri et al., 2018) and the mid-ocean ridge system (Saal et al., 2002; Le Voyer et al., 2017). Density of shading illustrates density of data. Horizontal lines are drawn through mean values of the MORB datasets.

Significant offsets between Haleyjabunga and Stapafell are seen for CO_2/Ba, H_2O/Ce, F/Nd and Cl/K. These offsets suggest that the mantle source for the Haleyjabunga melts may be more enriched in H_2O, F and Cl, than the Stapafell mantle source (relative to the trace elements). Haleyjabunga also appears to be more enriched in these elements than eruptions sampling typical Icelandic depleted mantle (Borgarhraun) and the depleted mantle underlying the Mid-Atlantic ridge and the East Pacific Rise (Siqueiros). In contrast, the Stapafell mantle source has H_2O/Ce within the range defined by MORB, F/Nd is higher, and Cl/K is comparable (though higher than the Borgarhraun mantle source). CO_2/Ba distributions also vary between the eruptions presented, but this is likely to be a result of varying degassing pressures and magma mixing[4].

Discussion and conclusions

Our results clearly demonstrate that mantle H_2O/Ce, F/Nd and Cl/K are heterogeneous on small inter-eruption length scales. In addition, the geochemically depleted Haleyjabunga eruption appears to be sampling more volatile rich mantle than the depleted mantle sampled by MORB and Borgarhraun. Helium isotope observations for Haleyjabunga suggest this eruption may also be sampling a primordial undegassed domain[5], potentially explaining the difference between it and the depleted mantle sampled by MORB and Borgarhraun. Further analysis is required to extract bounds on mantle CO_2 from this data, in light of the likelihood of mixing and degassing strongly controlling the CO_2-trace element systematics[4].

References

[1] Ahrens (1989) Origin and evolution of planetary and satellite atmospheres 328-385.

[2] J. Maclennan (2008) Geochimica et Cosmochimica 72, 4159-4176.

[3] M.F. Thirlwall et al. (2004) Geochimica et Cosmochimica Acta 68, 361-386.

[4] S. Matthews et al. (2017) Earth and Planetary Science Letters 480, 1-14.

[5] K. Breddam et al. (2000) Earth and Planetary Science Letters 176, 45-55.

CO_2 partitioning between plagioclase and melt

A. McCarthy & J. Blundy

[1]School of Earth Sciences, University of Bristol, Bristol BS8 1RJ, UK

Introduction

Volatiles, such as H_2O, CO_2 in arc magmas play fundamental roles in governing crystallization, eruption dynamics, and hydrothermal mineralisation [1]. Moreover, CO_2 fluxing during degassing of deep-seated magmas might affect overlying magmatic reservoirs with consequences for eruption dynamics and triggering. Melt inclusions are conventionally used to infer pre-eruptive volatile contents of arc magmas. However, inclusions only form after significant crystallisation of the host magma has taken place. Consequently, the initial magmatic volatile budget may not be reliably captured by melt inclusion analysis if some degassing precedes the onset of major crystallisation. Blundy et al., (2010) argue that this situation is commonly the case for volatile-bearing arc magmas, notably for CO_2, which is significantly less soluble and less abundant than H_2O. In that case, using melt inclusions to estimate original magmatic CO_2 can lead to significant underestimates of the original concentration, with profound implications for subduction zone CO_2 budgets.

An alternative strategy for constraining magmatic CO_2 contents is to use the CO_2 dissolved in the core of early-formed magmatic phenocrysts. A candidate mineral phase is plagioclase. Plagioclase displays a small solid solution with scapolite (meionite $3CaAl_2Si_2O_8.CaCO_3$ and sulfate meionite $3CaAl_2Si_2O_8.CaSO_4$) [2], which suggests that detectable amounts of CO_2 can be stored in the lattice of crystals grown from CO_2-bearing melts. Thus, being able to analyse CO_2 concentrations in plagioclase, and constraining experimentally the plagioclase-melt CO_2 partition coefficient could have widespread application in studies of arc magmas.

Scientific Objectives

A critical issue is whether CO_2 can be precisely measured in plagioclase. To assess this issue we took part in a one-day pilot-study at the NERC facility in Edinburgh using the SIMS Cameca IMS 4f in order to analyse plagioclase crystals from high-pressure (15 kbar) carbonate-bearing crystallization experiments produced at the University of Bristol. By selecting plagioclase from such carbonate-rich systems we expect dissolved CO_2 abundances to be maximised, providing a valuable test as to whether CO_2 can be incorporated significantly into plagioclase. Additionally, a plagioclase-bearing marble (anorthite + calcite assemblage) collected from Castione, Swiss-Italian Alps, is to be used as an initial natural sample in order to see if CO_2 is quantifiable in plagioclase derived from carbonate-rich rocks

Scientific Results

Preliminary results of measured CO_2 abundances in both experimental and natural plagioclase show that CO_2 concentrations reach ca. 12 ppm for the amphibolite-facies Castione Marble and between 5-122 ppm for high-pressure experiments at difference initial CO_2 ($CaCO_3$) concentrations. Preliminary calculated $K_d^{plagioclase\text{-}melt}$ for CO_2 (partition coefficient) is on the order of caesium (Kd=0.001). Though measured CO_2 abundances are distinctly lower than initially expected, suggesting a different mechanism of substitution then a scapolite-plagioclase solid solution, these results are still very encouraging. We expect in the near future to be able to refine our analytical procedure by increasing counting times, using higher beam currents and analysing CO_2 abundances using the Cameca 1270. We also aim to expand our study of natural samples by the analysis of large, homogeneous plagioclase from various high-pressure metamorphic- and magmatic rocks from environments most likely to contain elevated CO_2 concentrations.

References

[1] J. Blundy et al., (2010) Earth and Planetary Science Letters, **290**, 289-301

[2] J.R. Goldsmith et al., (1977) American Mineralogist, **62**, 1063-1081

[PAGE INTENTIONALLY LEFT BLANK]

Geochemistry of trace elements in fluorite from carbonatites

R.H. Mitchell

Department of Geology, Lakehead University, Thunder Bay, Ontario, Canada P7B 5E1

Long term objectives of the research

(1)To develop a matrix-matched standard for the analysis of trace elements in fluorite by SIMS;
(2)To determine the abundances of trace elements in fluorite occurring in diverse carbonatites;
(3)To correlate the cathodoluminescence (CL) spectra with rare earth element (REE) contents of fluorite.

Development of standard fluorite

Currently, the trace elements contents of fluorite (CaF_2) are typically determined by LA-ICP-MS as the presence of small inclusions of other minerals commonly precludes bulk analysis by solution ICP-MS. In this method fluorite trace element data are usually acquired against NIST or USGS glass standards. As the matrices of the silicate glass standards and CaF_2 are very different these standards are not necessary suitable for fluorite analysis. Typically, fluorites are zoned with respect to their optical and CL colours and to develop a suitable matrix matched standard has required a search for a natural fluorite sample of exceptional purity. On the basis of optical, back-scattered electron and CL-imagery a sample of polycrystalline purple fluorite from the Dong Pao carbonatite (North Vietnam) was found to be a suitable candidate for a SIMS standard. A second potential standard of green fluorite from the Okorusu carbonatite (Namibia) was also investigated. These fluorites were analysed by LA-ICP-MS using 213 and 193 nm lasers at the University of Manitoba and Laurentian University, respectively, and by SIMS at the Edinburgh Ion Microprobe Facility. Bulk data were also obtained by solution ICP-MS (ActivationLabs. Ontario). Additional data for Sr were obtained by standard EMP methods using celestite as a Sr standard at the University of Edinburgh.
The SIMS analysis was undertaken using the Cameca IMS 4f instrument using Au-coated polished grain mounts. Measurements were made with a $^{16}O^-$ beam of 14.5 keV energy, and 10 cycles each of 150 seconds counting time. Isotopes measured were: ^{7}Li; ^{9}Be; ^{19}F; ^{23}Na; ^{30}Si; ^{42}Ca; ^{59}Co(CaO); ^{88}Sr; ^{89}Y; $^{130.5}$background; ^{138}Ba; ^{139}La; ^{140}Ce; ^{141}Pr; ^{143}Nd; ^{149}Sm; ^{151}Eu; ^{156}Gd; ^{157}Gd; ^{158}Gd; ^{159}Tb; ^{161}Dy; ^{165}Ho; ^{167}Er; ^{169}Tm; ^{171}Yb; ^{175}Lu. External calibration standards were GSD-1G basaltic glass with 51.33 wt.% Ca as an internal standard assuming stoichiometric fluorite. Molecular interferences by light REE oxides were removed by energy filtering at –120 V offset. Corrections were made to the Tb, Dy, Er, Tm, Yb and Lu data to account for REE-fluoride interferences.

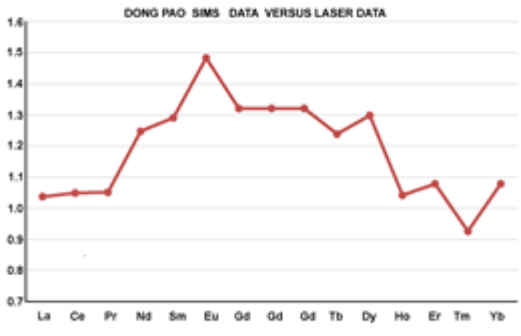

Figure 1. Relative abundances of REE obtained by SIMS GSD-1G versus laser NIST-610

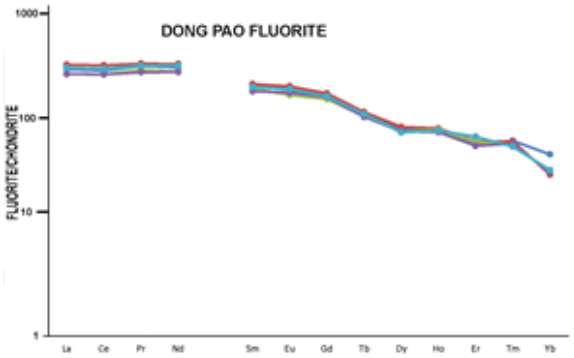

Figure 2. REE abundances in Dong Pao fluorite

Figure 1 illustrates the relative differences in REE abundances in fluorite versus laser methods and indicates that the SIMS ion yields are different for each REE. SIMS REE abundances are always greater than the laser abundances. Fig.2 shows that Dong Pao fluorite

is very homogeneous with respect all REE and that smooth chondrite distribution patters are evident.

Figs 3 and 4 illustrate CL spectra and SIMS-REE distribution patterns for fluorite from the Ashram Deposit of the Eldor carbonatite [1]. These data, and those shown in Fig.2, indicate that useful REE distribution patterns can be obtained for fluorite using GSD-1G as an external SIMS standard. The CL spectra of the Ashram fluorite is dominated by emission lines of Dy and Tb, as expected from the HREE enrichment of this fluorite. Analysis of fluorites from several carbonatite complexes revealed that HREE enrichment of fluorite is characteristic of this paragenesis and that CL spectra are dominated by Sm, Eu, Dy and Tb emission lines.

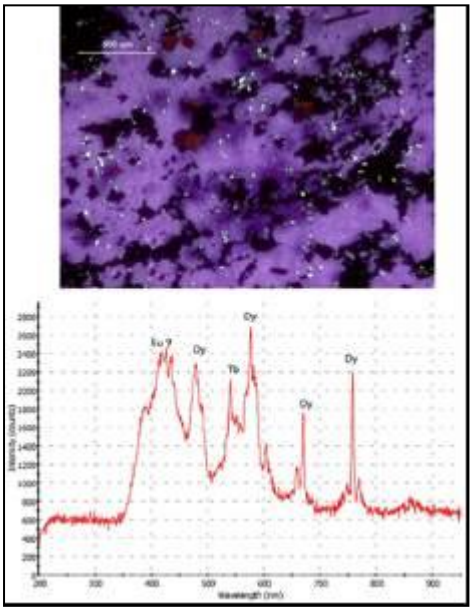

Fig.3 CL spectra fluorite

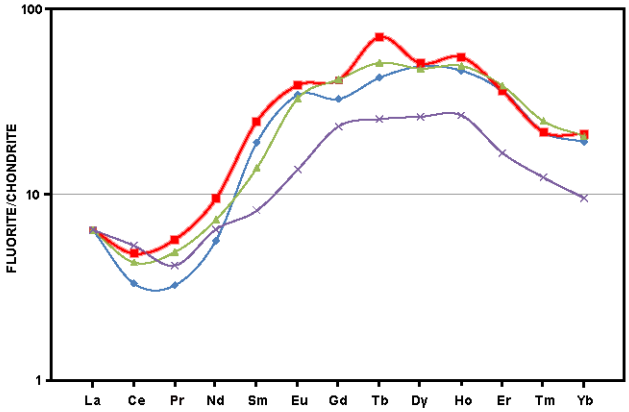

Fig.4 SIMS-REE distribution in Ashram fluorite

As yet the accuracy of the SIMS-REE determinations remains uncertain as analysis of Dong Pao fluorite by various techniques without matrix matched glass standards gives a range of compositions for a given REE. For example, the average Sm contents (ppm) of Dong Pao fluorite were found to range from 33.4 (SIMS-GSD-1), 25.9 (213 nm laser-NIST-610), to 26.9 (193 nm laser NIST 610), although overall REE distribution patterns are similar.

Other elements analysed by SIMS show a wide range of abundances with Sr being the major trace element ranging from c.350 to 3000 ppm. As with the REE, the accuracy of these data is uncertain as GSD-1 was used as a reference standard. For Dong Pao fluorite average Sr contents (ppm) range from 3100 (SIMS-GSD-1), 2731 (213 nm laser NIST-610), 2708 (193 nm laser NIST 610); to 2979 (WDS-EMP- $SrSO_4$).

The SIMS analyses indicated the presence of significant amounts of Be in fluorite from carbonatites ranging from not detectable to 15.9 ppm, and representing a $CaBeF_4$component [2]. The presence of Be as a trace element in fluorite has previously been reported only once by semi-quantitative optical spectrographic methods [3]

References

[1] Mitchell, R.H., and Smith D.L. (2017) Ore Geology Reviews, **86**, 784-806

[2] Counts, W.E., Roy ,R., Osborn, E.F., (1953) Journal of the American Ceramic Society **36,** 12-17

[3] Allen, R.D. (1952) American Mineralogist **37**, 910-930

Protracted assembly of magmas feeding large basaltic fissure eruptions

E. J. F. Mutch[1], J. Maclennan[1], M. Hartley[2] & M. Edmonds[1]

[1]Department of Earth Sciences, Univ. Cambridge, Downing Street, Cambridge, CB2 3EQ, UK
[2]School of Earth and Environmental Sciences, Williamson Building, Oxford Road, Univ. Manchester M13 9PL

Introduction

The Laki eruption (Skaftár Fires) of AD 1783-1784 was one of the largest basaltic fissure eruptions in historical times in which 122 Mt of sulphur dioxide was ejected into the atmosphere causing widespread climatic effects in the northern hemisphere and leading to famine across much of Europe [1,2]. Part of the Grímsvötn volcanic system in Iceland, it is one of the best studied small scale analogues of a flood basalt eruption. Approximately 14.7 km^3 of lava and ~0.4 km^3 dense rock equivalent of tephra were erupted from a 27 km fissure that developed sequentially SW to NE in 10 en echelon segments [3]. The crystal cargo consists of olivine (Fo_{70-85} cores with Fo_{52-70} rims), clinopyroxene and plagioclase (An_{65-89} cores and An_{50-65} rims) macrocrysts that change in composition and proportion throughout the duration of the eruption [4]. The plagioclase macrocrysts show a diverse range in crystal zoning patterns, often typified by a high-anorthite core, oscillatory zoned mantles and low-anorthite rims. Each zone records concurrent crystallisation and mixing in a dynamic mid-crustal magma reservoir that is being fed by a suite of different melts with different trace element compositions [5]. We have modelled the diffusive modification of trace elements across plagioclase zones to gain an important insight into crystal residence times and thus the timescales over which these magmas are assembled and mixed prior to this large catastrophic fissure eruption.

Methods

We handpicked primitive plagioclase macrocrysts from fresh glassy tephra of eruptive episode VII, mounted them in epoxy and diamond polished. Using a Cameca 1270 instrument, we measured trace element compositional profiles (Li, Mg, Sr, Ti, Rb, La, Y, Ba, Ce and K) from the edge of the plagioclase macrocrysts, across their rims and oscillatory mantles, and into their cores. Profiles up to 1200 µm in length, using 10 µm spots, were measured in order to assess long-range compositional variation. High resolution step scan profiles, with 2-3 µm spacing, were then measured over a shorter interval (typically 200-300 µm in length) to capture short length-scale diffusive modification. EPMA profiles were then measured to characterise major element composition and normalise the SIMS data.

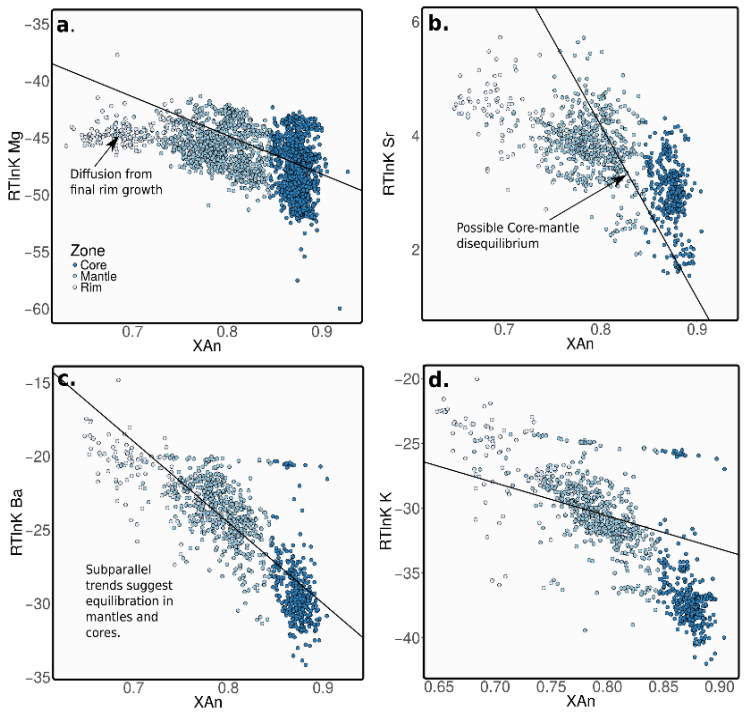

Figure 1. Calculated partition coefficients (RTlnK) vs. anorthite content plots for all collected data; (a) Mg, (b) Sr, (c) Ba and (d) K. Points have been colour-coded base on the zone they were collected. In most cases the core and mantle data have arrays that run subparallel to experimentally determined partitioning behaviour (black lines) suggestive of equilibrium. Deviation from these lines at carrier liquid conditions indicates disequilibrium and diffusive modification, which can be observed for the crystal rims.

We have developed finite-element forward models using FEniCS to track the compositional evolution of plagioclase trace elements from calculated initial conditions through time until the model matched the observed profile; thus giving us a diffusive timescale. A total of 19 'coarse' profiles and 13 step scan profiles were measured across plagioclase macrocrysts at the EIMF.

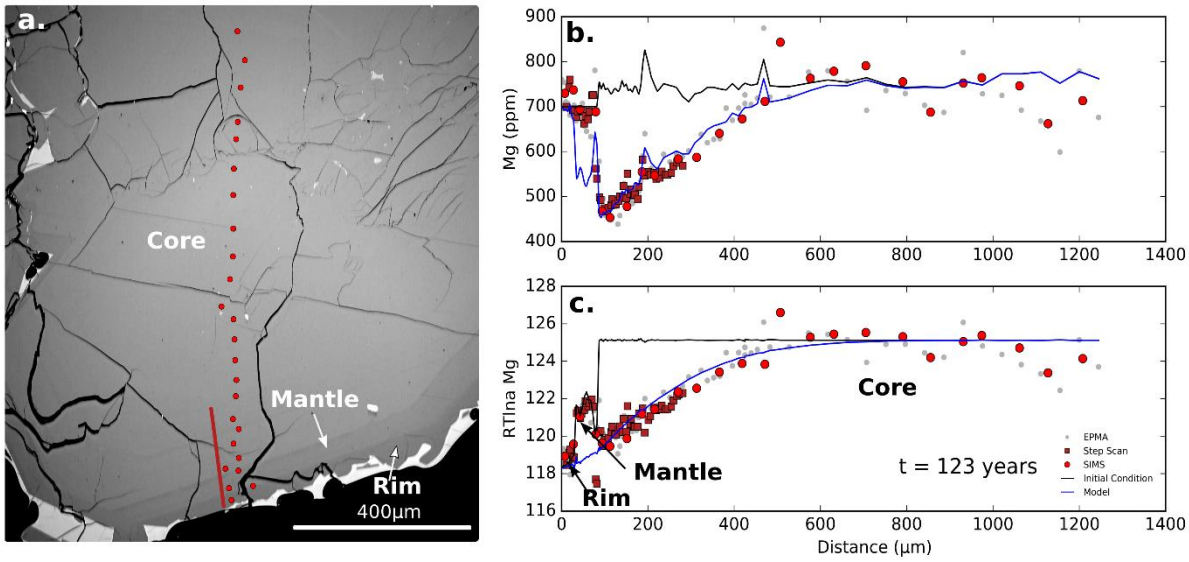

Figure 2. (a) BSE image of a plagioclase macrocryst with core Mg disequilibrium, and single-zone mantle and rim. The location of coarse SIMS spots (red points) and the step scan profile (red line) are also shown. (b) 1D finite-element model of Mg diffusion between the crystal core and mantle. The black line shows the estimated initial condition and the blue line the model fit (123 years). (c) The same models plotted relative to the activity of Mg (RTlna), which is dependent on anorthite content.

Results

By examining how calculated partition coefficients (RTlnK) for a given measurement deviates from known partitioning relationships for plagioclase [6], we can assess the amount of disequilibria and diffusive modification in each macrocryst. Fig. 1 shows that the majority of crystal mantles and cores have completely equilibrated for Mg as most mantle and core points lie on linear arrays parallel to the experimentally determined partitioning behaviour. Disequilibria for slower diffusing elements such as Sr, Ba and K is more difficult to assess given the greater uncertainty in their partitioning behaviours. Deviation from linearity observed between crystal rims and mantles likely reflects crystal growth in the final carrier liquid and rapid transport to the surface on the order of 10 days, which has been previously estimated by using diffusion profiles in olivine [7]. A sub-population of three texturally different plagioclase crystals (coarser crystal size with thinner mantles composed of one individual zone) show extensive Mg disequilibrium in their cores (Fig 2a). 1D finite-element models of Mg diffusion in these crystals indicate that they had a maximum residence time of approximately 120 years assuming a storage temperature of 1150 °C (Fig 2b-c). In this instance the mantle composition was used as a boundary condition meaning these timescales represent the time between the onset of mantle growth and when diffusion effectively stops upon quenching during eruption.

Discussion

The crystals with mature oscillatory-zoned mantles have been sequestered for a considerable period of time. To reach complete Mg equilibrium across crystals typically 1 mm in diameter would require timescales of ca. 1000 years at resident temperatures of 1150 °C, which provides a theoretical lower limit of long-term storage times. The unequilibrated crystals have thinner mantles and have younger relative ages. They have experienced fewer melt mixing events and thus represent one of the latest melt replenishment events prior to eruption. All of the observations combined suggest that the final magma, and its crystal cargo, that fed the Laki eruption was incrementally assembled over a protracted period of time on the order of 100s of years with new melt injections at regular intervals. These timescales of crystal storage support interpretations of U-series disequilibria that crystal storage in Icelandic magmatic systems can last thousands of years [8], and also that central volcanoes in Iceland, such as Grímsvötn, are fed by extensive magma plumbing systems that are continually being fed from below.

References

[1] Thordarson & Self (2003) *J Geophys Res: Atm 108* (D1); [2] Schmidt ea (2012) *J Geophys Res: Atm* 117 (D23); [3] Thordarson, & Self. (1993), *Bull. Volcanology 55*, 233-263; [4] Passmore ea (2012) *J Petrol.* egs061.; [5] Neave ea (2013) *J Petrol.* egt027; [6] Bindeman ea (1998) *Geochim Cosmochim Acta, 62*, 1175-93; [7] Hartley ea (2016) *Earth Planet Sci Lett 439*, 58-70; [8] Cooper K. ea (2016) *Contrib Min Pet 171*, 1-19.

Fluorine and Cl partitioning between olivine and silicate melt under lunar mantle conditions

N.J. Potts & G. D. Bromiley

School of GeoSciences, University of Edinburgh, Edinburgh EH9 3JW, UK

Background

Isotopic similarities between the Earth and Moon have led to the hypothesis that the Moon is derived largely from bulk silicate Earth material; most likely following a giant impact between a Mars-sized planetessimal and the proto-Earth. Subsequently, Earth has been progressively modified by melting and plate tectonics, while the Moon has remained relatively unchanged over the past 4.5 billion years, preserving a much better record of the early Earth-Moon system and, by extension, of the early inner solar system. Of particular importance is the Moon's ability to provide insight into the role of volatiles during planetary formation and early evolution.

It has now been shown that lunar volcanic glasses and Mare basalts contain significant quantities of volatiles[1] (i.e. F, Cl, S, H_2O), implying that at least part of the lunar mantle is volatile-rich. Overlapping water contents between Mare basalts and terrestrial mid-oceanic basalts have been used to imply that the water contents of the lunar mantle might be similar to that of Earth's mantle[3], implying that volatiles were accreted to the Earth before the Moon-forming event. In contrast, considerably lower values of fluorine and chlorine in the lunar mantle compared to the Earth have been used to suggest the Moon is depleted in volatiles compared to the Earth, implying delivery of volatiles post-Moon formation. Direct comparison of volatile contents with modern terrestrial magmas, however, is highly misleading, as lunar magmas formed under more reducing conditions. Existing estimates of the lunar mantle volatile contents are based on values of H, F, Cl, S partitioning between minerals and melt under the more oxidising conditions of Earth's modern upper mantle. Under these conditions, volatiles are known to be highly incompatible and readily incorporated in magmas, with only small amounts (ppm level) remaining in residual minerals as structural defects. The inherent assumption of existing studies, therefore, is that fO_2 has no influence on volatile partitioning.

A novel high-pressure/temperature experimental setup was invoked to allow us to determine H, F, and Cl partitioning under, lunar-relevant, fO_2. Experiments were conducted over a P-T range consistent with existing models to determine H, F, Cl, partitioning at low fO_2 in lunar systems. A one-day application was required to test the experimental design to ensure the retention of volatiles during experiments and to inform the direction of further experiments.

Results

Measurements of F, Cl, and H were made in orthopyroxene, and quenched melt in three experiments. Results highlighted how considerable amounts of F can partition into orthopyroxene alongside H, while no Cl partitions into this mantle forming phase. A negative correlation between F and H partitioning into orthopyroxene was found in the three experiments measured, while more H was found to partition into orthopyroxene than previously reported in the literature. These results demonstrate the effectiveness of our experimental design in terms of volatile retention under highly reducing conditions, and showed how couple substitutions mechanisms between F and H must be explored in further experiments. The lack of Cl retained in mantle forming minerals shows how, after solidification of a planetary mantle, a planet can become relatively enriched in F compared to Cl. This result fits with observed trends in F/Cl ratios of the Earth and Moon, highlighting the importance of understanding the processes impacting volatiles and their behaviour during planet formation, if we are to understand their origin in planets. This one-day pilot led into a more in depth study, which began in March 2018. Publication resulting from this work will be include results from the larger analysis session in March 2018.

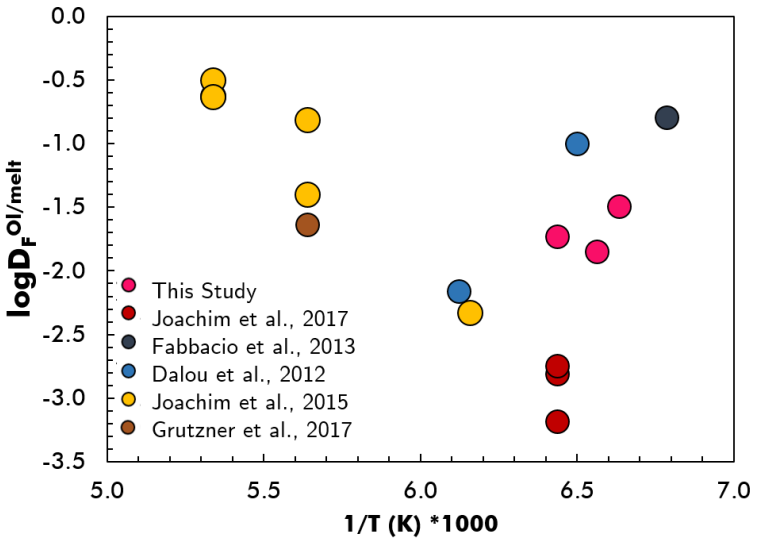

Figure 1. Fluorine partitioning versus T for experiments in this study and the literature.

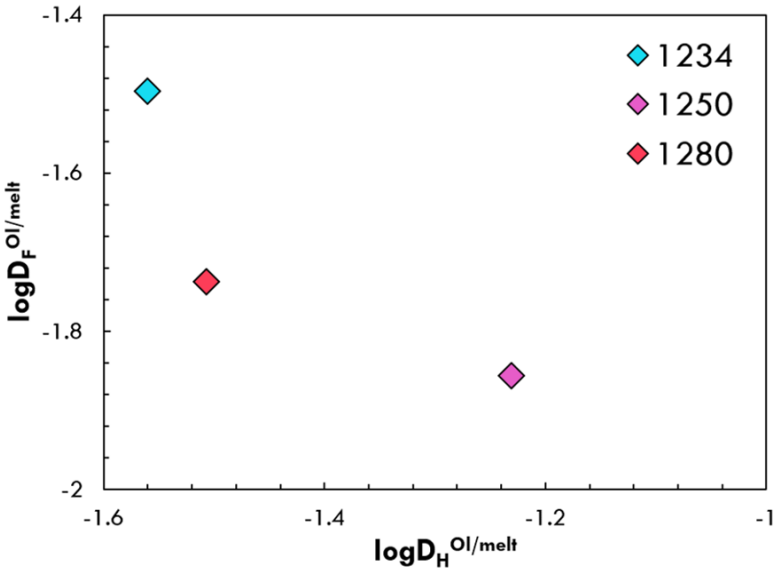

Figure 2. Fluorine partitioning versus H partitioning for experiments measured in this study.

Apatite-melt partitioning, the role of C

N.J. Potts[1], M. Anand[2] & G. D. Bromiley[1]

[1]School of GeoSciences, University of Edinburgh, Edinburgh EH9 3JW, UK
[2]The Open University, Milton Keynes, MK6 4LL, UK

Background

Apatite is the main volatile-bearing phase in lunar samples and is ubiquitous throughout the lunar rock collection, making it an ideal candidate to serve as a probe to reconstruct the volatile content of the interior of the Moon. Translating measurements of hydroxyl, fluorine, and chlorine in apatite to volatile abundances in the parent melt, however, remains a major challenge. We conducted a study in which high-pressure experiments were performed to quantify apatite-silicate melt volatile partitioning using, for the first time, silicate melt compositions that are similar to those from which lunar apatite crystallizes. Fluorapatite was equilibrated with silicate melt to constrain the partitioning of added volatiles. Melt and apatite volatile (F, Cl and H_2O) contents were measured by ion microprobe. Our results confirm that apatite with similar F, Cl, and H_2O contents can crystallize from silicate melts with variable H_2O contents and show that significant amounts of H_2O can be partitioned into apatite while F is still available in the melt. Combining results from this study with literature data yields simple descriptions for the partitioning of F and Cl between apatite and melt and a new, empirical predictive model that relates the water content of melts from which apatite crystallizes to the volatile contents of apatite.

A caveat to our results, however, is a recent study found considerable C could sit within the apatite X site. As the experiments in this study were performed in graphite buckets, within Pt capsules to provide an fO_2 of ~IW. If all the Fe_2O_3 of our starting material did not dissociate into FeO, then considerable free O_2 would be available to bound with C from the graphite bucket, leading to considerable CO_2 dissolved in the starting material. If this is the case, CO_2 is thought to compete with F, Cl, and OH to fill the crystallographic X site which may impact the model developed in the above study. Measurements of C within experimental grains were, therefore, crucial to provide further understanding and constraints on methods of apatite partitioning study, the thermodynamics of apatite partitioning to the crystallographic X site and allow for further development of the model proposed in our study.

Results

Measurements of apatite grains were made on the Cameca 4f. No discernible CO_2 was measured within these grains, while less than 700 ppm CO_2 was measured in surrounding glasses. This confirms that all Fe was present as 2+ rather than 3+ in our starting material, consistent with an fO_2 of IW+2 to IW-1, as required.

References

[1] R.A. Berner et al. (1983) American Journal of Science **283**, 641-683
[2] M.E. Raymo and W.F. Ruddiman (1992) Nature **359**, 117-122

[PAGE INTENTIONALLY LEFT BLANK]

Tracking the evolution of slab fluids at the Izu-Bonin arc with B isotopes

I.P. Savov [1] & J.C.M. De Hoog[2]

[1]School of Earth & Environment, University of Leeds, Leeds LS2 9JT, UK
[2]School of GeoSciences, University of Edinburgh, Edinburgh EH9 3JW, UK

During 1 day reconnaissance SIMS work we have successfully measured the B and $\delta^{11}B$ isotope ratios in 14 melt inclusions (MI) trapped in pyroxenes extracted from various core depths of Site U1348, drilled during IODP Expedition 351 to the Amami Basin in the Izu-Bonin-Mariana (IBM) region (Arculus et al., 2015). Site U1438 core is unique in that it penetrated the 49 M.yrs old basement representing very depleted tholeiitic basalts erupted just prior to the subduction (arc) initiation (Ishizuka et al., 2018). Together with the pre-arc basement we also recovered >1300m of exceptional volcaniclastic sediment cover, preserving a record of the entire proto-IBM arc development and subsequent destruction. The goal of our study was to see if there are trends in the B and $\delta^{11}B$ with the recorded increases in magma production rates with depth/time (Brandl et al., 2017). The $\delta^{11}B$ ratios vary from 5.5 to 10.7 ‰ and the B concentrations vary from 4 to 52 ppm.

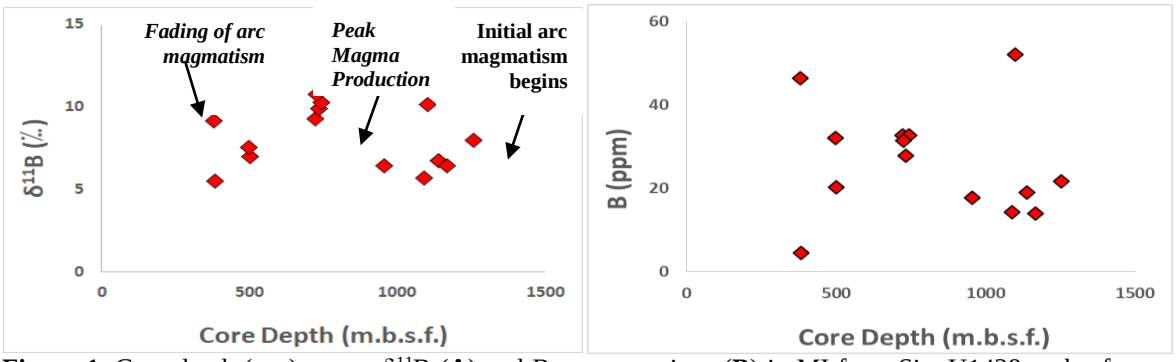

Figure 1. Core depth (age) versus $\delta^{11}B$ (**A**) and B concentrations (**B**) in MI from Site U1438; m.b.s.f.= meters below sea floor. It is clear that B and $\delta^{11}B$ do not vary systematically with core depth, although the core captures gradually increasing and then decreasing arc magma production (melt outfluxes) as evidenced from the sedimentology and the overall MI petrology (Brandl et al., 2017).

Although the preliminary results of the post-Eocene MI suite are limited, it seems that boron does not vary systematically with core depth i.e. age (Figure 1). Interestingly the MI we studied show excellent positive correlation between B and $\delta^{11}B$ (Figure 2). This relationship seems to be independent of any other MI chemical parameter. Our results also resemble the overall heavy $\delta^{11}B$ measured in tephras from the Miocene-to-modern Izu arc (Straub and Layne, 2001). We interpret the combined high B and $\delta^{11}B$ dataset as highlighting the extreme fluid mobile nature of boron, which seems to be added to the arc magmas immediately after the subduction begins from a forearc melange fluids (with high $\delta^{11}B$) irrespectively of variations in the slab fluid outfluxes, degree and style of melting, or subduction zone geometry.

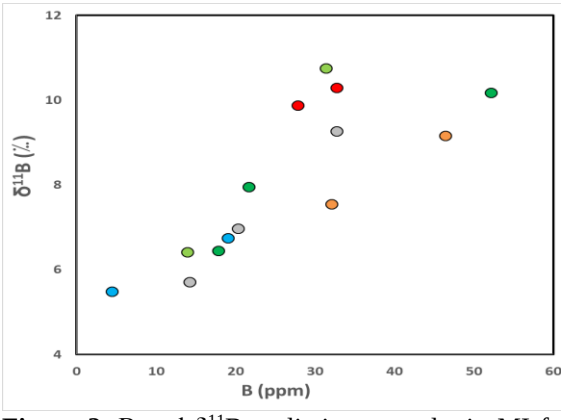

Figure 2. B and $\delta^{11}B$ preliminary results in MI from Exp. 351. Interestingly, the rear arc samples (red) are with $\delta^{11}B$ and B that are indistinguishable compared to the front arc MI (light & dark green). The evolved (dacite-rhyolite) MI (orange) are with the same $\delta^{11}B$ and B as those from the mafic samples.

References

[1] Arculus et al.. (2015) Nature Geosci. 8, 728-733; [2] Straub SM, Layne GD (2002). Earth Planet Sci Lett 198, 25–39; [3] Ishizuka, O., Hickey-Vargas R., Arculus R., Yogodzinski G., Savov, I.P., Kusano, Y., McCarthy, A.,, Brandl, P., Sudo, M. (2018). Earth Planet Sci. Lett. 481, 80–90; [4] Brandl., P., Hamada, M.; Arculus, R., Johnson; K., Marsaglia, K., Savov, I.P., Ishizuka, O., (2017). Earth Planet Sci. Lett. 461, 73-84.

[PAGE INTENTIONALLY LEFT BLANK]

Origin of mantle eclogite xenoliths from Chino Valley, Arizona, USA

D. Schulze[1], L. Malik[1], J. Valley[2], D. Davis[1], H. Helmstaedt[3]& S.Yokoyama[1]

[1]Dept. of Earth Sciences, University of Toronto, Toronto, Ontario Canada
[2]Dept. of Geology and Geophysics, University of Wisconsin, Madison, Wisconsin USA
[3]Dept. of Geological Sciences and Geological Engineering, Queen's University, Kingston, Ontario Canada

Mantle-derived xenoliths from the Oligocene Sullivan Buttes Latite in central Arizona, located in the Transition Zone between the Colorado Plateau and the Basin and Range provinces, are dominated by garnet, clinopyroxene and pargasitic amphibole. Oxygen isotope compositions of the garnets ($\delta^{18}O_{V\text{-}SMOW}$, determined by laser fluorination at the University of Wisconsin) are in the range +6.0 to +10.4‰. These values are anomalously high for rocks from the upper mantle, and suggest that the eclogite xenoliths are metamorphic rocks with protoliths that underwent interaction with seawater at low temperatures and were ultimately emplaced beneath the crust in central Arizona by subduction. As such, knowledge of the age of formation of the eclogites is critical in interpreting the tectonic history of the southwestern United States.

Some of the eclogite xenoliths contain zircon, but they are typically small (<20 microns) and low in uranium, resulting in difficulties in determining their ages by the U/Pb method. Zircon ages of two samples (LA ICP-MS at the University of Toronto) are 130+/-9 Ma (Th/U = 0.5) and 66+/-5 Ma (Th/U = 0.01). We have begun zircon dating by SIMS at EIMF, with results to date for one sample, the younger of the two samples dated by LA ICP-MS. Twelve zircons were analysed with results identical to the Toronto data (63.8+/-2.6 Ma). The project will continue with further SIMS dating of zircon from these eclogites.

The higher Th/U value of the older sample is consistent with a magmatic origin for the zircon in this sample, and suggests the protolith was Mesozoic oceanic crust (basalt or gabbro) belonging to the Farallon Plate. The low Th/U value of the younger sample is consistent with a metamorphic origin for these zircon and is consistent with formation of zircon in the basic rocks of the plate during subduction in Cenozoic time.

[PAGE INTENTIONALLY LEFT BLANK]

Apatite-melt partitioning; the role of fO_2

T. Stokes, G. Bromiley, K. Saunders & N. Potts

School of GeoSciences, University of Edinburgh, Edinburgh EH9 3JW, UK

Introduction

Apatite is a crucial accessory mineral when examining the trace element budget of magmas and understanding the distribution of volatiles in melts. This ubiquitous mineral is found in sedimentary, metamorphic and igneous rocks, and our understanding of apatite in extra-terrestrial samples has even helped us revaluate the volatile budget of the Moon [1]. Apatite also has the ability to survive serval episodes of crustal anataxis, making it a suitable mineral to provide insight into conditions early in Earth's history. Due to apatite's ability to incorporate numerous trace elements in appreciable amounts, it provides insight into the chemistry of magmas, and possibly the redox state during mantle melting. One parameter which may be important in determining the concentration of redox sensitive elements in apatite is oxygen fugacity (fO_2) [2,3]. Miles et al. [2] proposed that the concentration of Mn in apatite varies as a function of fO_2; however, experimental vigour was needed to confirm this relationship and identify other parameters controlling the partitioning of Mn between apatite and melt (e.g. melt structure, aluminosity, temperature, pressure).

Piston cylinder experiments

Mn partitioning experiments between apatite-melt were carried out on a variety of compositions from haplobasaltic to rhyolitic using a piston cylinder apparatus. Experiments were designed to form apatite with only Cl and H_2O, or, F and H_2O to understand the effect of anion content on D_{Mn} (apatite-melt). Oxygen fugacity was controlled by using a double capsule technique [4], or the use of a graphite lined Pt capsules, or left to buffer at the intrinsic fO_2 exerted by the apparatus. Product runs contained apatite and quenched glass. Capsules were mounted in indium, and major/minor element chemistry was quantified using EPMA.

Rationale for using SIMS

A one-day pilot application was needed to check that water was still present within the quenched glass at the end of each experimental run, as diffusion of H_2 is needed to control fO_2. Identifying the presence of water was, therefore, crucial in testing the experimental protocol used. Also, OH is a vital component of the apatite X site, and can only be estimated based on back calculating EPMA totals. Robust measurements of F, Cl and OH, which can only be obtained via SIMS, were necessary as the Ca(2) site in apatite is structurally linked to the contents of the X site, potentially controlling the species of Ca(2) site anion.

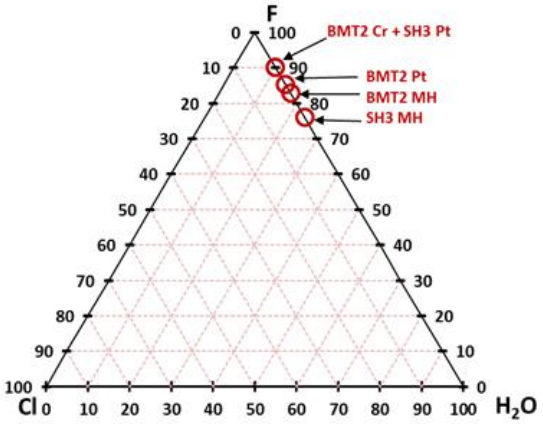

Figure 1. Apatite anion composition. Normalised to 100 % Mol fraction.

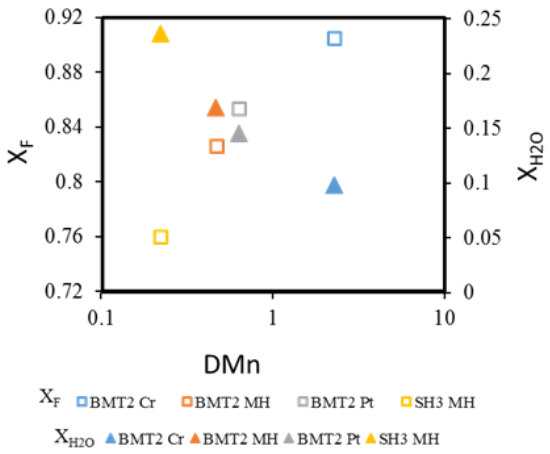

Figure 2. X_F/X_{H2O} vs D_{Mn}. X_F symbols are unfilled squares, whilst X_{H2O} are filled triangles

SIMS results

All sample glasses analysed contained significant amounts of H_2O, but we were unable to quantify values. Capsules analysed were all from the F-H_2O series of experiments, with all apatite compositions dominated by a F component. Apatite grown under more oxidised conditions contained more H_2O which either indicates an effect of fO_2 on H_2O partitioning, or that these runs resulted in glasses which contain greater wt% H_2O (Fig. 1). Consolidation of SIMS and EPMA data allows us to examine how D_{Mn} varies with the anion site content. D_{Mn} vs X_F content (Fig. 2) shows D_{Mn} increases with mole fraction F, and decreases with mole fraction H_2O in apatite.

Another outcome of the SIMS session was that some apatite crystals contained significant amounts of C as carbonate. Recent work by [5] noted that C is often incorporated with OH in the X site; Fig. 3 shows a similar relationship for samples studied here. A high wt% C in apatite also suggests there will be significant amounts of CO_2 in the melt; this may, in turn, inlfuence melt structure and, by extension, apatite-melt element partitioning.

This one-day study was a pilot for a larger application which was successful in the November 2017 round of IMF proposals. A week of time was dedicated to this larger project in January 2018, together with data from this pilot study, work is currently being prepared for publication. A key finding from this study is that both anion and cation apatite-melt partitioning are intrinsically linked, casting doubt on previous work which suggests that apatite chemistry provides a simple probe of redox state in magmas, or on the volatile content of planetary interiors.

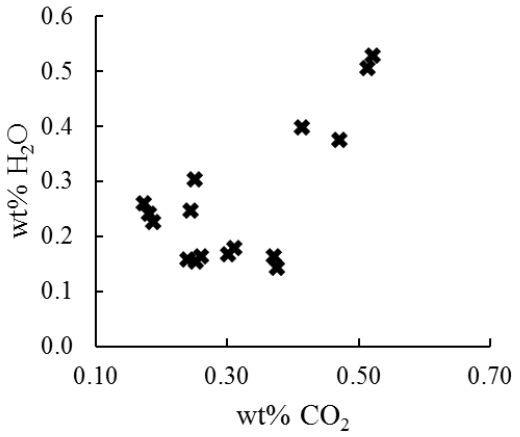

Figure 3. Wt% CO_2 vs wt% H_2O apatite for all experiments

References

[1] F.M. McCubbin et al. (2010) Proc. Natl. Acad. Sci. **107**, 11223–11228.
[2] A.J. Miles et al. (2014) Geochim. Cosmochim. Acta **132**, 101–119.
[3] B.A. Konecke et al. (2017) Am. Mineral. **102**, 548–557.
[4] H.P. Eugster (1957) J. Chem. Phys. **26**, 1760–1761.
[5] J. Riker et al. (2018), Am. Mineral. **103**, 260–270.

Tracing geodynamic changes in Paleoproterozoic rocks from SE Brazil

C. Storey[1], H. Moreira[1], J. Darling[1], M. Fowler[1] & L. Seixas[2]

[1]School of Earth and Environmental Sciences, University of Portsmouth, Portsmouth PO1 3QL, UK
[2]Departamento de Geologia, Escola de Minas, Universidade Federal de Ouro Preto, Brazil 35400-000

Background

Evolution of the continental crust has been studied intensely over the past few decades. The use of *in-situ* U-Pb and Lu-Hf isotopic systems in zircons has greatly improved our understanding of the source(s) of magmas that built the continental crust. Oxygen isotopes have more recently also been used as a filter for Hf model ages, distinguishing "mantle-like" zircons from "hybrid" ones with significant upper crustal components. This approach enables distinction of real juvenile additions to the crust from reworked pre-existing crust, which then permits better constraints on crustal growth rates [1, 2].

Aims and objectives

This project aims to resolve geodynamic processes during the Palaeoproterozoic, a critical time period in the transition to modern tectonic processes, by applying U-Pb, Lu-Hf and O isotope systematics to zircons from Palaeoproterozoic igneous rocks within the Mineiro Belt, an orogenic belt that bounds the Archaean southern São Francisco craton, Brazil. These igneous rocks represent the largest occurrence of plutonic trondhjemite-tonalite-granodiorite (TTG) magmatism intruded during the so-called "global magmatic shutdown" at 2.45 to 2.2 Ga [3], proposed due to the paucity of evolved igneous rocks with ages within this interval, and more recently re-defined as a "magmatic lull" between 2.3 to 2.2 Ga [4]. The belt contains a large juvenile magmatic arc, with an age of ca. 2.1 Ga, which is geochemically similar to Late Archaean mantle-derived sanukitoids [5]. Contemporaneous 2.1 Ga high Ba-Sr granitoids comprise another suite, distinguished from the sanukitoids by the depletion in compatible elements [6]. This age relationship of TTG followed by sanukitoid magmatism provides evidence of geodynamic changes, which has been associated with the onset of modern-style subduction-driven plate tectonics and the opening up of mantle wedges above steepened subduction zones [7]. However, elsewhere on Earth the transition from TTG to sanukitoid magmatism occurred at around 2.9-2.7 Ga. Hence, this area records a much younger transition during a time period widely believed to have generated very little evolved new crust. The belt also contains ca. 2.18 Ga old tonalites that are less evolved than the 2.13 Ga high Ba-Sr magmas and have a different geochemical evolution marked by assimilation of older mafic xenoliths. The plutonic rocks are surrounded by sedimentary sequences that are sourced from this basement and contain abundant detrital zircons. Our study will give significant insights into an important and poorly understood interval of time in terms of evolved magma generation, building of new crust and the implications for the onset and evolution of subduction-driven plate tectonics.

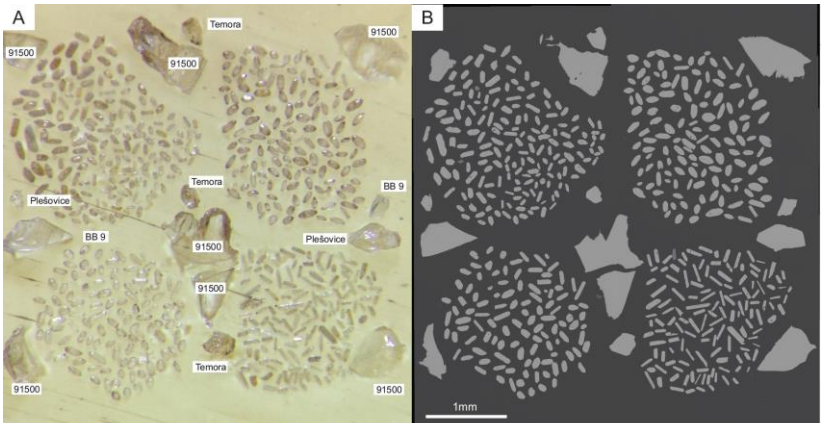

Figure 1. A) Zircon grains and reference materials on parcel tape. B) Backscatter image of one of the mounts produced in this study.

Sample preparation

Zircon grains were hand-picked and positioned in square shape on parcel tape, in which sides are smaller than 5 mm (diagonals < 7 mm). A 25 mm diameter round mount was then centred on top of the grains, where epoxy resin was poured and dried in a vacuum chamber. Reference materials were arranged at the middle and corners of the square (Fig. 1). The grains show minimal polishing relief that is

indistinguishable from the epoxy surface. Combined with the high sensitivity of the Cameca IMS-1270 from 15 µm spots, the oxygen secondary ion yielded on average 3 x 10^9 cps and 6 x 10^6 cps for masses ^{16}O and ^{18}O, respectively, and most of the $\delta^{18}O$ values have a precision better than 0.25‰ (2SD).

Results

During 5 days in January 2018, some 400 zircon grains from granitoids and metasedimentary rocks from the Mineiro Belt were analysed for oxygen isotopes. Zircons from the early 2.35 Ga TTG magmas have a narrow range of values consistent with a depleted mantle source to lower mafic ocean crust. In progressively younger rocks, some crustal contamination is identified by a broader spectrum towards $\delta^{18}O$ above mantle values (Fig.2). The oldest rocks (ca. 2.35 Ga) are TTG in composition and have $\delta^{18}O$ between 4.2 and 5.0 ‰. The youngest suite of rocks (ca. 2.13 Ga) are sanukitoids and have $\delta^{18}O$ values between 5.5 and 6.7 ‰, reflecting a crustal contribution, possibly from subducted sediments in a metasomatised mantle source. The suite of ca. 2.13 Ga rocks (high Ba-Sr granitoids) have a broader $\delta^{18}O$ composition, ranging from 2.8 to 7.5 ‰. The lowest values are likely due to U-Pb discordance (yet to be confirmed), but the highest values are consistent with crustal assimilation. The suite of ca. 2.18 Ga rocks (tonalites) have an average $\delta^{18}O$ composition of 5.5 ‰, indicating derivation from an uncontaminated mantle derived source. An extensive passive margin is inferred for the early stages of the Mineiro Belt tectonic setting, whereas underplating melt and/or contamination of the mantle wedge from a subduction zone explains the isotopic and geochemical signature of the younger magmas. U-Pb and Lu-Hf analyses will further validate the range of $\delta^{18}O$ values found in the zircons and contribute to the debate about mantle derived contributions and continental crust growth rates in the Palaeoproterozoic.

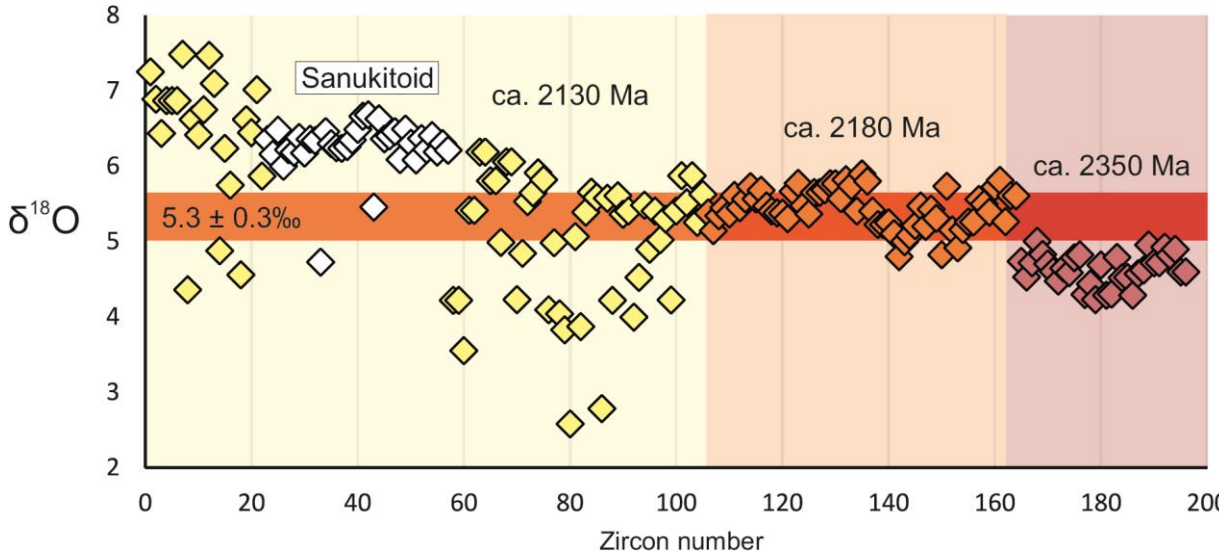

Figure 2. Oxygen analyses from zircon grains of igneous rocks. 5.5 ± 0.3 ‰ (1SD) is the $\delta^{18}O$ value of zircons in equilibrium with mantle melts [8]

References

[1] Hawkesworth, C.J., Kemp, A.I.S., 2006. Chem. Geol. 226, 144–162; [2] Dhuime, B., Hawkesworth, C.J., Cawood, P.A., Storey, C.D., 2012. Science 335, 1334–1336; [3] Condie, K.C., O'Neill, C., Aster, R.C., 2009. EPSL 282, 294–298; [4] Spencer, C.J., Murphy, J.B., Kirkland, C.L., Liu, Y. and Mitchell, R.N., 2018. Nature Geo. 11, 97-101; [5] Seixas, L.A.R., Bardintzeff, J-M., Stevenson, R., Bonin, B., 2013. Prec. Res. 238, 18–41; [6] Moreira, H., Seixas, L., Storey, C., Fowler, M., Lasalle, S., Stevenson, R. and Lana, C., 2018. Geos. Front.; [7] Martin, H., Moyen, J.-F., Rapp, R., 2010. Transactions of the Royal Society of Edinburgh-Earth Sciences. 100, 15–33. [8] Valley, 2005, CMP 150, 561-580.

Crystallization and degassing of volatile-rich magmas from Tanganasoga volcano, El Hierro

Z. Taracsák[1], M.E. Hartley[1], R. Burgess[1], M. Edmonds[2], M-A. Longpré[3]

[1]School of Earth & Environmental Sciences, University of Manchester, Manchester M13 9PL, UK
[2]Department of Earth Sciences, University of Cambridge, Cambridge CB2 3EQ, UK
[3]School of Earth and Environmental Sciences, Queens College, City University of New York, Flushing, NY 11367, USA

Background and Motivations

El Hierro, the westernmost island of the Canary Islands, produced the last volcanic eruption in the island chain between October 2011 and March 2012. More than 0.3 km^3 magma erupted off-shore of the southern tip of the island. This activity was monitored by both seismic and surface gas measurement stations, the latter indicating high (up to 2500 t/day) emissions of CO_2 on the surface before and during the eruption [1]. Melt inclusions hosted within olivines show the melt feeding the eruption was highly enriched in CO_2 and S and other volatiles [2]. However, no data on volatile systematics from older eruptions were available from the island, including its main volcanic edifice, Tanganasoga volcano. Our goal was to investigate if this volatile enrichment has been present in El Hierro magmas in the last 20000 years, and if so, why and how this enrichment forms, as well as where and how exsolution/degassing of volatiles takes place.

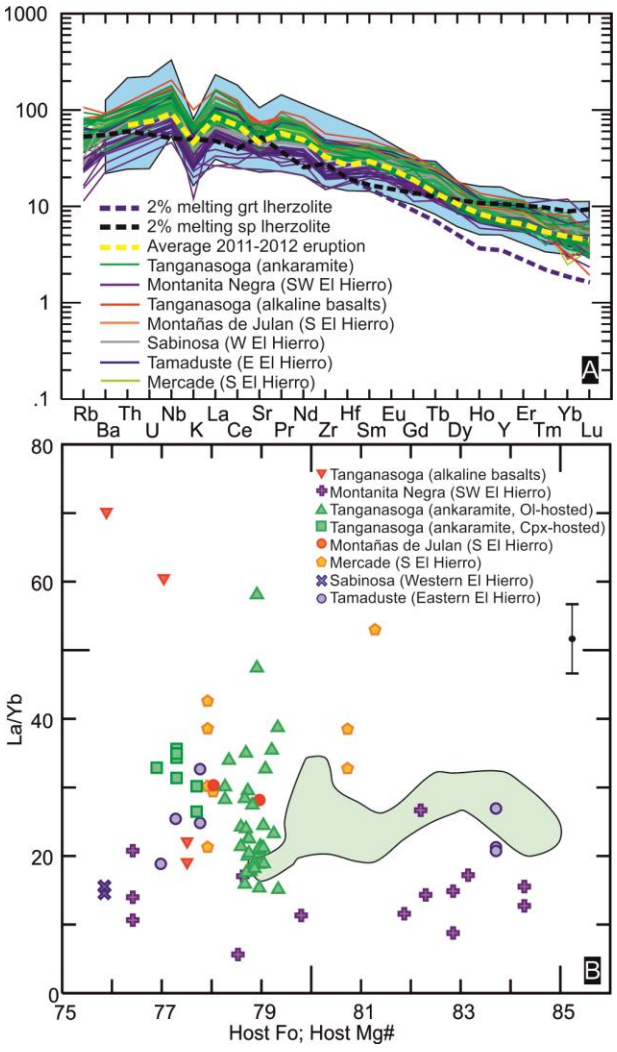

Figure 1: Trace element composition of MIs normalised to primitive mantle (A) and La/Yb ratio vs host forsterite content/Mg-number (B).

Results

93 olivine and clinopyroxene-hosted melt inclusions (MIs) and 13 groundmass glasses (all naturally quenched glasses) were measured for volatile (H_2O, CO_2, F) and trace elements from samples representing the latest stage (past 12 ka) of subaerial volcanism on El Hierro using the CAMECA IMS-4f instrument. SIMS analyses were followed by EPMA analyses of major elements and S and Cl.

Trace element concentrations fall within the range of previous whole rock compositions (including the 2011-2012 eruption; Fig. 1A). La/Yb ratios of MIs show large variation (15-80) compared to MIs from the 2011-2012 eruption (Fig. 1B). Even within one sample, the Tanganasoga ankaramite, the variation of La/Yb is larger than previously recorded in both whole rock samples and MIs. Variability of La/Yb is not related to host forsterite content/Mg-number; even within a range of Fo<1.5 variability is half an order of magnitude (most notably within the Tanganagosa ankaramite). MIs likely represent melt batches from variably enriched mantle domains that have been stored separately before MI entrapment, and mixed together at a later stage to form the magma feeding the eruptions.

CO_2 and H_2O concentrations in MIs vary between 0-3600 ppm and 0.08-2.22 wt%, respectively (Fig. 2A). These concentrations are in the range observed in 2011-2012 eruption MIs, and are one of the most volatile-enriched melts measured on oceanic islands to date.

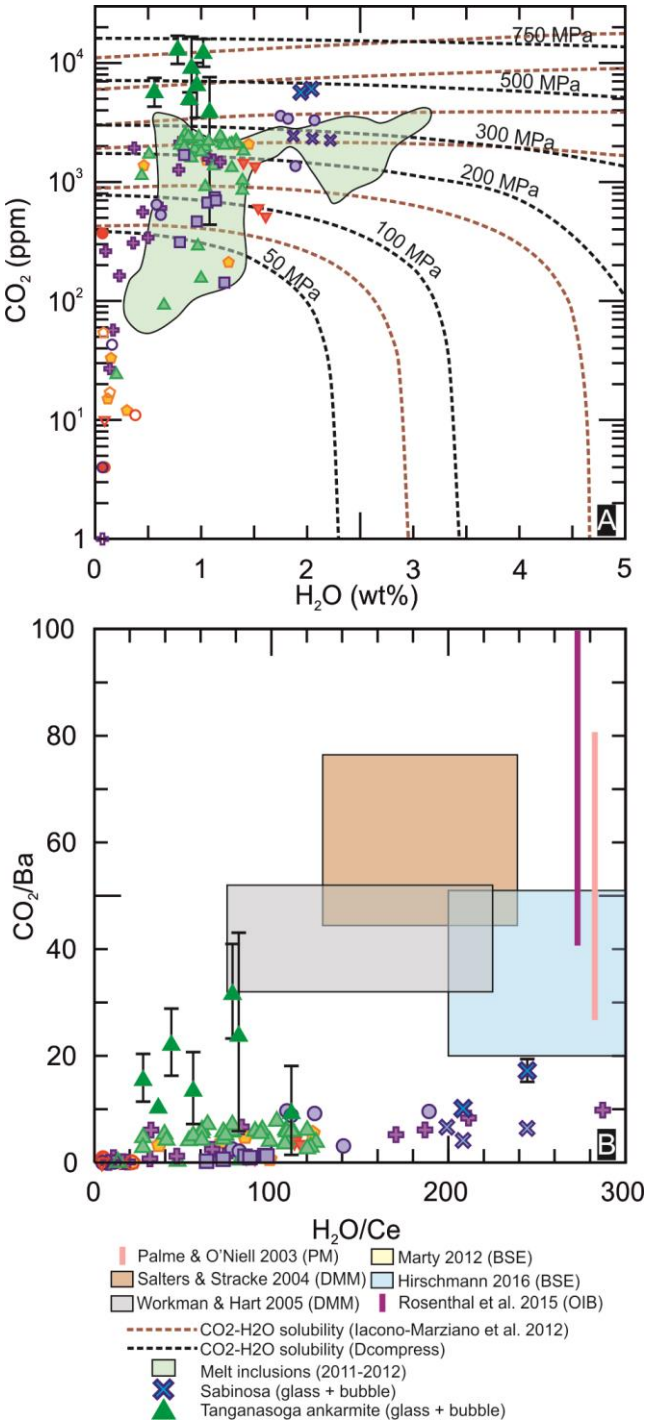

Figure 2: CO_2 vs. H_2O diagram of El Hierro MIs, showing solubility isobars (A). CO_2/Ba and H_2O/Ce ratios measured in MIs (B). Squares and lines indicate literature data on CO_2/Ba and H_2O/Ce ratios in the mantle.

Nonetheless, deep exsolution of CO_2 still likely occurred, as shown by very low CO_2/Ba ratio of the MIs (<10; Fig. 2B). Even if CO_2 sequestered into inclusion-hosted bubbles (measureable by Raman spectrometry) is taken into account, CO_2/Ba ratios only increase to 20-30, which is below most estimates of CO_2/Ba in melts from a primitive mantle-like source. The maximum saturation pressure of the melt inclusions is 300-780 MPa (10-25 km) using reconstructed (i.e. glass plus bubble) CO_2 concentrations. The reconstructed CO_2-H_2O saturation pressures overlap with the results of clinopyroxene-melt barometry (400-1000 MPa) carried out on different sample suites from El Hierro [2, 3].

H_2O/Ce systematics of MIs show large variation (20-290; **fig. 2/B**). This is likely controlled by shallow degassing (in case of low-H_2O, low-CO_2 MIs) and diffusive re-equilibration during crystallisation and mixing of more water-rich and poor magmas in the uppermost mantle.

Our samples show El Hierro has been fed by magmas with very high CO_2, S and F concentrations (CO_2 content of the un-degassed primary magma was likely above 1.5 wt%), originating from a mantle source containing at least two components represented by high and low La/Yb melts, possibly containing recycled C and F. This heterogeneity is also observed in the isotopic compositions of whole-rocks [4]. The ascending magma became fluid saturated at mantle depths of ~35-40 km, and exsolution and degassing of volatiles continued until eruption. This deep degassing process would explain high CO_2 fluxes on the surface during the 2011-2012 eruption [1]. MIs from Tanganasoga volcano indicate a complex plumbing system with multiple interconnected sills storing magmas with different trace element enrichment levels before eruption.

References

[1] Melián et al. (2014) Journal of Geophysical Research: Solid Earth **119**, 6976–6991
[2] Longpré et al. (2017) Earth and Planetary Science Letters, **460,** 268-280.
[3] Stroncik et al. (2008) Contribution to Mineralogy and Petrology, **157**, 593–607.
[4] Day et al. (2010) Geochimica et Chosmochemica Acta **74**, 6565–6589

Boron isotope systematics of veined (metasomatised) mantle xenoliths from Kamchatka arc volcanoes

L. Tomanikova, I. Savov & J. Harvey

School of Earth and Environment, University of Leeds, Leeds LS2 9JT, UK

Project rationale

Direct observations of the processes of element transfer and isotope fractionations associated with slab dehydration in subduction zones are not possible. However, pieces of fragmented metasomatised (veined) subarc mantle are often erupted at volcanic arcs such as in Kamchatka, Russia. These veined mantle xenoliths record evidence of interaction between the subarc mantle and slab-sourced hydrous fluids/melts. IN the Kamchatka subduction zone, the origin of the fluid with which these minerals were in equilibrium remains, as yet, unknown, primarily because the boron isotope systematics have not been studied in detail.

Background

Boron and $\delta^{11}B$ have been widely used in studies of the fate of slab-derived fluids in subduction zones[1]. They are particularly sensitive tracers of slab-sourced metasomatic agents because of the highly fluid-mobile behaviour of B, which is enriched in the subducting oceanic lithosphere relative to B-depleted mantle[2]. However, this versatile tracer has not previously been employed in the investigation of FME inputs and fluxes in metasomatised sub-arc mantle xenoliths. Mantle xenoliths from Shiveluch and Avachinsky record evidence of mantle wedge metasomatism in the form of veins rich in phlogopite, amphibole, orthopyroxene and clinopyroxene; a characteristic subduction-related vein paragenesis (Figure 1). The B isotope composition of the vein minerals will be sensitive to the source of dehydration reactions occurring in the slab with different isotopic signature of fluids derived via dehydration of the altered oceanic crust (AOC)[3] and serpentinite[4]. The aim of the project was to determine the variability of [B] and B isotope fractionation in the mantle wedge below the Kamchatka arc and to inform on the evolution of subduction-related fluids during progressive dehydration of a subducting slab below the two Kamchatka arc transect volcanoes.

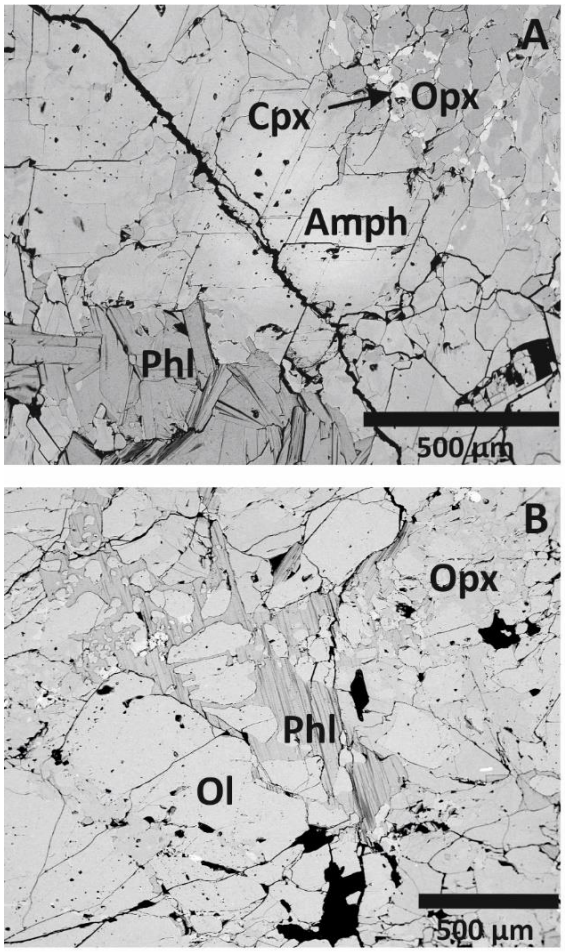

Figure 1. Back-scattered electron images of hydrous vein minerals in Shiveluch mantle xenoliths. A) A typical vein consisting of phlogopite and amphibole cross-cutting Shiveluch harzburgite SH98X-16 and B) poikilitic phlogopite in Shiveluch dunite SHIV-16-12-06.

This was achieved via B and $\delta^{11}B$ analysis of vein minerals (phlogopite, amphibole), olivine and glasses in ultramafic xenoliths.

Results and discussion

All vein minerals have low B contents and are dominated by negative $\delta^{11}B$ ratios (Figure 2). Amphibole and phlogopite B contents range from 0.2 to 6.4 µg g^{-1} and from 0.3 to 3.1 µg g^{-1}, respectively and their $\delta^{11}B$ range from +0.9 to -12.1‰ and from -0.5 to -16.6‰, respectively. Boron contents and $\delta^{11}B$ of olivine in mantle xenolith SHIV-16-12-06 range from 0.5 to 1.4 µg g^{-1} and -4.9 to -13.8‰, respectively, while the B content of primary mantle olivine in Avachinsky xenoliths was below detection limit.

Avachinsky vein minerals are lower in B (0.2-0.9 µg g^{-1}) than Shiveluch vein minerals (0.2-6.4 µg g^{-1}) and lighter in $\delta^{11}B$ (-3.6 to -16.6‰) relative to those of Shiveluch (+0.9 to -13.8‰). Boron contents and $\delta^{11}B$ of Kamchatka mantle xenoliths plot between the MORB and depleted mantle (DM) compositions[2], are depleted in B, and are light in $\delta^{11}B$ with respect to Kamchatka arc lavas (B = 11.2 to 36.3 µg g^{-1}; $\delta^{11}B$ = -3.7 to +5.6‰)[1].

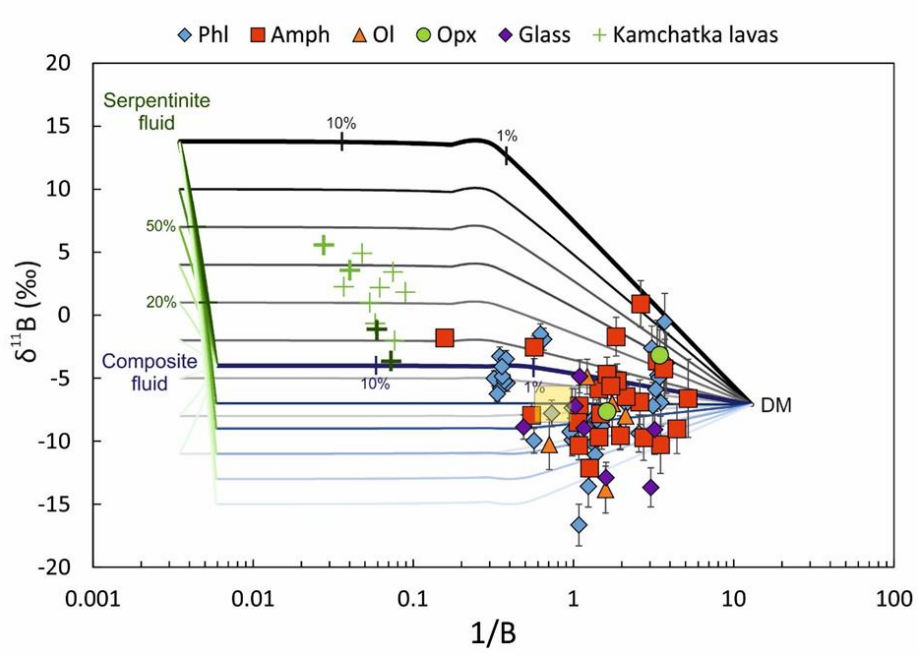

Figure 2. $\delta^{11}B$ vs B contents in vein minerals and glasses in Avachinsky and Shiveluch mantle xenoliths, Kamchatka arc volcanoes[1] and MORB glasses (yellow square)[2] and mixing relationship between depleted mantle (DM)[2], serpentinite and composite fluid comprising 90% AOC and 10% sediment[4]. Bold green crosses represent Avachinsky and Shiveluch volcanoes and bold dark green crosses represent Sredinny Range volcanoes which display a systematic decrease in serpentinite fluid component in the Kamchatka arc volcanics sources with increasing depth-to-slab[1].

The absence of both B enrichments and large isotope fractionations provide support for the mobility of B in fluids and its transient nature in the mantle wedge. Data points which in Figure 3 plot above the mixing line between DM and composite fluid require up to 3% serpentinite fluid component with $\delta^{11}B$ of -2‰. On the other hand, Kamchatka arc lavas require up to 50% serpentinite fluid component in their source to generate their high B and heavy $\delta^{11}B$ systematics. This inconsistency between the depleted B inventory of the metasomatised mantle and that of B enriched arc lavas is observed at both arc volcanoes, Shiveluch and Avachinsky, which implies early release of B in the forearc and its efficient transport through the subarc mantle. Contrary to the widely established model, flux melting of metasomatised mantle wedge above subducting slabs cannot alone produce uniformly B-rich and isotopically heavy arc basalts[1]. The magmas that form these basalts require interactions with heavy $\delta^{11}B$ fluids that can only be released from down-dragged forearc serpentinite[4], slab mantle serpentinite[5] or forearc-modified serpentinite mélange diapirs[6].

References

[1] T. Ishikawa et al. (2001) Geochimica et Cosmochimica Acta **65**, 4523-4537 [2] H. R. Marschall et al. (2017) Geochimica et Cosmochimica Acta **207**, 102-138 [3] S. Pabst et al. (2012) Lithos **132-133**, 162-179 [4] S. Tonarini et al. (2011) Earth and Planetary Science Letters **301**, 275-284 [5] M. Konrad-Schmolke et al. (2014) Lithos **208-209**, 393-414 [6] H. Marschall & J.C. Schumacher (2012) Nature Geoscience **5**, 862-867